ROTARY REGENERATOR DESIGN OPTIMISATION AND HEATING SURFACE SELECTION

by

D.C. Swanepoel

Thesis presented in partial fulfilment of the requirements for the degree of Master of Mechanical Engineering at the University of Stellenbosch

Thesis supervisor:
Prof. D.G. Kröger

Department of Mechanical Engineering
University of Stellenbosch
March 1995

DECLARATION

I, the undersigned, hereby declare that the work contained in this thesis is my own work and has not previously in its entirety or in part been submitted at any university for a degree.

16-02-95
....
Date

SYNOPSIS

The rotary regenerator is far from a new device and since its invention more than 70 years ago it has developed into a carefully engineered product. They are mainly used for gas to gas heat transfer and find application in electricity generating plants and in refrigeration and air conditioning systems amongst others. Today the challenge in regenerator design is the optimisation of the operating conditions and the development of improved heating surfaces. The objective of this study is to make a contribution in this respect. The design theory for regenerators is investigated and the dimensionless parameters on which the regenerator effectiveness depends are identified. Approximate solution methods for regenerators are evaluated by comparing their accuracy to more accurate numerical results. The best approximate solutions obtained from the accuracy analysis are used to formulate a regenerator design method. A computer program is written to thermally evaluate or design a rotary regenerator. The program uses either the approximate theory or more accurate numerical methods, depending on user specification. The program can be used to optimise some of the operating conditions.

Several new heating surfaces are experimentally tested for their heat transfer and pressure drop characteristics. The performance of the heating surfaces is compared to each other in a specific regenerator application. A cost effectiveness parameter is defined for comparison purposes. It is shown by an example how the matrix rotational speed, the flow split ratio, the matrix wall thickness can be optimised.

Key words:
Rotary regenerator
Ljungström regenerator
Air preheater
Heating surfaces

SAMEVATTING

Die roterende regenerator is allesbehalwe 'n nuwe konsep. Dit is al meer as 70 jaar gelede uitgevind en het sederdien ontwikkel tot 'n gevorderde ingenieursproduk. Dit word uitsluitlik gebruik vir gas tot gas warmteruiling en vind onder andere toepassing in die elektrisiteitsvoorsienings en lugreëling-en-verkoelings bedrywe. Die groot uitdaging vandag in regenerator ontwerp is die optimering van die bedryfstoestande en die ontwikkeling van verbeterde warmteruilingsoppervlaktes. Hierdie studie het ten doel om 'n bydrae op hierdie gebied te maak. Die ontwerpsteorie vir regenerators is ondersoek en daar is uitgewys van watter dimensielose getalle die effektiwiteit afhang. Benaderde oplosteorieë is ondersoek en 'n evaluasie van die akkuraatheid van dié teorieë is gedoen deur dit met akkurate numeriese oplossings te vergelyk. 'n Benaderde oplosmetode is geformuleer deur gebruik te maak van die beste benaderde oplossings. 'n Rekenaarprogram vir die ontwerp en evaluasie van 'n regenerator is geskryf. Hierdie program kan beide die benaderde oplosmetode sowel as numeriese metodes hanteer. Die program kan ook gebruik word om van die bedryfstoestande to optimeer.

Die warmteoordrag en drukval eienskappe van verskeie nuwe warmteruilingsoppervlaktes is eksperimenteel bepaal. Die vermoë van die oppervlaktes is in 'n spesifieke toepassing met mekaar vergelyk. 'n Koste-effektiwiteits parameter is vir hierdie doel gedefineer. Daar word aan die hand van 'n voorbeeld geillustreer hoe die rotasie spoed van die matriks, die vloeiverdelingsverhouding, die matriks wanddikte en die keuse van matriks geoptimeer kan word.

Sleutelwoorde:
Roterende regenerator
Ljungström regenerator
Lug-voorverwarmer
Warmteruilings oppervlaktes

ACKNOWLEDGEMENTS

I would like to thank my thesis supervisor Prof. D.G. Kröger for his advice and encouragement throughout this investigation.

I also would like to thank everybody who assisted me, especially Mr K. Zietsman for his valuable technical assistance.

A special thanks to Annemarie and my parents for their moral support whenever I needed it.

TABLE OF CONTENTS

NOMENCLATURE

A	area	m^2
C	cost	$
C	heat capacity rate	W/K
CP	cost effectiveness parameter	kWh/$
c	specific heat	J/kgK
D	diameter	m
d_{hub}	hub diameter	m
F	flow period	s
f	Fanning friction factor	
G	mass flux	kg/sm^2
H	annual operating time	hours
h	convective heat transfer coefficient	W/m^2K
i	interest rate	
K	loss coefficient	
k	thermal conductivity	W/mK
L	disk height	m
M	mass	kg
N	rotational speed	rev/s
n	regenerator life	years
Ny	characteristic heat transfer parameter	m^{-1}
P	absolute pressure	N/m^2
Δp	pressure differential	N/m^2
q	heat transfer rate	J/s
R	thermal resistance	K/W
Ry	characteristic flow parameter	m^{-1}
R	universal gas constant	J/kgK
s	surface spacing	m
T	temperature	K
t	time	s
V	volume	m^3
$\dot{V}$	volume flow rate	m^3/s
v	velocity	m/s
W	mass flow rate	kg/s
x	leakage factor or fraction	
x	axial distance	m

Greek Symbols

α	area ratio	
β	area density	m^2/m^3
δ	plate thickness	m
ε	effectiveness	
ϕ	flow split ratio	
η	efficiency	
μ	dynamic viscosity	kg/sm
ρ	density	kg/m^3
σ	porosity	

Dimensionless Groups

A_k^*	matrix solid area ratio	$A_{k,min}/A_{k,max}$
Bi	Biot number	$\frac{h\delta}{2k}$
C^*	heat capacity ratio	C_{min}/C_{max}
C_r^*	matrix heat capacity ratio	C_r/C_{min}
$(hA)^*$	connection conductance ratio	$(hA)_{min}/(hA)_{max}$
Ntu_o	modified number of heat transfer units	$\frac{1}{C_{min}}\left[{}^{1}\!/\!_{(hA)_{min}} + {}^{1}\!/\!_{(hA)_{min}}\right]^{-1}$
Ntu	number of transfer units	(hA)/C
Pr	Prandtl number	$\mu c_p/k$
Re	Reynolds number	$\rho vd/\mu$
λ	Longitudinal conduction parameter	$\frac{k_w A_{k,t}}{LC_{min}}$

Subscripts

a	air
act	actual
c	cold gas side or contraction
d	dwell
e	equivalent or expansion
eu	electrical unit
eff	effective
fd	fan drive
fr	frontal
fs	fan static
gs	gas supply
h	hot gas side or hydraulic
he	heat exchanger
i	inlet side
int	internal
iso	isothermal
k	refer to matrix solid area for longitudinal conduction
m	mean or average or matrix
mu	unit of matrix material
max	maximum
min	minimum
o	outlet side or free flow when used with area
p	pressure
r	rotor
ref	reference
s	seal
t	total
w	matrix wall
∞	recuperator or ideal rotary regenerator rotating at infinite speed

CHAPTER 1

INTRODUCTION

The first Ljungström Rotary Regenerator was patented in 1922 and named after the Swedish Engineer, Frederick Ljungström, who designed it. Since its invention the development of the rotary regenerator has been continuous, covering the principles of thermodynamics, fluid mechanics and structural engineering. The idea of using a slowly rotating drum containing a tightly packed heating surface matrix to transfer heat between two gas streams is still the basis of present day designs. Originally the rotary regenerator was designed for use in electrical power generating stations. The incoming air to the boiler is preheated to improve the boiler economy and efficiency. Although this is still the most important application today they are also used in vehicular gas turbine power plants, in cryogenic refrigeration units and in the food dehydration industry. Today the rotary regenerator is a carefully engineered product which is highly reliable. The diameter of the drum can range from 350 mm to more than 15 m. This causes the heating matrix to weigh anything from a few kilograms to several hundreds of tons [82WA1]. Figure 1.1 shows a rotary regenerator.

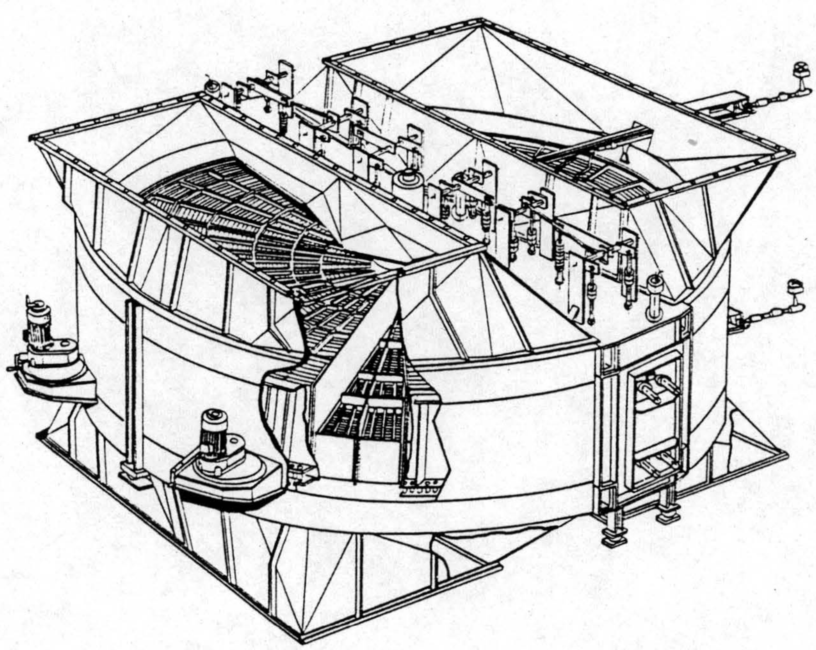

Figure 1.1: Ljungström Rotary Regenerator.

In a regenerator the heat is not transferred by passing it through plate or tube walls as in a recuperator. The heat is simply absorbed and released from the same surfaces as the entire mass of the heat exchanger elements is rotated in a continuous cycle through alternate streams of hot gas and cold gas.

The rising cost of energy over the past decade or two has compelled the manufacturing and process industry to re-examine the use of the rotary regenerator and other heat recovering systems. An important way to improve the effectiveness of a regenerator is the development of improved heating surfaces. The heat transfer elements are packed into baskets for easy handling and assembly. There are a great number of different surfaces in use today - each suited for a specific application. In figure 1.2 some typical surface elements can be seen. Figure 1.3 shows a basket fitted with heat transfer elements; ready for assembly in the regenerator drum.

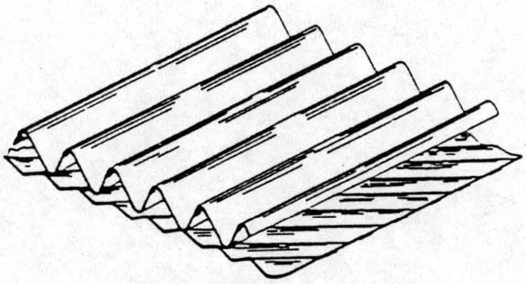

Corrugated undulated

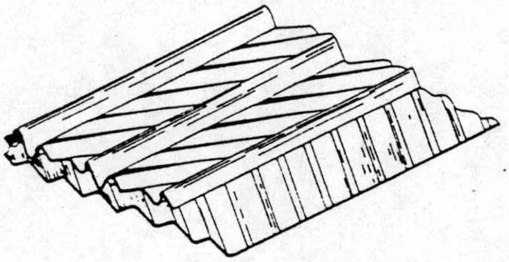

Double undulated

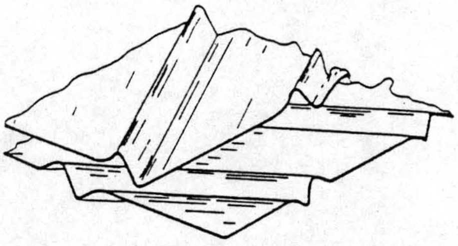

Flat notched crossed

Figure 1.2 Different heating surface elements.

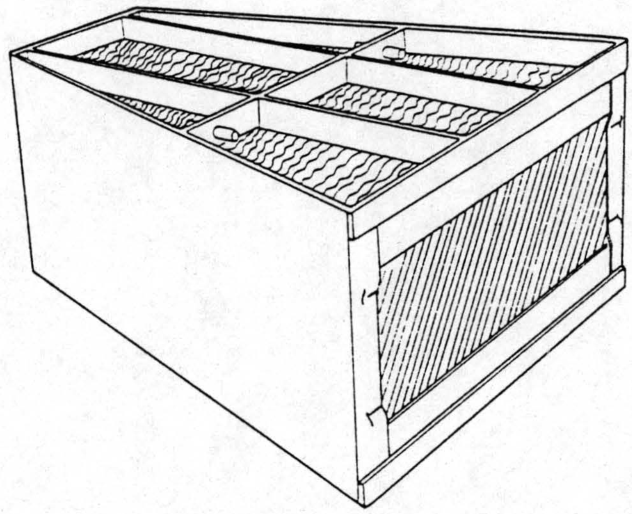

Figure 1.3: Heating surface elements fitted into a basket.

The development of improved heating surfaces requires that the heat transfer characteristics must be improved without producing an excessive pressure drop. An optimum heating surface for a specific application can only be determined by comparing the pressure drop and heat transfer characteristics of all the elements tested. The shape of the heating surface has a profound influence on the size and operating conditions of the regenerator.

The main objective of this thesis is twofold:

1. An experimental apparatus was designed to test numerous different shapes of new heating surfaces for their pressure drop and heat transfer characteristics. The mass flow rate and the plate spacing were varied during the tests for each different surface. The experimental set-up and procedures are described in Appendix A.

2. The thermal design theory for rotary regenerators was investigated. In Chapter 2 the basic differential equations are derived and it is shown on which dimensionless parameters the regenerator performance depends. No complete solution for the differential equations exists; therefore in Chapter 3 approximate solutions are presented and their accuracy is discussed. A practical and accurate rating or design procedure is formulated making use of the approximate solutions. A computer program was written employing this

design theory. The computer program enables the user to evaluate the performance of a rotary regenerator if the operating conditions, matrix specifications and disk dimensions are specified. Alternatively the user can design a rotary regenerator if the desired heat transfer rate and some of the operating conditions are given. In Chapter 4 the program is briefly discussed and a sample calculation is presented. In Chapter 5 the program is used to compare the different shapes of surfaces with each other in a specific application. The influence on the regenerator dimensions and operating conditions is investigated when different surfaces are used. The optimum surface must not only be able to produce a high heat transfer rate at a low pressure drop, but must result in the minimum cost. For this purpose a simplified cost model is introduced.

In short it can be said the objective of the thesis is to optimise the operation of a rotary regenerator. To accomplish this, there is a need for a comprehensive computer program employing the best design theory available and a simplified cost model for economic evaluation. Part of the optimisation process is the selection of the heating surfaces. Different heating surfaces were tested in a search for improved surfaces and to demonstrate how the designer would select a surface for a specific application.

CHAPTER 2

DESIGN THEORY FOR REGENERATORS

2.1 INTRODUCTION

A heat exchanger is a device used to transfer thermal energy between two or more fluids at different temperatures. Heat exchangers can be classified according to the transfer process into *direct contact type* and *indirect contact type* heat exchangers. In the direct contact type two fluid streams of different phases come into direct contact, exchange heat and then are separated again. In an indirect transfer type the two fluids are separated by a thin wall through which heat flows from the hot fluid to the cold fluid. Those heat exchangers in which there is a continuous flow of heat from the hot fluid to the cold fluid through a dividing wall are referred to as *recuperators*. In storage type heat exchangers the flow passage is occupied by only one of the fluids at a time. If the hot fluid is flowing through the passage heat is stored in the matrix wall. During the cold flow period the heat is transferred from the wall to the cold fluid again. This storage type of exchanger is generally referred to as a *regenerator* and will be the focus of our attention. Regenerators are exclusively used for gas to gas heat transfer applications.

In order to have a continuous operation in a regenerator, the fluid streams must be diverted to and from fixed matrixes as in a *fixed matrix regenerator*. Alternatively the matrix must be moved periodically in and out of the fixed streams of gases as in a *rotary regenerator*. A fixed matrix regenerator must have at least two matrixes in parallel. The hot and cold gases are ducted alternatively over each matrix by the operation of valves.

The object of this chapter is to set the background for solutions to the regenerator problem. The governing differential equations will be derived and it will be shown on which parameters the regenerator performance depends.

2.2 GOVERNING DIFFERENTIAL EQUATIONS

The design theory given in this section is basically as given by Shah [81SH1]. In fixed matrix type regenerators the fluid and matrix temperatures are a function of time and one spatial variable. In the rotary regenerator these temperatures are independent of time and a function of two spatial variables. The one being the axial distance and the second one the angle of rotation. However in rotary regenerators the angle of rotation is linear with time for a constant rotational speed. Thus for an observer travelling with the rotating matrix the rotation angle can be replaced by a time variable. The heat transfer analysis is identical for both types of regenerators if one chooses the reference coordinate system in this manner.

An idealised theory will be used in the derivation of the differential equations. In the next chapter some of the idealisations will be made invalid and their influence will be accounted for. These will include wall thermal resistance, carryover leakage and pressure leakage.

The following idealisations apply to the simplified theory:

1. Heat transfer between the heat exchanger and the surroundings is negligible.

2. Both fluids are uniformly distributed in the matrix during their respective flow periods and their mass flow rates do not vary with time.

3. The velocity and temperature of each fluid at the inlet are uniform over the flow cross section and are constant with time.

4. The fluid velocity on each side is considered constant with position, temperature and time throughout the matrix.

5. The convective heat transfer coefficients between the fluids and the matrix are constant with position, temperature and time.

6. The surface area of the matrix as well as the rotor mass is uniformly distributed.

7. The temperatures of both fluids and the matrix are dependant on the axial coordinate, x and the time, t.

8. The thermal properties of both fluids and the matrix are constant with temperature, time and position.

9. The temperature across the matrix wall thickness is uniform. The wall thermal resistance is thus equal to zero.

10. No mixing of the fluids occurs during the switch from hot flow to the cold flow. Also the fluid carryover is negligible relative to the flow rates, W_h and W_c.

The governing differential equations and boundary conditions that control the heat transfer process will now be derived. In figure 2.1 a counterflow rotary regenerator can be seen and in figure 2.2 the elemental flow passages are shown. The foregoing idealisations will be assumed to be applicable.

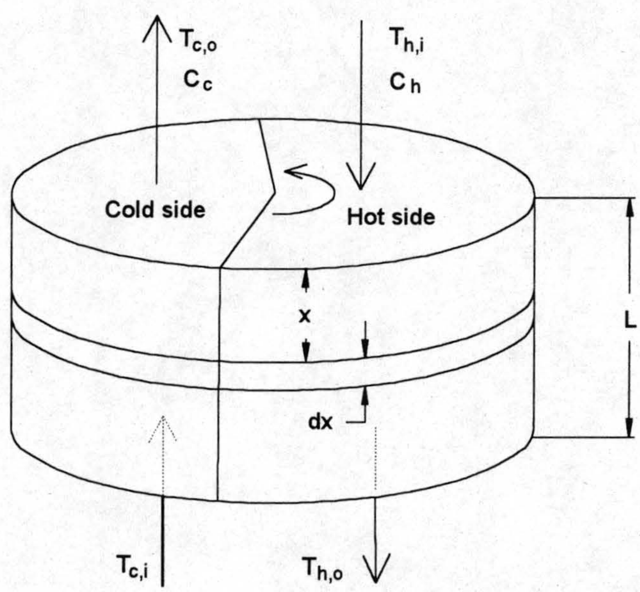

Figure 2.1: A rotary regenerator showing sections x and x+dx.

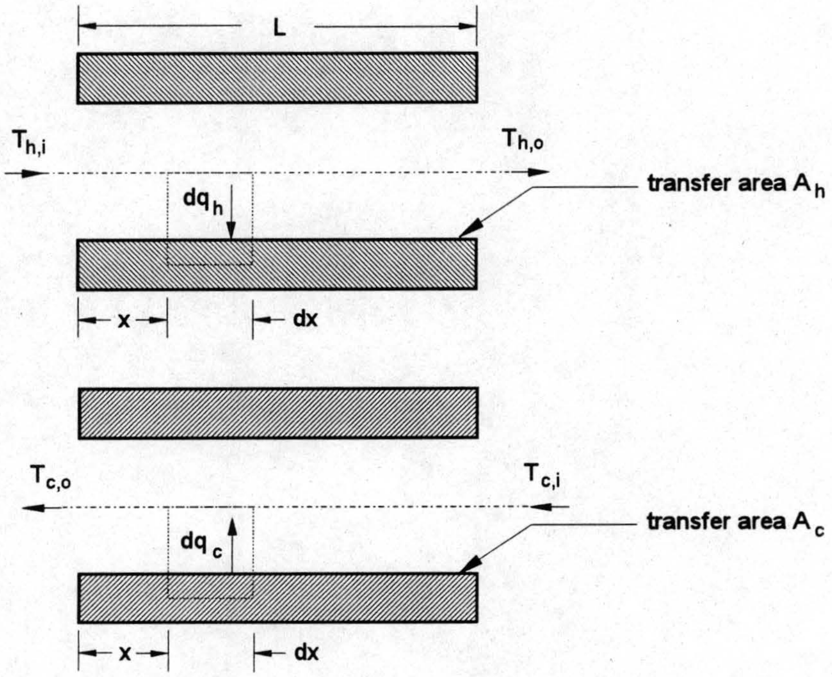

Figure 2.2: The regenerator matrix elemental flow passage during the hot and cold flow periods.

In the derivation of the differential equations all quantities considered, such as surface area, flow area and flow rate are associated with a complete cross section of the regenerator at x and x + dx. The differential fluid and matrix elements for the hot gas flow period are shown in figures 2.3 and 2.4 with the associated energy rate terms at a given instant of time.

Let us first define some of the terms that occur in the rate equations. The hot fluid capacity rate is C_h and M_h is the total mass of the hot fluid in the matrix. The hot fluid mass flow rate is W_h. The following relationships and definitions are applicable:

$$C_h = W_h c_{p,h}$$
$$W_h = M_h / t_{d\,h}$$

where $t_{d,h}$ is the dwell time of the hot fluid in the matrix and $c_{p,h}$ is the hot fluid specific heat at constant pressure. A_h is the total surface area of the matrix in contact with the hot fluid and h_h is the convective heat transfer coefficient between the matrix and the hot fluid. T_h and T_w are the hot fluid and matrix wall temperatures respectively. Note that the same definitions apply to the cold fluid.

The matrix wall thermal conductivity is k_w and c_w is the matrix wall specific heat. The solid area for longitudinal heat conduction is $A_{k,h}$. The mass of the matrix in contact with the hot fluid is $M_{w,h}$.

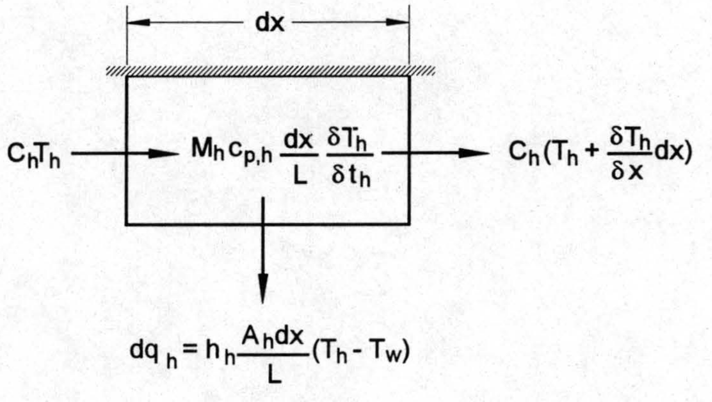

Figure 2.3: Differential fluid element with the associated energy rate terms.

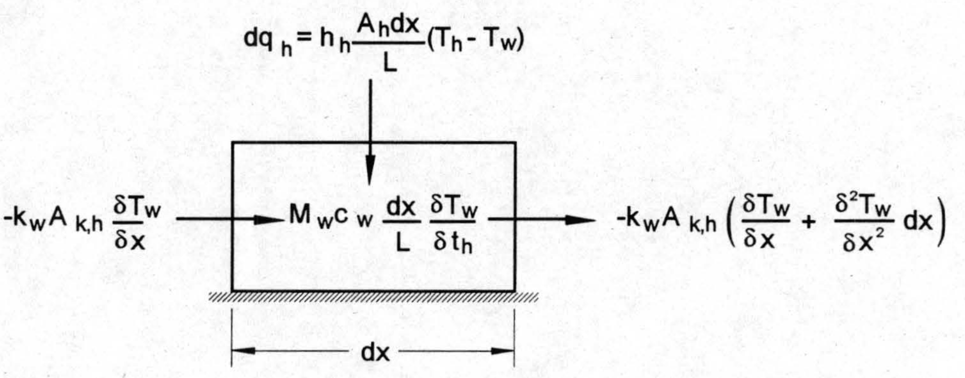

Figure 2.4: Differential matrix element with the associated energy rate terms.

The energy balance on the fluid element yields:

Rate of energy leaving the control volume - rate of energy entering the control volume + the rate of change of thermal energy of the fluid in the control volume = 0.

$$C_h\left(T_h + \frac{\partial T_h}{\partial x}dx\right) + h_h\left(\frac{A_h dx}{L}\right)(T_h - T_w) - C_h T_h + \left(M_h c_{p,h}\frac{dx}{L}\right)\frac{\partial T_h}{\partial t_h} = 0 \qquad (2.1)$$

The energy balance on the matrix element including the effect of longitudinal heat conduction yields:

$$-k_w A_{k,h}\left(\frac{\partial T_w}{\partial x}+\frac{\partial^2 T_w}{\partial x^2}dx\right)+k_w A_{k,h}\frac{\partial T_w}{\partial x}-h_h\left(\frac{A_h dx}{L}\right)\left(T_h-T_w\right)$$
$$+\left(M_{w,h}c_w\frac{dx}{L}\right)\frac{\partial T_w}{\partial t_h}=0 \tag{2.2}$$

Note that the wall thermal resistance was taken as zero implying that the matrix wall temperature is uniform at any x position.

Rearrange the above equations to find:

$$\frac{\partial T_h}{\partial t_h}+\frac{L}{t_{d,h}}\frac{\partial T_h}{\partial x}=\frac{(hA)_h\left(T_w-T_h\right)}{C_h t_{d,h}} \tag{2.3}$$

$$\frac{\partial^2 T_w}{\partial x^2}-\left(\frac{M_{w,h}c_w}{Lk_w A_{k,h}}\right)\frac{\partial T_w}{\partial t_h}=-\frac{(Ah)_h}{Lk_w A_{k,h}}\left(T_h-T_w\right) \tag{2.4}$$

Similar energy balances during the cold flow period result in the following differential equations:

$$\frac{\partial T_c}{\partial t_c}+\frac{L}{t_{d,c}}\frac{\partial T_c}{\partial x}=\frac{(hA)_c\left(T_c-T_w\right)}{C_c t_{d,c}} \tag{2.5}$$

$$\frac{\partial^2 T_w}{\partial x^2}-\left(\frac{M_{w,c}c_w}{Lk_w A_{k,c}}\right)\frac{\partial T_w}{\partial t_c}=-\frac{(Ah)_c}{Lk_w A_{k,c}}\left(T_w-T_c\right) \tag{2.6}$$

The boundary condition for the fluids is that the inlet temperature is constant and independent of time. The adiabatic boundary condition is applied to the matrix wall at x = 0 and x = L.

$T_h(0,t_h) = T_{h,i}$ = constant for $0 \leq t_h \leq F_h$
$T_c(L,t_c) = T_{c,i}$ = constant for $0 \leq t_c \leq F_c$

$$\frac{\partial T_w(0,t_h)}{\partial x}=\frac{\partial T_w(L,t_h)}{\partial x}=0 \qquad \text{for } 0 \leq t_h \leq F_h$$

$$\frac{\partial T_w(0,t_c)}{\partial x} = \frac{\partial T_w(L,t_c)}{\partial x} = 0 \qquad \text{for } 0 \le t_c \le F_c$$

Here F_h and F_c are the hot and cold flow periods respectively. The cyclic conditions for the wall temperature are:

$$T_w(x,t_h = F_h) = T_w(x,t_c = 0) \qquad \text{for } 0 \le x \le L$$
$$T_w(x,t_h = 0) = T_w(x,t_c = F_c) \qquad \text{for } 0 \le x \le L$$

From the four differential equations, boundary and periodic conditions it can be seen that the fluid and matrix temperatures are functions of the following variables and parameters.

$$\begin{aligned} T_h,T_c,T_w = f\{\, & x,t_h,t_c && \text{(independent variables)} \\ & T_{h,i},T_{c,i},C_h,C_c,t_{d,h},t_{d,c} && \text{(operating conditions)} \\ & M_{w,h},M_{w,c},(hA)_h,(hA)_c,L && \text{(design parameters)} \\ & F_h,F_c,c_w,k_w,A_{k,h},A_{k,c}\,\} && \text{(design parameters)} \end{aligned} \qquad (2.7)$$

2.3 DIMENSIONAL ANALYSES

The fluid and matrix temperatures depend on twenty dependant variables and parameters. To reduce this number suitable dimensionless groups will be defined. The choice of the groups is somewhat arbitrary but for rotary regenerators the effectiveness-number of transfer units (ε-Ntu) method is usually used. The reduced length-reduced period (Λ-Π) method is normally used for fixed matrix regenerators. The two methods are equivalent as shown by Shah [81SH1]. Only the ε-Ntu method will be discussed here.

Define the following dimensionless groups:

$$x^* = \frac{x}{L}$$

$$t_h^* = \frac{1}{F_h}\left(t_h - \frac{x}{L}t_{d,h}\right) \quad ; \quad t_c^* = \frac{1}{F_c}\left(t_c - \frac{x}{L}t_{d,c}\right)$$

$$T_h^* = \frac{T_h - T_{c,i}}{T_{h,i} - T_{c,i}} \quad ; \quad T_c^* = \frac{T_c - T_{c,i}}{T_{h,i} - T_{c,i}} \quad ; \quad T_w^* = \frac{T_w - T_{c,i}}{T_{h,i} - T_{c,i}}$$

$$Ntu_h = \frac{(hA)_h}{C_h} \; ; \; Ntu_c = \frac{(hA)_c}{C_c}$$

$$\lambda_h = \frac{k_h A_{k,h}}{LC_h} \; ; \; \lambda_c = \frac{k_h A_{k,c}}{LC_c}$$

$$C^*_{r,h} = \frac{M_{w,h} c_w}{F_h C_h} \; ; \; C^*_{r,c} = \frac{M_{w,c} c_w}{F_c C_c}$$

With the additional assumption that the dwell time of the fluid in the matrix is small compared to the flow period the differential equations and boundary conditions can be rewritten with the use of the above dimensionless groups.

For the hot flow period:

$$\frac{\partial T^*_h}{\partial x^*} = Ntu_h \left(T^*_w - T^*_h \right) \tag{2.8}$$

$$\frac{\partial^2 T^*_w}{\partial x^{*2}} - \frac{C^*_{r,h}}{\lambda_h} \frac{\partial T^*_w}{\partial t^*_h} = -\frac{Ntu_h}{\lambda_h} \left(T^*_h - T^*_w \right) \tag{2.9}$$

For the cold flow period:

$$\frac{\partial T^*_c}{\partial x^*} = Ntu_c \left(T^*_c - T^*_w \right) \tag{2.10}$$

$$\frac{\partial^2 T^*_w}{\partial x^{*2}} - \frac{C^*_{r,c}}{\lambda_c} \frac{\partial T^*_w}{\partial t^*_c} = -\frac{Ntu_c}{\lambda_c} \left(T^*_w - T^*_c \right) \tag{2.11}$$

Boundary conditions:

$$T^*_h\left(0, t^*_h\right) = 1 \qquad \text{for } 0 \le t^*_h \le 1$$

$$T^*_c\left(1, t^*_c\right) = 0 \qquad \text{for } 0 \le t^*_c \le 1$$

$$\frac{\partial T^*_w\left(0, t^*_h\right)}{\partial x^*} = \frac{\partial T^*_w\left(1, t^*_h\right)}{\partial x^*} = 0 \qquad \text{for } 0 \le t^*_h \le 1$$

$$\frac{\partial T_w^*(0,t_c^*)}{\partial x^*} = \frac{\partial T_w^*(1,t_c^*)}{\partial x^*} = 0 \qquad \text{for } 0 \le t_c^* \le 1$$

The cyclic conditions for the wall now become:

$$T_w^*(x^*, t_h^* = 1) = T_w^*(x^*, t_c^* = 0) \qquad \text{for } 0 \le x_h^* \le 1$$
$$T_w^*(x^*, t_h^* = 0) = T_w^*(x^*, t_c^* = 1) \qquad \text{for } 0 \le x_c^* \le 1$$

We have now reduced the number of independent variables and parameters from twenty to nine. The dimensionless temperatures are now a function of the following parameters.

$$T_h^*, T_c^*, T_w^* = f\left(x^*, t_h^*, t_c^*, Ntu_h, Ntu_c, \lambda_h, \lambda_c, C_{r,h}^*, C_{r,c}^*\right) \tag{2.12}$$

An alternative set of dimensionless variables can be defined from the set above. Ntu_h and Ntu_c can be combined to form Ntu_o and $(hA)^*$. The capacity rate ratios, $C_{r,h}^*$ and $C_{r,c}^*$ can be combined to form new ratios, namely C^* and C_r^*. The two dimensionless groups λ_h and λ_c can be combined to form λ and A_k^*.

We will denote the fluid with the smallest heat capacity rate, C as the minimum fluid and vice versa. The following definitions apply to the new variables.

$$Ntu_o = \frac{1}{C_{min}}\left[1/(hA)_h + 1/(hA)_c \right]^{-1} \quad ; \quad (hA)^* = \frac{(hA)_{min}}{(hA)_{max}}$$

$$C^* = \frac{C_{min}}{C_{max}} \quad ; \quad C_r^* = \frac{C_r}{C_{min}}$$

$$\lambda = \frac{k_w A_{k,t}}{L C_{min}} \quad ; \quad A_k^* = \frac{A_{k,min}}{A_{k,max}}$$

The functional relationship for the dimensionless outlet temperatures now becomes:

$$T_h^*, T_c^*, T_w^* = f\left(x^*, t_h^*, t_c^*, Ntu_o, (hA)^*, C_r^*, C^*, \lambda, A_k^*\right) \tag{2.13}$$

The alternative set has many advantages. The influence of $(hA)^*$ and A_k^* is small for fixed values of the other parameters as shown by Bahnke and Howard [64BA1]. This is a big advantage since the two parameters can practically be eliminated from equation (2.13). Another advantage is that the behaviour of a regenerator parallels that of a recuperator in the special case of infinite rotational speed or $C_r^* = \infty$. It will become clear in the next chapter that recuperator analysis is often used to find approximate solutions for regenerators.

The regenerator effectiveness, ε is defined as the actual heat transfer divided by the maximum possible heat transfer under the same operating conditions.

$$\varepsilon = \frac{C_h\left(\overline{T}_{h,i} - \overline{T}_{h,o}\right)}{C_{min}\left(\overline{T}_{h,i} - \overline{T}_{c,i}\right)} = \frac{C_c\left(\overline{T}_{c,o} - \overline{T}_{c,i}\right)}{C_{min}\left(\overline{T}_{h,i} - \overline{T}_{c,i}\right)} \tag{2.14}$$

where the bar indicates the time averaged temperature at the in- or outlet. For a rotary regenerator the time average is taken for an observer rotating with the matrix. The functional relationship for the effectiveness can thus be written as:

$$\varepsilon = f\left(Ntu_o, (hA)^*, C_r^*, C^*, \lambda, A_k^*\right) \tag{2.15}$$

It can be seen that the regenerator effectiveness still depends on six dimensionless parameters under all the idealisations made. In a direct contact type recuperator the effectiveness is only a function of Ntu and C^*. The parameters $(hA)^*$ and C_r^* arise because of the heat storing nature of a regenerator. The longitudinal heat conduction effect is accounted for by λ and A_k^*. No exact closed form analytical solution exists for the governing differential equations and boundary conditions. In the next chapter some approximate analytical and numerical results will be given.

CHAPTER 3

APPROXIMATE SOLUTIONS FOR A COUNTERFLOW REGENERATOR

3.1 INTRODUCTION

In the previous chapter it was established that the effectiveness of a regenerator is a function of six dimensionless parameters. To date there is no complete analytical solution for the governing differential equations and boundary conditions. In this chapter some partial and approximate solutions will be discussed. A computer program employing the finite difference scheme of Bahnke and Howard [64BA1] was written to evaluate the effectiveness of a counterflow regenerator for any range and combination of the six dimensionless parameters. The numerical scheme and solution method are shown in Appendix C. This was done to evaluate the approximate theories and correlations of several authors. The fluids and matrix properties were assumed to be constant. The numerical solution is subject to the same idealisations as given in Chapter 2. Numerical results from other authors are available in the literature ([58LA1], [64BA1], [83CH1] and [90RO1]). Usually the Gauss-Seidel method, based on single element calculation is used to solve the numerical equations. Chung-Hsiung Li [83CH1] proposed a method where a column of elements is solved at a time. He also allowed for variable fluids and matrix properties. The method of Chung-Hsiung Li [83CH1] is faster than the Gauss-Seidel method is inherently more stable. Variable fluid and matrix properties can easily be incorporated into the numerical solution methods. This will however increase the calculation time. Saunders and Smoleniec [51SA1] found that the error in effectiveness is usually less than 1 % if constant properties are assumed. However, they suggested that numerical solutions must allow for variable properties if significant variations in the fluids and matrix specific heats are anticipated.

The most important assumption in the derivation of the differential equations so far is that there is no mixing of the fluids due to pressure leakage or matrix rotation. The regenerator in the absence of leakage will be called the *ideal* regenerator. The method of solution is to find a solution for the ideal regenerator and then to model the influence of the leakage. In this chapter, solutions for the ideal regenerator will be given, it will be shown how influence of the leakage is modelled and how the pressure drop across the regenerator can be evaluated. At the end a solution method for the ideal regenerator will be formulated making use of the best approximate theories. The accuracy of this method will be checked against accurate numerical results.

As mentioned earlier, the effectiveness-number of transfer units (ε-Ntu) approach is usually used for rotary regenerators. The reduced length-reduced period (Λ-Π) method is normally used for fixed matrix regenerators. Only the ε-Ntu method will be discussed here. A comprehensive summary of regenerator design theory making use of the Λ-Π method can be found in [84]. In many cases, these methods are equivalent to the ε-Ntu approach.

3.2 IDEAL REGENERATOR SOLUTIONS

3.2.1 Solutions for the case of zero longitudinal heat conduction

In the case of zero longitudinal heat conduction the functional relationship for the effectiveness (equation (2.15)) becomes:

$$\varepsilon = f\left(Ntu_o, C_r^*, C^*, (hA)^*\right) \tag{3.1}$$

Note that if $C^* = 1$, the regenerator is said to be balanced. If $(hA)^* = 1$, it is labelled a symmetric regenerator. For the special case of infinite rotational speed, i.e. $C_r^* = \infty$ an analytical solution is available. The effectiveness is then given by the following relation.

$$\begin{aligned}\varepsilon_\infty &= \frac{1 - e^{-Ntu_o(1-C^*)}}{1 - C^* e^{-Ntu_o(1-C^*)}} \\ &= \frac{Ntu_o}{Ntu_o + 1} \quad \text{for } C^* = 1\end{aligned} \tag{3.2}$$

The above relation is identical to that of an indirect contact type recuperator. Ntu_o is identical to Ntu for a recuperator for only the case of zero wall thermal resistance. From now on we will denote the effectiveness of a regenerator with $C_r^* = \infty$ as ε_∞. Lambertson [58LA1] used a numerical finite difference procedure to calculate the regenerator effectiveness for the following ranges of the dimensionless parameters.

$$0.1 \le C^* \le 1 \;\;,\;\; 1 \le C_r^* \le 10 \;\;,\;\; 1 \le Ntu_o \le 10 \;\;,\;\; 0.25 \le (hA)^* \le 4$$

Lambertson [58LA1] reached the following conclusions:

1. As C^* decreases for given values of the other parameters, the effectiveness increases. This is also predicted by the equation for the limiting case of infinite rotational speed.
2. The influence of $(hA)^*$ is small for a given Ntu_o and for $C^* \ge 0.9$. In this range $(hA)^*$ can effectively be eliminated from the parameters. This was also the conclusion reached by Coppage and London [53CO1]. However for $C^* <$ 0.9 the influence becomes increasingly pronounced.
3. The effectiveness for values of $C_r^* > 5$ is very close to the case of infinite rotational speed.

Lambertson [58LA1] correlated the effect of C_r^*. Kays and London [84KA1] later modified the exponent from 1.87 to 1.93.

$$\varepsilon = \varepsilon_\infty \left(1 - \frac{1}{9 {C_r^*}^{1.93}} \right) \tag{3.3}$$

where ε_∞ is calculated from equation (3.2).

Razelos [79RA1] proposed the following method to calculate the regenerator effectiveness for the complete range of Ntu_o and C^*, and $C_r^* > 1$. As Lambertson, Razelos also disregarded the influence of $(hA)^*$ in the range 0.25 $< (hA)^* < 4$. From the specified values of Ntu_o, C^* and C_r^*, calculate $Ntu_{o,e}$ and $C_{r,e}^*$ for an equivalent balanced regenerator ($C^* = 1$).

$$Ntu_{o,e} = \frac{2 Ntu_o C^*}{1 + C^*} \tag{3.4}$$

$$C_{r,e} = \frac{2 C_r^* C^*}{1 + C^*} \tag{3.5}$$

Now calculate the effectiveness of the balanced regenerator using $Ntu_{o,e}$ and $C_{r,e}^*$ in equation (3.3) with $C^* = 1$.

$$\varepsilon_e = \frac{Ntu_{o,e}}{1+Ntu_{o,e}}\left(1-\frac{1}{9C_{r,e}^{*\ 1.93}}\right) \tag{3.6}$$

The effectiveness of the unbalanced regenerator can now be calculated from

$$\varepsilon = \frac{1-e^n}{1-C^*e^n} \quad \text{where } n = \varepsilon_e\left(C^{*2}-1\right)\Big/2C^*\left(1-\varepsilon_e\right) \tag{3.7}$$

The Razelos method [79RA1] was evaluated over a wide range of parameters. It was not used together with equation (3.6), but with numerical results for C^* = 1 to extend the results to $C^* < 1$ for $(hA)^* = 1$. This was done to isolate the ability of the Razelos method to account for the influence of C^*. It agrees with accurate numerical results within 1 % within the following ranges:

1. $1 < Ntu_o < 500$, $C_r^* > 1$, $0.7 < C^* < 1$
2. $1 < Ntu_o < 500$, $C_r^* > 1.5$, $0.5 < C^* < 1$
3. $1 < Ntu_o < 500$, $C_r^* > 2.5$, $0.3 < C^* < 1$

The Razelos method [79RA1] is extremely accurate over a wide range of parameters. It should however be used with caution for $C_r^* < 1.5$ and $C^* < 0.5$ where the error is high for large Ntu_o numbers. The error is for example 19 % for $Ntu_o = 500$, $C_r^* = 1$ and $C^* = 0.3$.

Baclic [85BA1] obtained a highly accurate closed form expression for the balanced, symmetric regenerator. He made use of a power series solution. Baclic [85BA1] applied the Galerkin method to solve the coeffients that arise in the analysis. Romie and Baclic [88RO1] showed how the coeffients can be obtained by an alternative method. They labelled it the Successive Integral Method (SIM). The results are valid for $C^* = 1$ and $(hA)^* = 1$.

$$\varepsilon = C_r^*\frac{1+7\beta_2-24\left\{B-2\left[R_1-A_1-90\left(N_1+2E\right)\right]\right\}}{1+9\beta_2-24\left\{B-6\left[R-A-20(N-3E)\right]\right\}} \tag{3.8}$$

where

$$B = 3\beta_3 - 13\beta_4 + 30(\beta_5 - \beta_6)$$
$$R = \beta_2[3\beta_4 - 5(3\beta_5 - 4\beta_6)]$$
$$A = \beta_3[3\beta_3 - 5(3\beta_4 + 4\beta_5 - 12\beta_6)]$$
$$N = \beta_4[2\beta_4 - 3(\beta_5 + \beta_6)] + 3\beta_5^2$$
$$E = \beta_2\beta_4\beta_6 - \beta_2\beta_5^2 - \beta_6\beta_3^2 + 2\beta_3\beta_4\beta_5 - \beta_4^3$$

$$N_1 = \beta_4[\beta_4 - 2(\beta_5 + \beta_6)] + 2\beta_5^2$$
$$A_1 = \beta_3[\beta_3 - 15(\beta_4 + 4\beta_5 - 12\beta_6)]$$
$$R_1 = \beta_2[\beta_4 - 15(\beta_5 - 2\beta_6)]$$

and

$$\beta_i = V_i\left(\frac{2Ntu_o}{C_r^*}, 2Ntu_o\right) \Big/ (2Ntu_o)^{i-1} \quad \text{with}$$

$$V_i(x,y) = e^{-(x+y)} \sum_{n=i-1}^{\infty} \frac{n!}{(i-1)!(n-i+1)!} (y/x)^{n/2} I_n\left(2\sqrt{xy}\right)$$

The Baclic equation [85BA1] is in excellent agreement with numerical results. The largest errors occur at high Ntu_o numbers and $C_r^* = 1$. At $Ntu_o = 500$ the error is about 0.3 %. The method can however be extended to produce answers to the desired accuracy. The method is not for hand calculation and the computing time needed is similar to that of finite difference methods.

The Razelos method [79RA1] for extending the results for a balanced regenerator to an unbalanced one requires the effectiveness of a balanced regenerator. Equation (3.6) was found to be inaccurate at high Ntu_o numbers. It is not always desirable to use a table and no relatively simple correlation could be found. Numerical results for a balanced symmetric ($C^* = (hA)^* = 1$) for the complete range of $C_r^* > 1$ and $0.5 < Ntu_o < 500$ were correlated as follows:

$$\varepsilon = \frac{Ntu_o}{1 + Ntu_o}\left(1 - \frac{1}{AC_r^{*n}}\right) \tag{3.9}$$

where

$$A = 15.78/Ntu_o + 3.2678\ln(Ntu_o) + 0.0019373[\ln(Ntu_o)]^5$$
$$n = 1.881 + 0.0331197[\ln(Ntu_o)]^2$$

Equation (3.9) agrees with accurate numerical results within 0.25 % for the range $C_r^* > 1$ and $0.5 < Ntu_o < 500$ and within 0.7 % for $C_r^* > 1$ and $0.5 < Ntu_o < 500$. The largest error is 0.69 % and occurs at $C_r^* = 1.5$ and $Ntu_o = 80$. Equation (3.9) can be used in place of equation (3.6) in the Razelos method [79RA1].

The influence of $(hA)^*$ was not taken into account by any of the approximate solutions so far. Usually it is quoted that the influence of $(hA)^*$ is small in the range $0.25 < (hA)^* < 4$ and the results are then given for $(hA)^* = 1$. Numerical results were calculated for $(hA)^* = 0.25$ and 4 and it was found that the deviation in the effectiveness $(\varepsilon_{(hA)^*=1} - \varepsilon_{(hA)^*=0.25\,;\,4})$ is less than 1 % within the following ranges:

1. $1.5 < Ntu_o < 500$, $C_r^* > 2.5$, $0.5 < C^* < 1$
2. $1.5 < Ntu_o < 500$, $C_r^* > 1.5$, $0.7 < C^* < 1$
3. $1.5 < Ntu_o < 500$, $C_r^* > 1$, $0.85 < C^* < 1$

Scaricabarozzi [89SC1] found some particular solutions for the differential equations discussed in Chapter 2. The additional assumptions are made that the heat capacities of the fluids are negligible compared to that of the matrix and that the axial heat conduction in the matrix is zero. A linearity solution is proposed that approximately satisfies the boundary conditions. He examined five cases where the solution is approximated with piece-wise linear or constant functions. The designer does not know beforehand which of the five cases applies best to his situation. It is a rather complicated procedure to find the most appropriate case. He claims an accuracy of less than 1 %. The results are only valid for symmetrical regenerators.

3.2.2 Effect of longitudinal heat conduction

The effect of longitudinal heat conduction in the regenerator is to reduce the effectiveness for a specified Ntu_o. Two additional dimensionless parameters, λ and A_k^* now play a role. Bahnke and Howard [64BA1] investigated the effect of longitudinal conduction in detail. They employed a finite difference method and determined the effectiveness for a rotary regenerator within the following ranges: $1 \le Ntu_o \le 100$, $0.9 \le C^* \le 1$, $1 \le C_r^* \le \infty$, $0.25 \le (hA)^* \le 1$, $0.25 \le A_k^* \le 1$, $0 \le \lambda \le 0.32$

They found that the influence and trends of the four dimensionless parameters of the previous section on the effectiveness are basically the same as the case of zero longitudinal conduction. The addition of conduction simply superimposes its effect on the heat exchanger. The effectiveness will decrease asymptotically with an increase in λ for the values of the other parameters fixed. They defined a conduction effect parameter that is the percentage reduction in effectiveness compared to the no conduction case. The conduction effect increases with an increase in Ntu_o for λ and all the other parameters fixed. They also found that the conduction area ratio A_k^* has only a small influence in the range of 0.25 to 1.

Hahnemann [48HA1] presented a closed form expression for the effectiveness which includes the conduction effect, but for the special case of infinite rotation speed. The expression is thus valid under the same circumstances as equation (3.2), but it includes the effect of λ. The full solution of Hahnemann is given in Appendix B. For the special case of $C^* = (hA)^* = 1.0$ it reduces to:

$$\varepsilon_{\infty,\lambda\neq 0} = 1 - \left[1 + Ntu_o - \kappa Ntu_o^3 / a^2\right]^{-1} \tag{3.10}$$

where

$$\kappa = 4 - \frac{8}{a}\left[1 - (1 - e^{-a})/\sinh(a)\right]$$

$$a = 2\sqrt{Ntu_o^2 + Mo_o}$$

$$Mo_o = \frac{Ntu_o}{\lambda}$$

Shah [75SH1] used the correlation of Lambertson for $\lambda = 0$ (equation (3.6)) and combined it in a way with the results of Hahnemann [48HA1] to arrive at the following correlation that includes the effect of longitudinal heat conduction.

$$\varepsilon = \varepsilon_\infty \left(1 - \frac{1}{9C_r^{*\,1.93}}\right)\left(1 - \frac{1}{2 - C^*}\left\{\frac{1}{1 + Ntu_o - (\kappa / a^2) Ntu_o^3} - \frac{1}{1 + Ntu_o}\right\}\right) \tag{3.11}$$

According to Shah [75SH1], equation (3.11) agrees within 0.5 % with the results of Bahnke and Howard [64BA1] for the following limited range of parameters: $3 \leq Ntu_o \leq 12$, $0.9 \leq C^* \leq 1$, $2 \leq C_r^* \leq \infty$, $0.5 \leq (hA)^* \leq 1$, $0 \leq \lambda \leq 0.04$. It agrees within 1 % if the range is extended as follows: $1 \leq Ntu_o \leq 20$, $0.25 \leq (hA)^* \leq 1$, $0 \leq \lambda \leq 0.08$. For gas turbine applications the above mentioned ranges are sufficient.

The following method was however more recently recommended by Shah [88SH1] to account for the longitudinal heat conduction effect.

$$\varepsilon_{\lambda \neq 0} = C_\lambda \varepsilon_{\lambda = 0}$$

$$\text{where } C_\lambda = \left(\frac{\varepsilon_{\infty,\lambda \neq 0}}{\varepsilon_{\infty,\lambda = 0}}\right) \tag{3.12}$$

The efficiency ratio in brackets is for a balanced recuperator. It is therefore postulated that the same ratio can be applied to unbalanced regenerators. The procedure that Shah [88SH1] recommends is as follows:

1. Use the Razelos method to compute $\varepsilon_{e,\lambda=0}$ for an equivalent balanced regenerator.
2. Compute C_λ from equation (3.12) using λ and $Ntu_{o,e}$.
3. Calculate $\varepsilon_{e,\lambda \neq 0} = C_\lambda \varepsilon_{e,\lambda=0}$.
4. Determine ε from equation (3.7) with ε_e replaced by $\varepsilon_{e,\lambda \neq 0}$.

This procedure yields ε which is accurate within 1 % for $1 \leq Ntu_o \leq 20$ and $C_r^* \geq 1$ when compared to the accurate numerical results.

Romie [91RO1] suggested the following method to take into account the influence of longitudinal heat conduction. Ntu_o is replaced by $G_L Ntu_o$ in the relationship for zero longitudinal conduction.

$$\varepsilon = f\left(G_L Ntu_o, C_r^*, C^*, (hA)^*\right) \tag{3.13}$$

The factor G_L is derived from recuperator analysis. The solution of Hahnemann [48HA1] for a recuperator including the effect of longitudinal conduction is quite long and will be denoted by:

$$\varepsilon_{\infty,\lambda\neq 0} = f\left(Ntu, C^*, (hA)^*, \lambda\right) \tag{3.14}$$

The factor G_L is found by using the expression for a counterflow recuperator.

$$\varepsilon_{\infty,\lambda\neq 0} = \frac{1 - e^{-G_L Ntu(1-C^*)}}{1 - C^* e^{-G_L Ntu(1-C^*)}} \tag{3.15}$$

from which

$$G_L = \frac{1}{Ntu(1-C^*)} Ln\left(\frac{1 - C^* \varepsilon_{\infty,\lambda\neq 0}}{1 - C^*}\right) \tag{3.16}$$

For $C^* = (hA)^* = 1$ it reduces to $G_L = \varepsilon_{\infty,\lambda\neq 0}/(Ntu(1-\varepsilon_{\infty,\lambda\neq 0}))$ where $\varepsilon_{\infty,\lambda\neq 0}$ is calculated from equation (3.10). The above method was compared to accurate numerical results in the following range of parameters: $1 \le Ntu_o \le 500$, $0.7 \le C^* \le 1$, $1 \le C_r^* \le \infty$, $0.25 \le ((hA)^*=A_k^*) \le 4$, $0 \le \lambda \le 0.16$. The error was less than 1 % in the following ranges:

1. $1 \le Ntu_o \le 500$, $0.8 \le C^* \le 1$, $1.5 \le C_r^* \le \infty$, $0.25 \le (hA)^* \le 1$, $0 \le \lambda \le 0.16$
2. $1 \le Ntu_o \le 500$, $0.9 \le C^* \le 1$, $1 \le C_r^* \le \infty$, $0.25 \le (hA)^* \le 1$, $0 \le \lambda \le 0.16$

The maximum error for $0.9 \le C^* \le 1$, $0.25 \le (hA)^* \le 1$ and the full range of all the other parameters was 1.6 %. For $C^* = 1$, G_L can be calculated using equation (3.10). However for $C^* < 1$, G_L must be calculated using the full equation as given by the functional relationship in equation (3.14). The Hahnemann [48HA1] solution is complex enough to discourage hand calculation and a computer program is needed to handle all the coefficients.

This method is more accurate than the method given by Shah [81SH1] especially at high Ntu_o numbers and $C^* < 1$. For hand calculations the method of Romie is suggested for $C^* = 1$ and the method of Shah for $C^* < 1$.

3.2.3 Effect of transverse heat conduction

One of the idealisations for the theory so far is that the matrix wall thermal resistance is zero. The temperature gradient in the wall thickness direction is zero. The zero wall thermal resistance is a good approximation for thin and metal matrixes, but for thick ceramic matrixes the wall resistance may not be negligible.

An equivalent thermal resistance is added to the convective resistances in the expression for Ntu_o to account for the effect of wall resistance. Hausen [83HA1] showed that this resistance can be expressed as

$$R = \left(\frac{\delta}{6k_w}\right)\left(\frac{1}{A_h} + \frac{1}{A_c}\right)\phi \tag{3.17}$$

The function ϕ reproduces the influence of the rapid temperature changes that are experienced by the surface immediately after flow reversal. As shown by Shah [81SH1], $\phi = 1$ corresponds to the case where the wall temperature is linear with time during the entire flow period at every x position. Hausen [83HA1] gives the following expression for ϕ.

$$\phi = 1 - (1/15)Z \qquad \text{for } Z \le 5 \tag{3.18a}$$

$$\phi = 2.142(0.3+2Z)^{-0.5} \qquad \text{for } Z \ge 5 \tag{3.18b}$$

where

$$Z = \frac{\delta C_r}{2k_w}\left(1/A_h + 1/A_c\right)$$

C_r is the capacity rate of the matrix. The expression for Ntu_o now becomes:

$$Ntu_o = \frac{1}{C_{min}}\left[1/(hA)_h + 1/(hA)_c + \frac{\delta\phi}{6k_w}\left(1/A_h + 1/A_c\right)\right]^{-1} \tag{3.19}$$

Hausen [83HA1] also supplies precise equations for the function ϕ. They are however in terms of infinite series and are too complicated for practical design purposes. Romie [91RO1] gives a factor G_T by which Ntu_o must be multiplied similar to the factor G_L for longitudinal conduction. He also makes use of Hausens ϕ function and it can be shown that this method is equivalent to the one above. Heggs et al. [80HE1] used a finite difference method to calculate the effectiveness of symmetric regenerator ($C^* = (hA)^* = 1$) with transverse heat conduction. Romie compared the ϕ method with the numerical results of Heggs [80HE1]. For $Ntu_o = 25$ and $C_r^* = 50$ the maximum error is -0.3 %. For $Ntu_o = 20$ and $C_r^* = 2$ the maximum error is -0.2 %, but for Ntu_o = 2.5 and $C_r^* = 1$ the maximum error was 3.3 %. The latter error is for a Biot number of 5. The error decreases with Bi and is close to zero at Bi = 1. In practice the Biot number will barely exceed unity for all kinds of practical matrixes. For thin metal matrixes Bi << 1 that further reduces the effect of transverse conduction. Heggs and Carpenter [79HE1] concluded that the ϕ method can be used to predict the effectiveness of a regenerator accurately. They however found that the method can be inaccurate if one is interested in the temperature - time response of the system.

3.3 INFLUENCE OF PRESSURE- AND CARRYOVER LEAKAGE

The leakages in regenerators can be classified [81SH1] into two categories: (1) pressure leakages as a result of the pressure difference between the two fluid streams and (2) carryover leakage, due to transport of one gas trapped in the matrix void volume into the other gas stream owing to matrix rotation or the flow reversal in a fixed matrix regenerator. The pressure leakage is often referred to as fluid bypass.

The pressure leakage is inherent in the operation of rotary regenerators and is a price to be paid for the advantage of compactness. Minor pressure leakages occur in fixed matrix regenerators at the control valves. Shah [81SH1] presents a simplified theory that accounts for the pressure and carryover leakages separately. However the two effects occur simultaneously and therefore should be considered together. Shah [88SH1] therefore presents the following model to account for the leakages simultaneously.

The pressure leakage mass flow rate is defined as ΔW_p. The mass of the cold fluid in the matrix void volume that is carried over to the hot fluid in one rotation is defined as ΔW_c. The hot fluid carryover, ΔW_h is similarly defined. The pressure and carryover leakages are expressed in dimensionless form as:

$$x_p = \frac{\Delta W_p}{W_c} \quad , \quad x_c = \frac{\Delta W_c}{W_c} \quad , \quad x_h = \frac{\Delta W_h}{W_h} \tag{3.20}$$

Figure 3.1 shows a simple model of a regenerator having fluid bypass and carrryover.

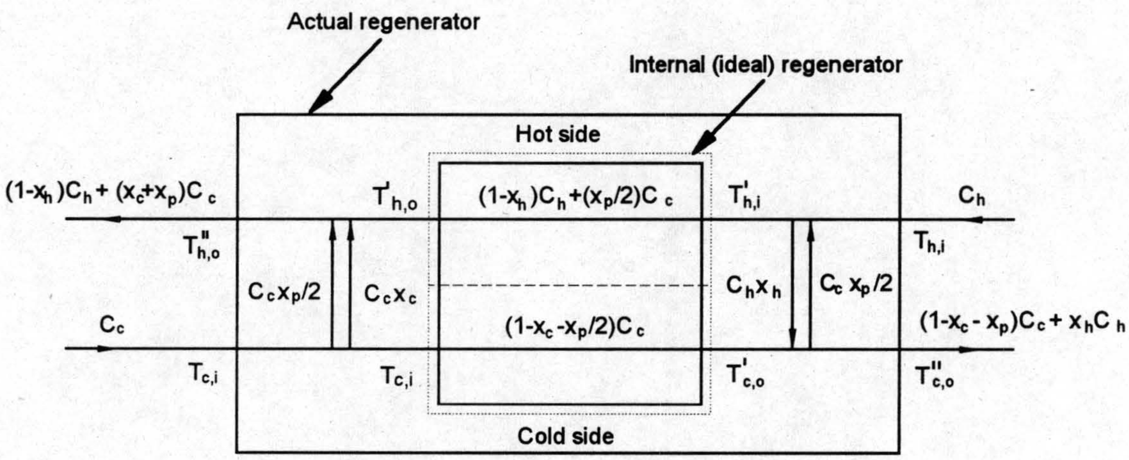

Figure 3.1: A regenerator model showing fluid bypass and carryover.

For the model in figure 3.1 the following additional assumptions were made:

1. The intermixing of the fluids occurs outside the matrix.

2. The high pressure side is considered as the cold side, therefore the pressure leakage is from the cold to the hot side. It is further assumed that half of the pressure leakage occurs at the one end and the other half at the opposite end of the matrix.

3. The leakage fluid temperatures are essentially the same as the main incoming fluid stream temperatures.

4. The fluids have constant and equal specific heats.

5. The cold side remains the minimum side after the carryover leakage.

The model assumes that there is the actual regenerator indicated by the solid outer line in figure 3.1 and an internal regenerator indicated by the dotted line. The fluid streams enter the internal regenerator with capacity rates C_h and C_c and temperatures $T_{c,i}$ and $T_{h,i}$. The pressure and carryover leakages then occur before the fluid streams enter or after they leave the internal regenerator. Due to the leakage, the hot and cold side mass flow rates and subsequently the capacity rate of the fluids in the internal regenerator is different from the inlet conditions for the actual regenerator. The hot side inlet temperature to the internal regenerator is now $T_{h,i}^{'}$. The internal regenerator is then treated as an ideal regenerator with no leakage and the outlet temperatures $T_{h,o}^{'}$ and $T_{c,o}^{'}$ are determined. The outlet mass flow rates and temperatures for the actual regenerator can then be determined. The outlet temperatures for the actual regenerator are $T_{h,o}^{''}$ and $T_{c,o}^{''}$.

On the basis of the regenerator model in figure 3.1 four different effectivenesses are defined to investigate the influence of pressure leakage and carryover.

1. The effectiveness of the ideal regenerator with zero fluid bypass or carryover is designated as ε_i and is defined by:

$$\varepsilon_i = \frac{C_c\left(T_{c,o} - T_{c,i}\right)}{C_{min}\left(T_{h,i} - T_{c,i}\right)} \tag{3.21}$$

2. The effectiveness of the internal regenerator (denoted by the dotted line in figure 3.1).

$$\varepsilon_{int} = \frac{\left(1 - x_c - x_p/2\right)C_c\left(T_{c,o}^{'} - T_{c,i}\right)}{\left(1 - x_c - x_p/2\right)C_c\left(T_{h,o}^{'} - T_{c,i}\right)} = \frac{\left(T_{c,o}^{'} - T_{c,i}\right)}{\left(T_{h,o}^{'} - T_{c,i}\right)} \tag{3.22}$$

This effectiveness is calculated in exactly the same way as the ideal regenerator, but the parameters Ntu_o, C^*, C_r^*, $(hA)^*$ will change slightly due to the different fluid flow rates through the internal regenerator. All the variables affected by the change in flow rate must be recalculated.

3. The actual regenerator is denoted by the outer solid lines and its effectiveness is defined as the ratio of the actual heat transfer to the maximum possible heat transfer with the same flow rates and inlet temperatures.

$$\varepsilon_{act} = \frac{\left[\left(1 - x_c - x_p\right)C_c + x_h C_h\right]T''_{c,o} - C_c T_{c,i}}{\left[\left(1 - x_c - x_p\right)C_c + x_h C_h\right]T_{h,i} - C_c T_{c,i}} \tag{3.23}$$

4. Since ε_{act} is based on the modified flow rates an effective regenerator effectiveness based on the original inlet capacities and temperatures is defined.

$$\begin{aligned} q_{actual} &= \varepsilon_{act}\left[\left[\left(1 - x_c - x_p\right)C_c + x_h C_h\right]T_{h,i} - C_c T_{c,i}\right] \\ &= \varepsilon_{eff} C_c \left(T_{h,i} - T_{c,i}\right) \end{aligned} \tag{3.24}$$

The temperatures $T'_{h,i}$, $T''_{c,o}$ and $T''_{h,o}$ can be calculated by doing an energy balance on the hot inlet, cold outlet and hot outlet streams.

3.4 PRESSURE DROP EVALUATION

So far methods to calculate the heat transfer rate in a rotary regenerator were presented. An equally important aspect in the design and optimisation of heat exchangers is the energy required to overcome the pressure drop across the matrix. Kays and London [84KA1] give the following model for plate fin heat exchangers. Rotary heat exchangers usually have cylindrical flow passages and therefore the components of the pressure drop are the same as for plate fin heat exchangers. The total pressure drop consists of the entrance effect, the core friction, flow acceleration and the exit effect. Consider the model shown in figure 3.2 for the pressure drop analysis:

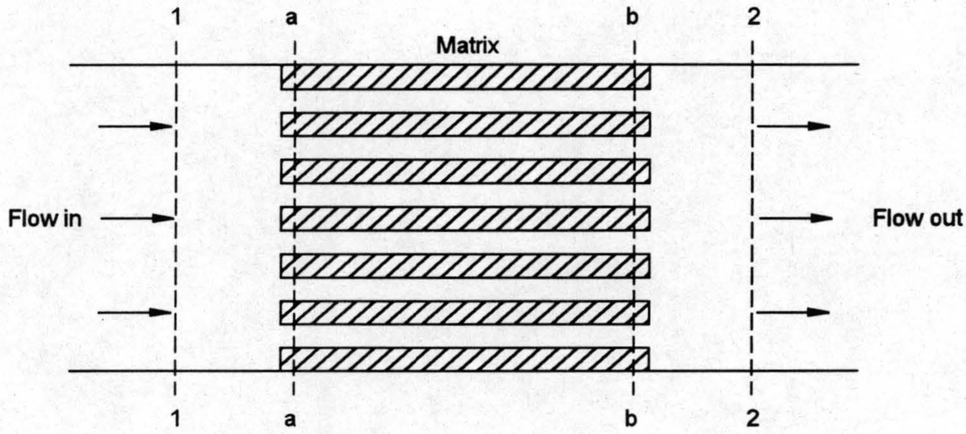

Figure 3.2: Heat exchanger core model for pressure drop analysis.

It will be assumed that the pressure changes from sections 1 to a and b to 2 is small compared to the total pressure, i.e. $\rho_1 = \rho_a$ and $\rho_b = \rho_2$. An energy balance between sections 1 and a yield:

$$\frac{v_1^2}{2} + \frac{P_1}{\rho_1} = \frac{v_a^2}{2} + \frac{P_a}{\rho_1} + K_c \frac{v_a^2}{2} \tag{3.25}$$

K_c is the contraction loss coefficient and is defined by the above equation. If we define the porosity σ as the ratio of the minimum free flow area to that of the frontal area of the matrix, equation (3.25) can be rearranged as follows:

$$P_1 - P_a = \frac{G^2}{2}\left[\left(1 + K_c - \sigma^2\right)/\rho_1\right] \tag{3.26}$$

Here G is the mass flux based on the minimum free flow area of the matrix. In a similar fashion the energy balance between sections b and 2 yields the following relation.

$$P_b - P_2 = -\frac{G^2}{2}\left[\left(1 - K_e - \sigma^2\right)/\rho_2\right] \tag{3.27}$$

The exit energy loss coefficient is K_e and is defined by equation (3.27). A momentum balance between sections a and b yield:

$$P_a - P_b = \frac{G^2}{2}\left[4f\frac{L}{D_h}\left(\frac{1}{\rho_m}\right) + 2\left(\frac{1}{\rho_2} - \frac{1}{\rho_1}\right)\right] \tag{3.28}$$

The flow length is L, D_h is the hydraulic diameter, f is the Fanning friction factor and ρ_m is the harmonic mean density and is defined by $(1/\rho_m) = 0.5(1/\rho_1+1/\rho_2)$. If we add up all the pressure losses between the inlet and outlet of the regenerator matrix we find the total pressure drop Δp.

$$\Delta p = \frac{G^2}{2}\left[4f\frac{L}{D_h}\left(\frac{1}{\rho_m}\right)+2\left(\frac{1}{\rho_o}-\frac{1}{\rho_i}\right)+(1+K_c-\sigma^2)\frac{1}{\rho_i}-(1-K_e-\sigma^2)\frac{1}{\rho_o}\right] \tag{3.29}$$

Note that in the above derivation the kinetic energy and momentum velocity distribution correction factors were taken as 1. This is approximately true for turbulent flows. Often in heat exchanger pressure drop analysis the exit and entrance losses are accounted for in the friction factor. Equation (3.29) then becomes:

$$\Delta p = \frac{G^2}{2}\left[4f_e\frac{L}{D_h}\left(\frac{1}{\rho_m}\right)+(1+\sigma^2)\left(\frac{1}{\rho_o}-\frac{1}{\rho_i}\right)\right] \tag{3.30}$$

where f_e is an effective friction factor

3.5 APPROXIMATE SOLUTION METHOD

In this section an approximate solution method for the ideal regenerator will be defined. The aim is to find a procedure that is relatively simple and sufficiently accurate. The computing time must be much less than the time required for a numerical solution. This is especially important when one is interested in optimisation.

1. With the design parameters and operating conditions known, calculate the six dimensionless parameters $Ntu_o, C^*, C_r^*, (hA)^*, \lambda$ and A_k^*. Ntu_o already includes the effect of transverse heat conduction and must be calculated from equation (3.19).
2. Calculate the longitudinal heat conduction correction factor G_L from equation (3.16). The recuperator efficiency $\varepsilon_{\infty,\lambda\neq 0}$ is calculated from the full Hahnemann relationship [48HA1] implied by equation (3.14) and shown in Appendix B. Correct Ntu_o by replacing it with $G_L Ntu_o$.

3. Calculate $Ntu_{o,e}$ and $C^*_{r,e}$ for an equivalent balanced regenerator using equations (3.4) and (3.5).

4. Calculate the effectiveness of the equivalent balanced regenerator using equation (3.9). In this case equation (3.8) would have been slightly more accurate, but the computing time for evaluating the infinite Bessel series is similar to that of finite difference methods.

5. The effectiveness of the original unbalanced regenerator can now be calculated from equation (3.7).

We have now established an approximate method that can be compared to accurate numerical results. The comparison was done over the following range of parameters: $1 \leq Ntu_o \leq 500$, $0.7 \leq C^* \leq 1$, $1 \leq C^*_r \leq \infty$, $0.25 \leq ((hA)^* = A^*_k) \leq 4$, $0 \leq \lambda \leq 0.16$. The ranges are sufficient to cover most applications. The error was less than 1 % within the following ranges:

1. $1 \leq Ntu_o \leq 500$, $0.7 \leq C^* \leq 1$, $2 \leq C^*_r \leq \infty$, $0.25 \leq (hA)^* \leq 4$, $0 \leq \lambda \leq 0.16$
2. $1 \leq Ntu_o \leq 500$, $0.8 \leq C^* \leq 1$, $1.5 \leq C^*_r \leq \infty$, $0.25 \leq (hA)^* \leq 4$, $0 \leq \lambda \leq 0.16$
3. $1 \leq Ntu_o \leq 500$, $0.7 \leq C^* \leq 1$, $1.5 \leq C^*_r \leq \infty$, $0.25 \leq (hA)^* \leq 1$, $0 \leq \lambda \leq 0.04$
4. $1 \leq Ntu_o \leq 15$, $0.9 \leq C^* \leq 1$, $1 \leq C^*_r \leq \infty$, $0.25 \leq (hA)^* \leq 4$, $0 \leq \lambda \leq 0.16$

The maximum error for $C^*_r \geq 1.5$ and the full range of all the other parameters was 1.7 %. It is worth mentioning that in the comparison run the approximate method took approximately 500 times less computing time than the numerical method. This of course, depends on the accuracy desired in the numerical method. In this case the numerical results were good to four significant figures.

CHAPTER 4

SOFTWARE DESCRIPTION AND SAMPLE CALCULATION

4.1 INTRODUCTION

In this chapter the basic layout of a PC program written to evaluate and design a rotary regenerator is described. A sample calculation for a part of the program is presented. In Chapter 3 the basic theory for the regenerator solution is given. The sample calculation serves as method to show how this theory must be integrated to thermally design a rotary regenerator. Finer detail of the theory is introduced in the process. A simplified cost effectiveness parameter is defined. The cost effectiveness parameter will serve as a method to compare alternatives. Alternatives may include alterations to the regenerator operating conditions, rotating disk dimensions and type of matrix used.

4.2 PROGRAM DESCRIPTION

A PC software package was written in Borland Pascal Version 7.0 for the thermal evaluation and design of a counterflow rotary regenerator. The program consists mainly of two parts namely: 1) Evaluation or Rating and 2) Design or Sizing. In the evaluation problem the designer specifies the operating conditions (mass flow rates, inlet temperatures, inlet pressures, disk rotational speed), rotating disk dimensions (outer diameter, hub diameter, disk height, ratio of area split between hot and cold fluid) and the matrix properties (plate spacing, wall thickness, material thermophysical properties, heat transfer and pressure drop correlations for the matrix). The object is then to find the outlet gas temperatures, the total heat transfer rate and the pressure drop across the regenerator.

In the design problem all the operating conditions are specified as in the case of the rating problem, except for the disk rotational speed. Of the disk dimensions only the outer diameter is specified and all the matrix properties are specified except for the matrix wall thickness. The overall effectiveness or equivalently the total heat transfer rate desired is specified. The disk rotational speed, the hot to cold fluid flow split ratio and the matrix wall thickness are then varied. At each combination of the varied parameters the disk height is calculated that will deliver the required heat transfer rate. The calculation of a cost effectiveness parameter enables the designer to choose the most economic viable option. The cost effectiveness parameter will be described in more detail later in the chapter.

The program is 'user friendly' with an easy to use menu system. It allows for on-screen data entry and editing. The data entry is checked to fall in ranges practical in regenerator design. In this way program errors are minimised. The entered data can be stored by the program as the new default values that will be retrieved automatically the next time the program is used. For air, the thermophysical properties are built into the program. For gases other than air a file with thermophysical property data must be supplied. The program automatically calculates polynome equations to represent the data for further use during the solution process.

In figure 4.1 a flow diagram of the Evaluation part of the program can be seen. In order to explain the flow diagram a few concepts must be clear. A Pascal program mainly consists of *procedures* and *functions*. A procedure is a group of statements performing a specific task. A function is similar to a procedure, but can only have one output. When a program gets large it is advisable to make use of *units*. A unit is a sub-program or a library of procedures and functions that can be used by the main program.

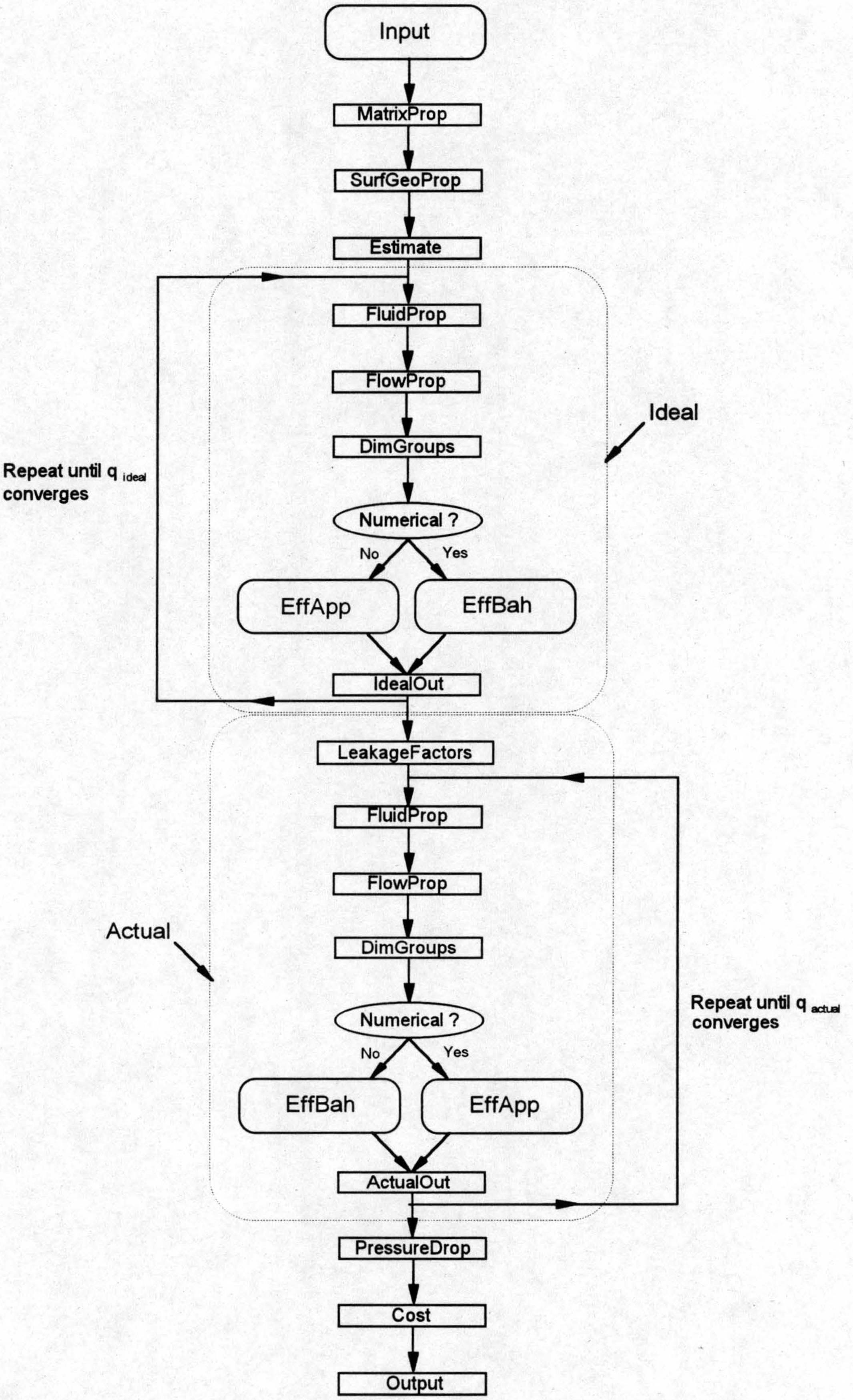

Figure 4.1: A flow diagram for the Evaluation part of the program.

A brief description of the main program elements to solve the Evaluation problem will now follow.

Unit Input:
This unit handles the user-program interface. It allows for all the data entry, editing and storing. A user manual is given with the program to assist the user in using the program and entering the input data.

Procedure MatrixProp:
This procedure calculates the porosity, the surface area density and the mass of the matrix. In the case where the matrix is not of the parallel plate fin type the user will have to supply this information as part of the input.

Procedure SurfGeoProp:
In this procedure the relevant surface areas and geometrical properties of the matrix are calculated. The frontal area, free flow area, air side heat transfer area, solid matrix area for longitudinal heat conduction and the matrix volume are calculated. The above mentioned areas are calculated for the hot and the cold gas sides.

Procedure Estimate:
This procedure estimates the fluids mean gas temperatures to start the iteration process for the solution of the ideal regenerator.

Procedure FluidProp:
This procedure calculates the thermophysical properties of the gases at the appropriate mean temperatures.

Procedure FlowProp:
This procedure calculates the heat transfer characteristics of the matrix from the supplied heat transfer correlations. It also corrects the heat transfer coefficients for variation in gas thermophysical properties.

Procedure Dimgroups:
This procedure calculates the six dimensionless groups needed to calculate the effectiveness of a regenerator in the absence of leakage. These groups depend on the operating conditions and matrix configuration.

Unit Effec:

This unit takes as input the above mentioned dimensionless parameters and then calculates the effectiveness of the regenerator in the absence of gas pressure leakage and carryover leakage. The unit can calculate the effectiveness by one of two methods, depending on user specification.

1. An approximate theory, making use of the solutions and solution method discussed in Chapter 3. This method is indicated by EffApp in the flow diagram.
2. A finite difference method where the rotor is divided into a finite number of elements. Energy balances are then written for each element and the system is solved iteratively. The numerical scheme and solution method are discussed in Appendix C. The method is by Bahnke and Howard [64BA1] and is indicated by EffBah in the flow diagram.

Procedure IdealOut:

In this procedure the outlet temperatures and the heat transfer rate for the ideal regenerator are calculated making use of the definition of the regenerator effectiveness and energy balances between the two gas streams.

Procedure LeakageFactors:

In a real regenerator gas trapped in one side of the matrix will be transported to the other side and vice versa due to matrix rotation. In this procedure the amount of carryover leakage is calculated based on the final converged conditions of the ideal regenerator.

The effect of the leakage is to change the mass flow rates of the respective gas streams. See figure 3.1 for a regenerator model showing the fluid bypass (pressure leakage) and carryover effects.

Procedure ActualOut:

This procedure calculates the outlet temperatures and heat transfer rate of the internal regenerator. It then uses this information together with information of the fluid bypass and carryover leakages to calculate the actual heat transfer rate and the temperatures of the gas streams leaving the actual regenerator.

Procedure Pressuredrop:

In this procedure the loss coefficient for the matrix under consideration is calculated from the supplied pressure drop correlation and corrected for variations in thermophysical properties. With the loss coefficient known the pressure drop across the matrix is evaluated for both the hot gas and cold gas sides.

Procedure Cost:

The cost effectiveness parameter as described later in this chapter is calculated in this procedure.

Procedure Output:

This procedure displays the main results on the screen and stores it in a data file.

In figure 4.2 a flow diagram for the Design section of the program can be seen. The Design problem is basically the Evaluation problem executed in reverse order. The method however is very different.

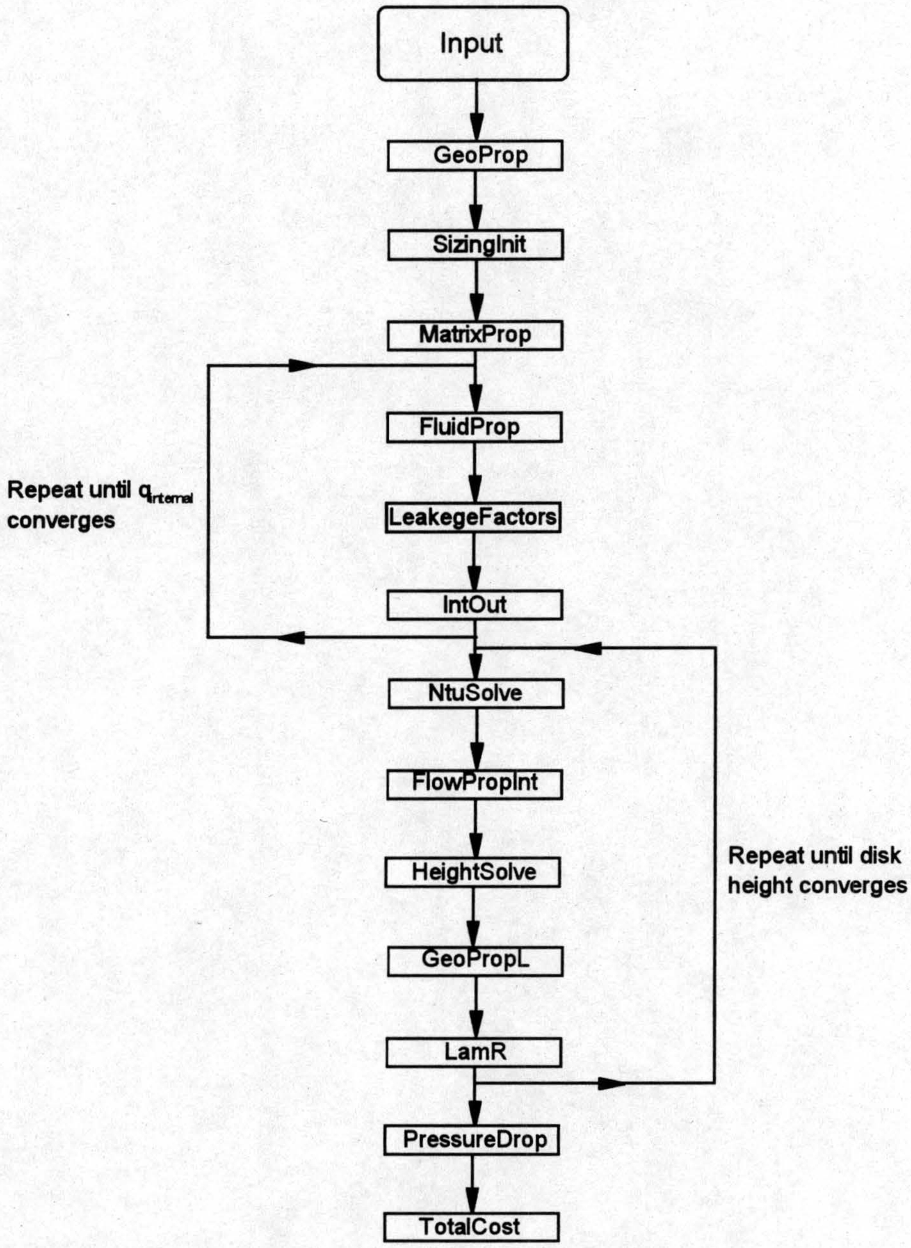

Figure 4.2: A flow diagram for the Design part of the program.

The Input unit is the same as described for the Evaluation problem. See the user manual for a detailed description on how to enter the desired program input.

Procedure GeoProp:

In the design problem the disk height is unknown. This procedure calculates all the relevant areas, except for that dependant on the disk height.

Procedure SizingInit:

This procedure assigns initial values to the mean temperatures, leakage factors and other variables to start the solution process.

Procedure IntOut:

In the Design problem the effectiveness and thus the heat transfer rate for the actual regenerator is specified. In this procedure the outlet conditions for the actual regenerator is used to calculate the heat transfer rate in the internal regenerator and subsequently the internal regenerator effectiveness.

Procedure NtuSolve:

In the Evaluation problem we calculated the effectiveness as a function of the six dimensionless parameters. In the design problem we know the effectiveness and three of the parameters, namely C^*, A_k^* and C_r^*. With the assumption that $hA^* = 1$ (the influence is negligible) and for the first iteration that $\lambda = 0$, Ntu_o can be solved. This is done in this procedure by varying Ntu_o until the desired effectiveness is obtained.

Procedure FlowPropInt:

This procedure calculates the heat transfer coefficient and flow properties for the internal regenerator.

Procedure HeightSolve:

This procedure solves for the height of the regenerator disk.

Procedure GeoPropL:

This procedure calculates the remainder of the geometrical properties and areas that requires the disk height to be known.

Procedure LamR:

In solving Ntu_o in the first iteration it was assumed that $\lambda = 0$ and that the matrix wall thermal resistance, $R = 0$. With all the geometrical properties now known, better values for the above mentioned parameters are calculated in this procedure for the next iteration.

The procedures PressureDrop and Cost are the same as described for the Evaluation problem.

Several other units are used by the program that is not directly part of the flow diagram, but that provides support in the solution process. The unit Math provides mathematical procedures needed by the program. The units Mtx and CurveFit provide the necessary procedures to perform the curve fits on thermophysical property data. Various other units that are not written by the author are used in the program. They will not be discussed here.

4.3 INPUT DATA FOR EVALUATION SAMPLE CALCULATION

The input data for this sample calculation is taken from [91LE1]. It is of a rotary regenerator in service as an air preheater in an electricity generation facility. The matrix pressure drop and heat transfer correlations are not taken from the above mentioned source, but are correlations of a surface tested by the author. The hot to cold flow split ratio was also changed from 1.0 to 1.1 to illustrate the effect of an unbalanced ratio.

4.3.1 Operating conditions

Cold gas inlet mass flow rate, W_c = 109 kg/s
Hot gas inlet mass flow rate, W_h = 109 kg/s
Disk rotational speed, N = 0.25 rpm
Cold gas inlet temperature, $T_{c,i}$ = 337 K
Cold gas inlet pressure, $P_{c,i}$ = 106.21 kPa
Hot gas inlet temperature, $T_{h,i}$ = 580.5 K
Hot gas inlet pressure, $P_{h,i}$ = 102.28 kPa
Pressure leakage fraction, x_p = 0.08 of cold gas flow rate

4.3.2 Disk dimensions

Disk outer diameter, D = 7.863 m
Hub diameter, d_{hub} = 2.237 m
Disk height, L = 2.58 m
Hot to cold gas flow split ratio, ϕ = 1.1 : 1
Seal face coverage fraction, x_s = 0.1 of total frontal area

4.3.3 Matrix properties

The matrix correlations are of the 11A surface of Type 1 at a spacing of 5 mm. See Appendix A for a description of the surface and the experimental set-up and procedure to arrive at the pressure drop and heat transfer correlations.

Plate spacing, $s = 5$ mm
Matrix wall thickness, $\delta = 0.5$ mm
Matrix wall thermal conductivity, $k_w = 51.9$ W/mK
Matrix wall density, $\rho_w = 7817$ kg/m³
Matrix wall specific heat, $c_w = 434$ J/kgK
Pressure drop correlation, $K_T = 84.943\,Ry_T^{-0.2903}$ $(1.5\times10^5 < Ry_T < 9\times10^5)$
Heat transfer correlation, $Ny_T = 9.033\,Ry_T^{0.8068}$ $(1.5\times10^5 < Ry_T < 9\times10^5)$
Reference length for correlations, $L_{ref} = 0.2$ m
Reference porosity, $\sigma_{ref} = 1.0$
Ratio of actual surface area to projected area, $\alpha = 1.2$

4.3.4 Cost calculation parameters

Fan static efficiency, $\eta_{fs} = 0.7$
Fan drive system efficiency, $\eta_{fd} = 0.9$
Annual operating time, H = 8750 hours
Expected regenerator life, n = 20 years
Annual interest rate, i = 0.1 (10%)
Unit cost of electrical power, $C_{eu} = 0.05$ \$/kWh
Matrix material cost, $C_{mu} = 1$ \$/kg

4.4 SOLUTION FOR IDEAL REGENERATOR

Note that during the sample calculation the full numbers accurate to 10 or more decimal places are used. In the text 2 to 6 decimal places are given. There may therefore be a discrepancy in decimal places between the figures on the left- and right hand side of a equality sign in the text. The answers are always calculated with the more accurate values.

4.4.1 Matrix properties

The porosity, σ is the ratio of the free flow area to the total frontal area.

$$\sigma = \frac{A_o}{A_{fr}} = 1 - \frac{\delta}{\delta + s} = 1 - \frac{0.5}{0.5 + 5} = 0.9091$$

The surface area density of the matrix, β and the effective mass of the matrix, M_w can be calculated as follows:

$$\beta = \frac{2\alpha}{s + \delta} = \frac{2(1.2)}{0.005 + 0.0005} = 436.3636 \text{ m}^3/\text{m}^2$$

$$M_w = \frac{\pi}{4}\left(D^2 - d_{hub}^2\right)(1 - \sigma)(1 - x_s)\rho_w L$$

$$= \frac{\pi}{4}(7.863^2 - 2.237^2)(1 - 0.9091)(1 - 0.1)(7817)(2.58) = 7.364116 \times 10^4 \text{ kg}$$

4.4.2 Geometrical and surface properties

The effective frontal area $A_{fr,t} = \pi/4(D^2 - d_{hub}^2)(1 - x_s) = \pi/4(7.863^2 - 2.237^2)(1 - x_s)$ $= 44.6284(1-0.1) = 40.1655$ m²

The cold gas side frontal area $A_{fr,c} = A_{fr,t}(1/(1+\phi)) = 19.1264$ m²

The hot gas side frontal area $A_{fr,h} = A_{fr,t}(\phi/(1+\phi)) = 21.0391$ m²

The total free flow frontal area $A_{o,t} = A_{fr,t}\sigma = 44.6284(0.9091) = 36.5141$ m²

The cold gas side free flow frontal area $A_{o,c} = A_o(1/(1+\phi)) = 17.3877$ m²

The hot gas side free flow frontal area $A_{o,h} = A_o(\phi/(1+\phi)) = 19.1264$ m²

The matrix effective volume, $V = A_{fr,t}L = 40.1655(2.58) = 103.6271$ m³

The total heat transfer area, $A_t = \beta V = 436.3636(103.6271) = 4.521908 \times 10^4$ m²

The cold gas heat transfer area $A_c = A_t(1/(1+\phi)) = 2.153290 \times 10^4$ m²

The hot gas heat transfer area $A_h = A_t(\phi/(1+\phi)) = 2.368619 \times 10^4$ m²

The solid matrix area for longitudinal heat conduction, $A_{k,t} = A_{fr,t} - A_{o,t}$ $= 3.6514$ m²

4.4.3 Fluid properties

The fluid properties must be calculated at the mean temperatures of the hot- and cold gases respectively. An iterative process is thus required. The final converged values for the mean gas temperatures are as follows:

$T_{h,m} = 483.29$ K

$T_{c,m} = 434.91$ K

The following properties were evaluated from the equations in Appendix D.

Table 4.1: Thermophysical properties for the ideal regenerator at the mean gas temperatures.

T (K)	μ (kg/ms)	k (W/mK)	c_p (J/kgK)	Pr
434.91	2.451881×10^{-5}	3.663099×10^{-2}	1020.913	0.6833
483.29	2.644000×10^{-5}	3.967366×10^{-2}	1028.250	0.6853

4.4.4 Flow properties

The cold side mass flux, $G_c = W_c/A_{fr,c} = 109/19.1264 = 5.6989$ kg/m²

The hot side mass flux, $G_h = W_h/A_{fr,h} = 109/21.0391 = 5.1808$ kg/m²

The cold side flow parameter, $Ry_c = G_c/\mu_c = 5.6989/2.451881\times10^{-5}$

$= 2.324304\times10^{5}$ m^{-1}

The hot side flow parameter, $Ry_h = G_h/\mu_h = 5.1808/2.451881\times10^{5}$

$= 1.959468\times10^{5}$ m^{-1}

The heat transfer correlation from the experimental testing, $Ny_T = 9.033Ry_T^{0.8068}$ can be rewritten as follows to be applicable to a plate fin matrix. See Appendix A for a derivation of the conversion method.

$$Ny = 9.033(Ry/\sigma)^{0.8068}(L/L_{ref})\sigma$$

$$Ny_c = 9.033(2.324304\times10^{5}/0.9091)^{0.8068}(2.58/0.2)(0.9091) = 2.443150\times10^{6}\ \text{m}^{-1}$$

$$Ny_h = 2.128736\times10^{6}\ \text{m}^{-1}$$

$Ny_c = 4.935115\times10^{5}$ m^{-1}

$Ny_h = 4.673649\times10^{5}$ m^{-1}

The above values for Ny are valid for conditions of constant fluid properties. In this case there is a temperature difference between the matrix wall and the gas in the flow passages and therefore a temperature correction will have to be applied. The temperature correction has the following form.

$$Ny = Ny_{iso}\left(\frac{T_w}{T_m}\right)^n$$

where T_w is the mean wall temperature and T_m the mean gas temperature. The exponent n is dependent on the flow conditions. For laminar flow n = 0. For turbulent flow n = -0.47 for heating and -0.36 for cooling [91KA1]. Let us first determine whether the flow is laminar or turbulent.

$$Re_c = (Ry_c/\sigma)(D_h) = (2.324304\times10^5/0.9091)(2)(0.005) = 2556$$
$$Re_h = (Ry_h/\sigma)(D_h) = (1.959468\times10^5/0.9091)(2)(0.005) = 2155$$

In the program the transition point was set at a Reynolds number of 2000. The flow is thus turbulent for both cases. The hydraulic diameter, D_h was taken as twice the plate spacing for parallel plates. In order to calculate the mean wall temperature on each side the heat transfer rate must be known. The mean wall temperatures from the previous iteration are:

$$T_{w,c} = 449.583 \text{ K}$$
$$T_{w,h} = 469.528 \text{ K}$$

When the heat transfer rate is known it will be shown how to calculate the mean wall temperatures. The temperature adjusted values for Ny then become

$$Ny_c = 2.443148\times10^6\left(\frac{449.583}{434.906}\right)^{-0.47} = 2.405334\times10^6 \text{ m}^{-1}$$

$$Ny_h = 2.128736\times10^6\left(\frac{469.529}{483.291}\right)^{-0.36} = 2.150994\times10^6 \text{ m}^{-1}$$

Making use of the definition of Ny as given by equation (A.7) we can calculate the heat transfer coefficient on each side.

$$(hA)_c = Ny_c\, Pr_c^{1/3}\, k_c A_{o,c} = 1.484356\times10^6 \text{ W/K}$$

$(hA)_h = 1.582903 \times 10^6 \ W/K$

$h_c = (hA)_c/A_c = 68.934 \ W/m^2K$
$h_h = (hA)_h/A_h = 66.828 \ W/m^2K$

4.4.5 Dimensionless Groups

In the previous chapters it was shown that the effectiveness of a rotary regenerator is dependant on six dimensionless variables. They are Ntu_o, C^*, $(hA)^*$, C_r^*, λ and A_k^*.

Capacity rates:
$C_c = W_c(c_{p,c}) = 109(1020.913) = 1.112795\times10^5$ W/K
$C_h = W_h(c_{p,h}) = 109(1028.250) = 1.120793\times10^5$ W/K
$C_r = M_w c_w N = 7.364116\times10^4(434)(0.25/60) = 1.331678\times10^5$ W/K

In this case we see that the cold fluid is the minimum fluid. Therefore:

$C^* = C_c/C_h = 0.9929$
$C_r^* = C_r/C_c = 1.1967$
$(hA)^* = (hA)_c/(hA)_h = 0.9377$
$A_k^* = A_{k,c}/A_{k,h} = 0.9091$

$$\lambda = \frac{A_{k,t}k_w}{C_c L} = \frac{(3.6514)(51.9)}{(1.112795\times10^5)(2.58)} = 6.600752\times10^{-4}$$

Equation (3.19) can be used to calculate Ntu_o. We first need to calculate the equivalent wall thermal resistance from equation (3.17).

$$Z = \frac{\delta C_r}{2k_w}\left(1/A_h + 1/A_c \right)$$
$$= \frac{(0.0005)(1.331678\times10^5)}{(2)(51.9)}\left(\frac{1}{2.368619\times10^4} + \frac{1}{2.153290\times10^4}\right)$$
$$= 5.687166\times10^{-5} \ m^{-2}$$

$Z < 5$, therefore use equation (3.18a) to calculate ϕ.

$\phi = 1 - (1/15)Z = 1 - (1/15)(5.687166\times10^{-5}) = 0.9999962$

The equivalent resistance is now according to equation (3.17)

$$R = \left(\frac{\delta}{6k_w}\right)\left(\frac{1}{A_h} + \frac{1}{A_c}\right)\phi$$
$$= \left(\frac{0.0005}{(6)(51.9)}\right)\left(\frac{1}{2.368619 \times 10^4} + \frac{1}{2.153290 \times 10^4}\right)(0.9999962)$$
$$= 1.423554 \times 10^{-10} \quad K/W$$

$$Ntu_o = \frac{1}{C_{min}}\left[\frac{1}{(hA)_h} + \frac{1}{(hA)_c} + R \right]^{-1}$$
$$= \frac{1}{1.112795 \times 10^5}\left[\frac{1}{1.582903 \times 10^6} + \frac{1}{1.484356 \times 10^6} + 1.423554 \times 10^{-10}\right]^{-1}$$
$$= 6.8830$$

In this example the wall thermal resistance is negligible in comparison with the convective resistances. This is usually the case for a thin metal matrix..

4.4.6 Effectiveness for ideal regenerator

The program has the option to calculate the effectiveness with a numerical procedure or with an approximate theory. The effectiveness will now be calculated by making use of the approximate theory as described in Chapter 3.

The effect of longitudinal conduction is taken into account by modifying Ntu_o with a factor G_L. To evaluate G_L from equation (3.16) we need the effectiveness of a recuperator implied by equation (3.13) and shown in Appendix B. It is quite long and not suitable for hand calculation. The effectiveness was evaluated with the computer program using the Hahnemann [48HA1] method.

This gives $\varepsilon_{\infty,\lambda\neq0} = 0.8743$

The Hahnemann [48HA1] solution can be checked against the numerical solution with an infinite C_r^*. The numerical solution gives $\varepsilon_{\infty,\lambda\neq0} = 0.8731$ for the same dimensionless groups, but with $C_r^* = 10$. A high C_r^* implies a high rotational speed where the effectiveness of a regenerator and a recuperator are identical. There is practically no further increase in the effectiveness for higher values of C_r^*, therefore a value of 10 can be regarded as 'infinite'. We will continue the rest of the calculations with ε = 0.8743.

G_L can now be calculated from equation (3.16)

$$G_L = \frac{1}{Ntu_o(1-C^*)} Ln\left(\frac{1-C^*\varepsilon_{\infty,\lambda\neq 0}}{1-C^*}\right)$$
$$= \frac{1}{(6.8830)(1-0.9929)} Ln\left(\frac{1-(0.9929)(0.8743)}{1-0.9929}\right) = 0.9958$$

G_L is very close to unity. This is an indication that reduction in effectiveness due to the longitudinal conduction effect will be very small. The modified Ntu_o now becomes $G_L Ntu_o$ = 6.8524 and will simply be denoted by Ntu_o again.

The Razelos method [79RA1] together with equation (3.9) will be used to calculate the effectiveness. Firstly we need to calculate the parameters for an equivalent balanced regenerator (C^* = 1) from equations (3.4) and (3.5).

$$Ntu_{o,e} = \frac{2Ntu_o C^*}{1+C^*} = \frac{(2)(6.8524)(0.9929)}{1+0.9929} = 6.8279$$

$$C_{r,e} = \frac{2C_r^* C^*}{1+C^*} = \frac{(2)(1.1967)(0.9929)}{1+0.9929} = 1.1924$$

The effectiveness for the balanced regenerator is now calculated from equation (3.9)

$$A = 15.78/Ntu_{o,e} + 3.2678 \ln(Ntu_{o,e}) + 0.0019373[\ln(Ntu_{o,e})]^5 = 8.6393$$
$$n = 1.881 + 0.0331197[\ln(Ntu_{o,e})]^2 = 2.0032$$

$$\varepsilon_e = \frac{Ntu_{o,e}}{1+Ntu_{o,e}}\left(1-\frac{1}{AC_{r,e}^{*\,n}}\right) = \frac{6.8279}{1+6.8279}\left(1-\frac{1}{(8.6393)(1.1924)^{2.0032}}\right)$$
$$= 0.8013$$

The effectiveness of the unbalanced regenerator can now be calculated. Equation (3.7) gives:

$$\varepsilon = \frac{1-e^{n}}{1-C^{*}e^{n}} = \frac{1-e^{-0.02888}}{1-0.9929e^{-0.02888}} = 0.8041$$

where $\varepsilon_e\left(C^{*2}-1\right)/2C^{*}\left(1-\varepsilon_e\right) = 0.8013(0.9929^2-1)/(2)\left(0.9929(1-0.8013)\right)$
$= -0.02888$

The effectiveness for the balanced regenerator is very close to that of the unbalanced regenerator. This is so because the regenerator is nearly balanced ($C^* = 0.9929$). We have now calculated the effectiveness for the ideal regenerator taking into account all six the dimensionless parameters with the exception of $(hA)^*$, the influence of which is ignored in the range $0.25 < (hA)^* < 4$. As a check for the approximate method the effectiveness was also calculated by the numerical procedure given in Appendix C. This yields $\varepsilon = 0.8076$. The difference in this case is negligibly small.

The heat transfer rate from the hot- to the cold gas for the ideal regenerator can now be calculated from the definition of the ideal effectiveness (equation (3.21)).

$q_i = \varepsilon_i C_{min}(T_{h,i}-T_{c,i}) = (0.8041)(1.112795\times10^5)(580.5-337) = 21789.51$ kW

From the energy balance $q_i = C_c(T_{c,o}-T_{c,i}) = C_h(T_{h,i}-T_{h,o})$ the outlet and mean gas temperatures can be calculated.

$T_{c,o} = 532.81$ K
$T_{h,o} = 386.09$ K
$T_{c,m} = 434.90$ K
$T_{h,m} = 483.29$ K

The mean temperatures for the hot and cold gas are practically the same as the initial values used at the start of the calculation. The solution is therefore converged. The mean matrix wall temperatures can now be calculated.

$$T_{w,c} = T_{c,m} + \frac{q_{int}}{(hA)_c} = 434.90 + \frac{21789.51\times10^3}{1.484356\times10^6} = 449.58 \text{ K}$$

$$T_{w,h} = T_{h,m} - \frac{q_{int}}{(hA)_c} = 483.29 - \frac{21789.51\times10^3}{1.582903\times10^6} = 469.52 \text{ K}$$

4.5 SOLUTION FOR REGENERATOR WITH FINITE LEAKAGE

So far we have neglected the influence of the pressure leakage and the carryover of the gases due to the matrix rotation. We will now correct the effectiveness for these enthalpy losses. Refer to figure 3.1 for a regenerator model taking into account the losses.

4.5.1 Leakage factors

The leakage factors are defined by equation (3.20). The pressure leakage factor x_p is constant and is specified as part of the input data. The carryover leakage factors x_c and x_h are dependent on the operating conditions and the disk geometry.

The total rotation time = 1/N = 240 s. The cold gas flow time, $F_c = 240/(1+\phi) = 240/(1+1.1) = 114.2857$ s. The hot gas flow time, $F_h = 240(\phi)/(1+\phi) = 240(1)/(1+1.1) = 125.7143$ s.

$$\Delta W_c = \frac{\rho_{c,m} A_{o,c} L}{F_c} = \frac{P_{c,i} A_{o,c} L}{R T_{c,m} F_c} = \frac{(106.21\times 10^3)(17.3877)(2.58)}{(287.08)(434.904)(114.2857)} = 0.3339 \text{ kg/s}$$

$$\Delta W_h = \frac{\rho_{h,m} A_{o,h} L}{F_h} = \frac{P_{h,i} A_{o,h} L}{R T_{h,m} F_h} = \frac{(102.28\times 10^3)(19.1264)(2.58)}{(287.08)(483.294)(125.7143)} = 0.2894 \text{ kg/s}$$

We can now calculate x_c and x_h from their definition as given by equation (3.20). The result is

$x_c = 0.3339/109 = 3.0635\times10^{-3}$
$x_h = 0.2894/109 = 2.6547\times10^{-3}$

4.5.2 Internal regenerator properties

The internal regenerators have different gas flow rates than the ideal regenerator. The change in the flow rates will also affect the fluid properties, the flow properties and the dimensionless groups.

The modified flow rates can be calculated as follows.

$$W'_c = W_c\left(1 - x_c - \frac{x_p}{2}\right) = 109\left(1 - 3.0635\times10^{-3} - \frac{0.08}{2}\right) = 104.3061 \text{ kg/s}$$

$$W'_h = W_h(1 - x_h) + W_c\frac{x_p}{2} = 109(1 - 2.6547\times10^{-3}) + 109\frac{0.08}{2} = 113.0706 \text{ kg/s}$$

As in the case of the ideal regenerator an iterative process is required. The final converged values are as follows:

$T'_{c,m} = 438.03$ K
$T'_{h,m} = 487.15$ K

The fluid properties are evaluated from the equations in Appendix D.

Table 4.2: Thermophysical properties for the internal regenerator at the mean gas temperatures.

T (K)	μ (kg/ms)	k (W/mK)	c_p (J/kgK)	Pr
438.03	2.464646×10^{-5}	3.683319×10^{-2}	1021.347	0.6834
487.15	2.658822×10^{-5}	3.990850×10^{-2}	1028.887	0.6855

The flow properties for the internal regenerator can now be evaluated.

$G_c = W'_c/A_{fr,c} = 104.3061/19.1264 = 5.4535$ kg/m²
$G_h = W'_h/A_{fr,h} = 113.0706/21.0391 = 5.3743$ kg/m²
$Ry_c = G_c/\mu_c = 5.4535/2.464646\times10^{-5} = 2.212692\times10^{5}$ m^{-1}
$Ry_h = G_h/\mu_h = 5.3743/2.658822\times10^{-5} = 2.021314\times10^{5}$ m^{-1}

Similar to the case of the ideal regenerator the temperature corrected heat transfer parameters are:

$Ny_c = 2.311173\times10^{5}$ m^{-1}
$Ny_h = 2.204447\times10^{5}$ m^{-1}

$(hA)_c = Ny_c\, Pr_c^{1/3}\, k_c A_{fr,c} = 1.434147\times10^{6}$ W/K
$(hA)_h = 1.632009\times10^{6}$ W/K

$h_c = (hA)_c/A_c = 66.6039$ W/m²K
$h_h = (hA)_h/A_h = 68.9013$ W/m²K

The dimensionless groups for the internal regenerator can now be evaluated.

Capacity rates:
$C_c = W'_c(c_{p,c}) = 104.3061(1021.347) = 1.065327\times10^5$ W/K
$C_h = W'_h(c_{p,h}) = 113.0706(1028.887) = 1.163370\times10^5$ W/K
$C_r = M_w c_w N = 7.364116\times10^5(434)(0.25/60) = 1.331678\times10^5$ W/K

The cold gas remains the minimum fluid, therefore:

$C^* = C_c/C_h = 0.9157$
$C_r^* = C_w/C_c = 1.2500$
$(hA)^* = (hA)_c/(hA)_h = 0.8788$
$A_k^* = A_{k,c}/A_{k,h} = 0.9091$

$$\lambda = \frac{A_{k,t}k_w}{C_c L} = \frac{(3.6514)(51.9)}{(1.065327\times10^5)(2.58)} = 6.894859\times10^{-4}$$

The equivalent wall thermal resistance does not change and is the same as for the ideal regenerator.

$R = 1.423554\times10^{-10}$ K/W

$$Ntu_o = \frac{1}{C_{min}}\left[\frac{1}{(hA)_h} + \frac{1}{(hA)_c} + R\right]^{-1}$$
$$= \frac{1}{1.065327\times10^5}\left[\frac{1}{1.434147\times10^6} + \frac{1}{1.632009\times10^6} + 1.423554\times10^{-10}\right]^{-1}$$
$$= 7.1647$$

4.5.3 Internal regenerator effectiveness

Similar to the ideal regenerator the effectiveness for the internal regenerator will now be calculated.

The Hahnemann [48HA1] solution gives $\varepsilon_{\infty,\lambda\neq0} = 0.9064$ for the equivalent recuperator.

G_L is now once again calculated from equation (3.16)

$$G_L = \frac{1}{Ntu_o(1-C^*)} Ln\left(\frac{1-C^*\varepsilon_{\infty,\lambda\neq 0}}{1-C^*}\right)$$
$$= \frac{1}{(6.8949)(1-0.9157)} Ln\left(\frac{1-(0.9157)(0.9064)}{1-0.9157}\right) = 0.995515$$

The modified Ntu_o now becomes $G_L Ntu_o = 7.1325$.

The Razelos method [79RA1] is used to calculate the effectiveness.

$$Ntu_{o,e} = \frac{2Ntu_o C^*}{1+C^*} = \frac{(2)(7.1325)(0.9157)}{1+0.9157} = 6.8188$$

$$C_{r,e} = \frac{2C_r^* C^*}{1+C^*} = \frac{(2)(1.2500)(0.9157)}{1+0.9157} = 1.1950$$

The effectiveness for the balanced internal regenerator is now calculated from equation (3.9)

$$A = 15.78 / Ntu_{o,e} + 3.2678 \ln(Ntu_{o,e}) + 0.0019373[\ln(Ntu_{o,e})]^5 = 8.6378$$
$$n = 1.881 + 0.0331197[\ln(Ntu_{o,e})]^2 = 2.0031$$

$$\varepsilon_e = \frac{Ntu_{o,e}}{1+Ntu_{o,e}}\left(1-\frac{1}{AC_{r,e}^{*\,n}}\right) = \frac{6.8188}{1+6.8188}\left(1-\frac{1}{(8.6378)(4.58645)^{2.0031}}\right)$$
$$= 0.8014$$

The effectiveness of the unbalanced regenerator is given by equation (3.7).

$$\varepsilon = \frac{1-e^n}{1-C^*e^n} = \frac{1-e^{-0.3558}}{1-0.9157e^{-0.3558}} = 0.8353$$

where $\varepsilon_e\left(C^{*2}-1\right)/2C^*(1-\varepsilon_e) = 0.8014(0.9157^2-1)/(2)(0.9157(1-0.8014))=$ -0.3558

The relevant temperatures and the heat transfer rate for the internal regenerator can now be calculated. The effectiveness of the internal regenerator is defined by equation (3.22). Here C_c and C_h are the original values from the ideal regenerator analysis.

$$\varepsilon_{int} = \frac{\left(1 - x_c - x_p / 2\right) C_c \left(T'_{c,o} - T_{c,i}\right)}{\left(1 - x_c - x_p / 2\right) C_c \left(T'_{h,i} - T_{c,i}\right)} = \frac{\left(T'_{c,o} - T_{c,i}\right)}{\left(T'_{h,o} - T_{c,i}\right)}$$

The above equation together with an energy balance on the hot gas inlet stream yields the following expression for the temperature of the cold gas leaving the internal regenerator.

$$T'_{c,o} = \left[\frac{\varepsilon_{int} A + T_{c,i}\left(1 - \varepsilon_{int}\right)}{B}\right] = \left[\frac{(0.8353)(558.2696) + (337)(1 - 0.8353)}{0.9680}\right]$$
$$= 539.06 \text{ K}$$

where

$$A = \frac{T_{h,i} C_h \left(1 - x_h\right)}{\left(1 - x_h\right) C_h + 0.5 x_p C_c}$$
$$= \frac{(580.5)(1.120793 \times 10^5)(1 - 2.6547 \times 10^{-3})}{(1 - 2.6547 \times 10^{-3})(1.120793 \times 10^5) + 0.5(0.08)(1.112795 \times 10^5)} = 558.2696$$

and

$$B = \frac{1 - 0.5 x_p C_c \varepsilon_{int}}{\left(1 - x_h\right) C_h + 0.5 x_p C_c}$$
$$= \frac{1 - 0.5(0.08)(1.112795 \times 10^5)(0.8353)}{(1 - 2.6547 \times 10^{-3})(1.120793 \times 10^5) + 0.5(0.08)(1.112795 \times 10^5)} = 0.9680$$

The definition of the internal regenerator effectiveness can now be used to calculate the hot gas inlet temperature.

$$T'_{h,i} = \frac{\left(T'_{c,o} - T'_{c,i}\right) + \varepsilon_{int} T'_{c,i}}{\varepsilon_{int}} = \frac{(539.06 - 337) + (0.8353)(337)}{0.8353} = 578.91 \text{ K}$$

The heat transfer rate in the internal regenerator is

$$q_{int} = \left(T'_{c,o} - T'_{c,i}\right)\left(1 - x_c - 0.5 x_p\right) C_c$$
$$= (539.06 - 337)(1 - 3.0635 \times 10^{-3} - 0.5(0.08))(1.112795 \times 10^5) = 21517.34 \text{ kW}$$

The temperature of the hot gas leaving the internal regenerator can finally be calculated.

$$T'_{h,o} = T'_{h,i} - \frac{q_{int}}{(1-x_h)C_h + 0.5x_pC_c}$$

$$= 578.91 - \frac{21517.34\times10^3}{(1\text{-}2.6547\times10^{-3})(1.120793\times10^5)+0.5(0.08)(1.112795\times10^5)}$$

$$= 393.79\text{ K}$$

4.5.4 Actual regenerator effectiveness

After the gas streams leave the internal regenerator the carryover gas from the opposite sides enters the streams. The outlet temperatures from the actual regenerator can be calculated by doing energy balances on the departing streams.

$$T''_{c,o} = \frac{T'_{c,o}(1-x_c-x_p)C_c + T'_{h,i}x_hC_h}{(1-x_c-x_p)C_c + x_hC_h}$$

$$= \frac{(539.06)(0.91694)(1.112795\times10^5)+(578.91)(2.6547\times10^{-3})(1.120793\times10^5)}{(0.91694)(1.112795\times10^5)+(2.6547\times10^{-3})(1.120793\times10^5)}$$

$$= 539.18\text{ K}$$

$$T''_{h,o} = \frac{T'_{h,o}\left((1-x_h)C_h + 0.5x_pC_c\right) + T'_{c,i}(x_c+0.5x_p)C_c}{(1-x_h)C_h + (x_p+x_c)C_c}$$

$$= \frac{\begin{bmatrix}(393.79)\left((0.997346)(1.120793\times10^5)+0.5(0.08)(1.112795\times10^5)\right)\\ +(337)(3.0635\times10^{-3}+0.5(0.08))(1.112795\times10^5)\end{bmatrix}}{(0.997346)(1.120793\times10^5)+(0.08+3.0635\times10^{-3})(1.112795\times10^5)}$$

$$= 391.54\text{ K}$$

The effectiveness of the actual regenerator is defined by equation (3.23) and is the ratio of the actual heat transfer to the maximum possible heat transfer for the actual regenerator.

$$\varepsilon_{act} = \frac{\left[\left(1-x_c-x_p\right)C_c + x_h C_h\right]T''_{c,o} - C_c T_{c,i}}{\left[\left(1-x_c-x_p\right)C_c + x_h C_h\right]T_{h,i} - C_c T_{c,i}}$$

$$= \frac{\left[(0.91694)(1.112795\times10^5)+(2.6547\times10^{-3})(1.120793\times10^5)\right]539.18-(1.112795\times10^5)(337)}{\left[(0.91694)(1.112795\times10^5)+(2.6547\times10^{-3})(1.120793\times10^5)\right]580.5-(1.112795\times10^5)(337)}$$

$= 0.8069$

The denominator of the above relation represents the actual heat transfer rate.

$q_{act} = 17675.18$ kW

The actual regenerator effectiveness, ε_{act} is defined in terms of the modified flow rates. We can calculate the effective effectiveness that is based on the original flow rates.

$$\varepsilon_{eff} = \frac{q_{act}}{C_c\left(T_{h,i} - T_{c,i}\right)} = \frac{17675.18\times10^3}{(1.112795\times10^5)(580.5-337)} = 0.6523$$

As a final check for the energy balance we can calculate the energy losses from the cold stream before and after the internal regenerator.

The inlet energy loss = $C_c T_{c,i}(x_c+0.5x_p)$
= $(1.112795\times10^5)(337)(3.0635\times10^{-3} + 0.08/2) = 1614.93$ kW.

The outlet energy loss = $C_c T'_{c,o}(0.5x_p) - C_h T'_{h,i} x_h$
= $(1.112795\times10^5)(539.06)(0.08/2) - (1.127093\times10^5)(578.91)(2.6547\times10^{-3})$
= 2227.22 kW.

Energy balance requires that q_{int} - inlet loss - outlet loss = q_{act}. The right hand side gives 21517.34 - 1614.93 -2227.22 = 17675.19 that is exactly equal to the actual heat transfer rate. The ideal heat transfer without any leakage and carryover losses is 21789.51 kW. There is therefore a 18.9 % reduction in the heat transfer rate due to the pressure leakage and carryover.

4.6 PRESSURE DROP EVALUATION

The pressure drop is evaluated over the internal regenerator. The modified mass flow rates will therefore be used. The total pressure drop consists of a few components, namely the core friction, the momentum effect and the exit and entrance losses. In the analysis that will follow it is assumed that the loss coefficient, K includes the entrance and exit effects. The total pressure drop is given by equation (3.30). The version given here is slightly different, because a loss coefficient, K is known from experimental data which is indicative of the friction factor (see Appendix A for details). In the relation below G is based on the total frontal area of the heat exchanger.

$$\Delta p = \frac{G^2}{2}\left[\frac{K}{\rho_m} + \frac{(1+\sigma^2)}{\sigma^2}\left(\frac{1}{\rho_o} - \frac{1}{\rho_i}\right)\right]$$

From the heat transfer analysis we know the mean temperatures and mass fluxes for the internal regenerator.

$T'_{c,m} = (337+539.06)/2 = 438.03$ K
$T'_{h,m} = (578.91+393.79)/2 = 486.35$ K
$G_c = 5.4535$ kg/m²
$G_h = 5.3743$ kg/m²

The viscosities at the mean temperatures are:

$\mu_c = 2.464645\times10^{-5}$ kg/ms
$\mu_h = 2.655776\times10^{-5}$ kg/ms

The flow parameter $Ry = G/\mu$ is now calculated for both gas streams.

$Ry_c = 2.225995\times10^{5}$ m^{-1}
$Ry_h = 2.433961\times10^{5}$ m^{-1}

The pressure drop correlation obtained during the experimental testing, $K_T = 84.943 Ry_T^{-0.2903}$ can be rewritten as follows to be applicable to a plate fin matrix. See Appendix A for more detail.

$$K = 84.943(Ry)^{-0.2903}(L/L_{ref})\sigma^{-(-0.2903+2)}$$

$$K_c = 84.943(2.225995 \times 10^5)^{-0.2903}(2.58/0.2)(0.9091)^{-1.7097} = 36.2123$$
$$K_h = 37.1635$$

As in the case of the characteristic heat transfer parameter, Ny a temperature correction has to be applied. The temperature correction has the following form:

$$K = K_{iso}\left(\frac{T_w}{T_m}\right)^m$$

For laminar flow m = 0.81 if the gas is cooled and m = 1.0 if the gas is heated. For turbulent flow m = -0.1 for both heating and cooling [91KA1]. The flow is turbulent on both the hot and the cold sides as was seen earlier. The mean matrix wall temperatures for the internal regenerator are:

$$T_{w,h} = T_{h,m} - \frac{q_{int}}{(hA)_h} = 486.35 - \frac{21517.34 \times 10^3}{1.632009 \times 10^6} = 473.17 \text{ K}$$

$$T_{w,c} = T_{c,m} + \frac{q_{int}}{(hA)_c} = 438.03 + \frac{21517.34 \times 10^3}{1.434147 \times 10^6} = 453.03 \text{ K}$$

The temperature adjusted values then become

$$K_c = 36.2123\left(\frac{453.03}{438.03}\right)^{-0.1} = 36.09$$

$$K_h = 37.1635\left(\frac{473.17}{486.35}\right)^{-0.1} = 37.26$$

Densities:

$$\rho_{c,i} = \frac{P_{c,i}}{RT'_{c,i}} = \frac{106.21 \times 10^3}{(287.08)(337)} = 1.0978 \text{ kg/m}^3$$

$$\rho_{h,i} = \frac{P_{h,i}}{RT'_{h,i}} = \frac{102.28 \times 10^3}{(287.08)(578.91)} = 0.6154 \text{ kg/m}^3$$

The calculation of the outlet densities requires the pressure drop across the matrix to be known. The final converged values for the pressure drop are:

$$\Delta p_c = 720.32 \text{ Pa}$$
$$\Delta p_h = 656.09 \text{ Pa}$$

$$\rho_{c,o} = \frac{P_{c,i} - \Delta p_c}{RT'_{c,o}} = \frac{106.21 \times 10^3 - 656.09}{(287.08)(539.06)} = 0.6821 \text{ kg/m}^3$$

$$\rho_{h,o} = \frac{P_{h,i} - \Delta p_h}{RT'_{h,o}} = \frac{102.28 \times 10^3 - 720.32}{(287.08)(393.79)} = 0.8984 \text{ kg/m}^3$$

$$\rho_{m,c} = 0.5\left[\frac{1}{\rho_{i,c}} + \frac{1}{\rho_{o,c}}\right]^{-1} = 0.5\left[\frac{1}{1.0978} + \frac{1}{0.6821}\right]^{-1} = 0.8414 \text{ kg/m}^3$$

$$\rho_{m,h} = 0.5\left[\frac{1}{\rho_{i,h}} + \frac{1}{\rho_{o,h}}\right]^{-1} = 0.5\left[\frac{1}{0.6154} + \frac{1}{0.8984}\right]^{-1} = 0.7305 \text{ kg/m}^3$$

The pressure drop for each side can now be evaluated.

$$\Delta p_c = \frac{G_c^2}{2}\left[\frac{K_c}{\rho_{m,c}} + \frac{(1+\sigma^2)}{\sigma^2}\left(\frac{1}{\rho_{o,c}} - \frac{1}{\rho_{i,c}}\right)\right]$$
$$= \frac{(5.4535)^2}{2}\left[\frac{36.09}{0.8414} + \frac{1+0.9091^2}{0.9091^2}\left(\frac{1}{0.6821} - \frac{1}{1.0978}\right)\right] = 656.1 \text{ Pa}$$

$$\Delta p_h = \frac{G_h^2}{2}\left[\frac{K_h}{\rho_{m,h}} + \frac{(1+\sigma^2)}{\sigma^2}\left(\frac{1}{\rho_{o,h}} - \frac{1}{\rho_{i,h}}\right)\right]$$
$$= \frac{(5.3743)^2}{2}\left[\frac{37.26}{0.7305} + \frac{1+0.9091^2}{0.9091^2}\left(\frac{1}{0.8984} - \frac{1}{0.6154}\right)\right] = 720.3 \text{ Pa}$$

4.7 COST EFFECTIVENESS PARAMETER

In engineering processes or projects the objective is usually to obtain the highest output per unit input. This statement is an expression of a physical efficiency and measures the success of an engineering activity in a physical environment. This efficiency is always less than 100 %. However, engineering projects must always be concerned with two levels of efficiency. On the first level there are physical efficiencies and on the second level there are economic efficiencies. Economic efficiencies are expressed as economic gain per unit input of cost. These efficiencies must be greater then 100 % for the undertaking to be economically successful. Physical efficiencies are related to economic efficiencies. Good physical efficiencies pave the way for economic feasibility, but are not a guarantee for economic success. Physical efficiencies are always significant, but only to the extent that they contribute to economic efficiency.

A very simplified cost effectiveness parameter for the regenerator will now be presented. The parameter is not necessarily an indication of the actual costs involved and should rather be seen as an approximate method for comparing alternatives. For the scope of this work the interest lies with the matrix material. The object is to determine the effect on the size of the regenerator and basic energy costs when different matrix materials are used. Detailed information regarding the capital and operating costs of rotary regenerators is scarce and difficult to obtain.

The two main cost elements are the cost of the pumping power and the cost of the matrix material. Both costs will be expressed as an equivalent annual cost.

4.7.1 Gas supply cost

The required input electrical power to move the volume of gas through the matrix can be expressed as

$$P_e = \frac{\dot{V}\Delta p}{\eta_{fs}\eta_{fd}}$$

In the above expression $\dot{V} = W/\rho$ is the volume flow rate (m^3/s) and Δp is the pressure drop across the matrix in Pa. The fan static efficiency is η_{fs} and the fan drive system efficiency (electric motor and gears) is η_{fd}. In a regenerator there are a hot and a cold gas stream with different flow rates. The total electrical power input to the fan is thus

$$P_e = \frac{\dot{V}_c \Delta p_c + \dot{V}_h \Delta p_h}{\eta_{fs}\eta_{fd}} = \frac{(104.3061/0.8414)656.1 + (113.0706/0.7305)720.3}{(0.7)(0.9)}$$
$$= 306.09 \text{ kW}$$

The annual cost of the gas supply can be expressed as

$$C_{gs} = (P_e)(H)(C_{eu}) = (306.09)(8750)(0.05) = 133\ 914.2\ \$$$

Here H is the number of operating hours per year and C_{eu} is the unit cost of electricity (\$/kWh).

4.7.2 Matrix material cost

The annual matrix material cost consists of a capital investment that is levelled over the life of the plant at a certain interest rate. The equivalent annual capital investment for material can be expressed as

$$C_m = M_w C_{mu} W_{ca}$$

Here M_w is the mass of the matrix in kg. The matrix material cost is C_m (\$/kg) and W_{ca} is the factor that levels the capital investment over the life of the plant. From the present economic analysis W_{ca} can be expressed as

$$W_{ca} = \frac{(1+i)^n i}{(1+i)^n - 1} = \frac{(1+0.1)^{20} 0.1}{(1+0.1)^{20} - 1} = 0.11746$$

where i is the annual interest rate and n is the number of years. Therefore

$$C_m = (7.364116 \times 10^4)(1)(0.11746) = 8649.86\ \$$$

It should be noted that for this particular regenerator the annual pumping cost C_{gs} is an order of magnitude higher than the annualised material cost, C_m.

4.7.3 Cost effectiveness parameter

The cost effectiveness parameter is defined as

$$CP = (q_{actual})(H)/(C_{gs} + C_m) = (17675.2)(8750)/(133\,914.2 + 8649.86)$$
$$= 1084.84 \text{ kWh/\$}$$

The cost effectiveness parameter is an indication of the amount of energy that can be regenerated per dollar annual investment.

4.8 SOFTWARE LIMITATIONS

The program assumes a single layered layout of the regenerator matrix. The program will have to be modified extensively to cater for more than one layer. For thin metal matrixes where the effect of longitudinal heat conduction and wall thermal resistance is negligible it is a good approximation to assume a single layered matrix layout, providing that the thermophysical properties of the matrix material in the different layers do not differ substantially. Multi layered layouts are used sometimes because of the certain practical considerations [84WO1]. For excess temperature at the hot end, scale resistant material is used. Corrosion often occurs at the cold end when the gas contains sulphur trioxide and the matrix temperature falls below the gas dew point. In the latter case corrosion resistant materials are used and the matrix wall thickness is increased.

The program has the ability to accept matrix correlations for a certain disk height and then to extend the correlations for the specified height. This can only be done if the friction coefficient and heat transfer coefficient were tested under fully developed hydraulic and thermal conditions. Furthermore the program assumes that the inlet- and exit pressure losses are included in the correlation for the loss coefficient K. If the inlet and exit losses contribute substantially to the loss coefficient large errors can result if the loss coefficient is extrapolated to different disk heights. Care should therefore be taken by the user of the program to not use correlations under conditions very different from the test conditions.

CHAPTER 5

REGENERATOR PERFORMANCE OPTIMISATION AND HEATING SURFACE SELECTION

5.1 INTRODUCTION

The object of this chapter is to show how the workings of a regenerator can be optimised with regard to the operating conditions and the selection of the heating surface. To show how the operating conditions can be optimised a single matrix surface will be used. In the second part of the chapter the different heating surfaces tested in the experimental work will be compared to each other at their respective optimum operating points. The experimental set-up, procedures and results are shown in Appendix A. It will be shown how the disk dimensions and optimum operating point are influenced by using different heating surfaces and different spacings between the surfaces. The performances of the surfaces are compared to each other by the use of the earlier defined cost effectiveness parameter.

There are a large number of applications and conditions one can use to evaluate the performances of the surfaces and it is possible that the outcome will be different every time. In this chapter a single example was taken and it is shown how the designer can choose some of the operating conditions and heating surfaces to arrive at a good design.

The regenerator data used in the evaluation sample calculation of Chapter 4 will be used with a few alterations. The operating conditions are the same as specified in section 4.3.1 except for the disk rotational speed which now becomes a variable. The disk dimensions are the same as in section 4.3.2, but the disk height and flow split ratio are made variable. The matrix density, specific heat and thermal conductivity are taken as in section 4.3.3, but the plate spacing, wall thickness and type of matrix used was not fixed. The cost effectiveness parameters are also the same as in section 4.3.4 except for the unit cost of electrical power.

The optimisation process requires that the regenerator effectiveness or equivalently the desired heat transfer rate is specified. The disk outer diameter was not taken as an optimisation variable, because it was found that the largest possible frontal area always produces the most cost effective answer. It is therefore up to the designer to specify the largest possible outer diameter for the rotating disk which can be practically implemented in the specific system.

5.2 OPTIMISATION OF OPERATING CONDITIONS USING A SPECIFIC HEATING SURFACE

The design option of the program discussed in Chapter 4 was used to show how to optimise some of the operating conditions. The disk rotational speed, the hot to cold gas flow split ratio and the plate thickness were varied in the optimisation process. The heat transfer and pressure drop correlations of the 11A surface were used. The surface spacing is 5 mm. See Appendix A for details of the surfaces.

5.2.1 Effect of disk rotational speed and matrix plate thickness

The effectiveness of an ideal regenerator (no pressure leakage or carryover) increases with an increase in rotational speed and asymptotically approaches that of a recuperator as predicted by equation (3.3). This is also evident from numerical results. In a real regenerator however, an increase in rotational speed increases the gas carryover which in turn reduces the regenerator effectiveness. These two effects oppose each other. The effectiveness first increases with an increase in rotational speed and then decreases indicating an optimum value at some rotational speed. If the effectiveness is held constant as was done in this case the required surface area or disk height will show a minimum at some rotational speed. In figure 5.1 it can be seen how the hot fluid leakage fraction increases with rotational speed. The cold fluid leakage fraction follows a similar pattern.

It can be seen from figure 5.1 that the leakage fraction increases more or less linearly with an increase in rotational speed. The leakage fraction increases slightly if the plate thickness is increased at a constant rotational speed. This is so because a decrease in plate thickness at a constant spacing increases the matrix void volume and thus the amount of gas trapped in the matrix for transport to the opposite side.

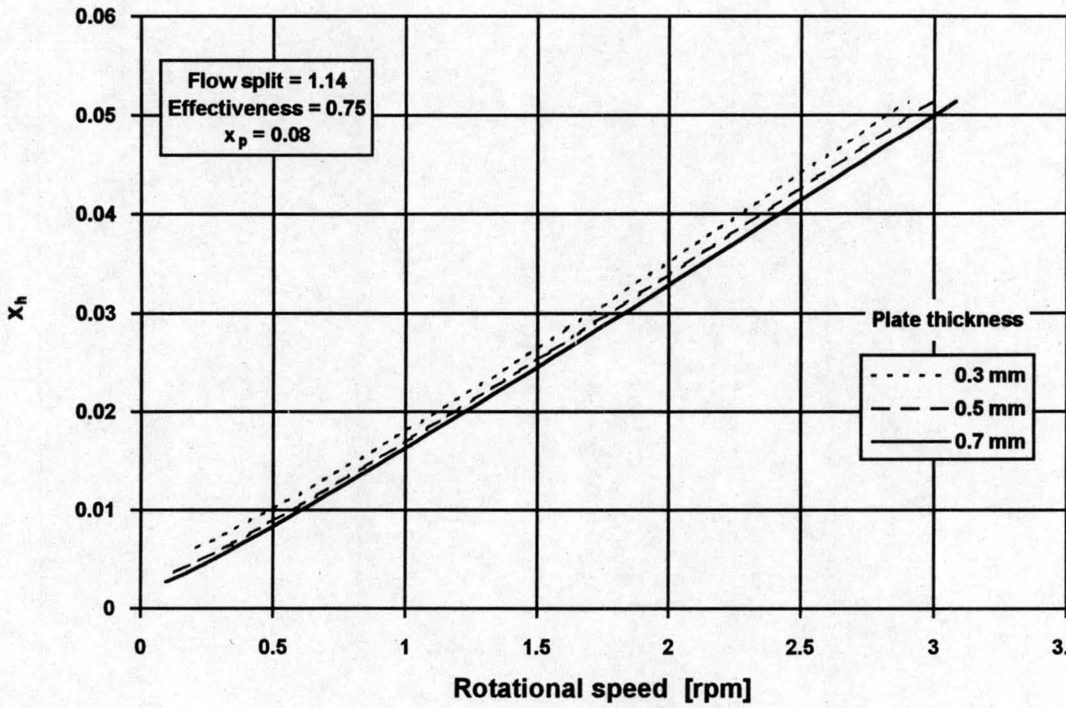

Figure 5.1: Hot fluid carryover leakage fraction at various plate thicknesses for the 11A surface of Type 1 at a spacing of 5 mm.

In figure 5.2 it can be seen that there is a minimum disk height for every plate thickness as the disk rotational speed is increased. The optimum disk rotational speed is defined as the speed that requires the minimum disk height for a specified effectiveness.

In the literature it is indicated that regenerators usually operate at rotational speeds of 1 to 3 rpm ([66GR1] and [84WO1]). For this example the optimum speeds are in the same range. The optimum speed increases with a decrease in plate thickness as can be seen from figure 5.2. This can be explained as follows. The effectiveness of an ideal regenerator increases with an increase in C_r^* as is evident from equation (3.3). If equation (3.3) is plotted it can be seen that the effectiveness increases rapidly if C_r^* is increased for relatively low values of C_r^*. At high values of C_r^* there is practically no further increase in the effectiveness if C_r^* is increased and the effectiveness approaches that of an equivalent recuperator. In turn it can be seen from the relation, $C_r^* = M_w c_w N/C_{min}$., that C_r^* can be increased by increasing the matrix rotational speed or increasing the matrix mass (plate thickness). A regenerator with thicker plate thicknesses for the heating surfaces will more rapidly reach the point where an increase in rotational speed has only a small increase in effectiveness. The deteriorating effect of gas carryover will therefore be more prominent for heavy matrixes than for relatively thin matrixes at small rotational speeds. The optimal rotational speed is thus limited to a lower value for heavy matrixes.

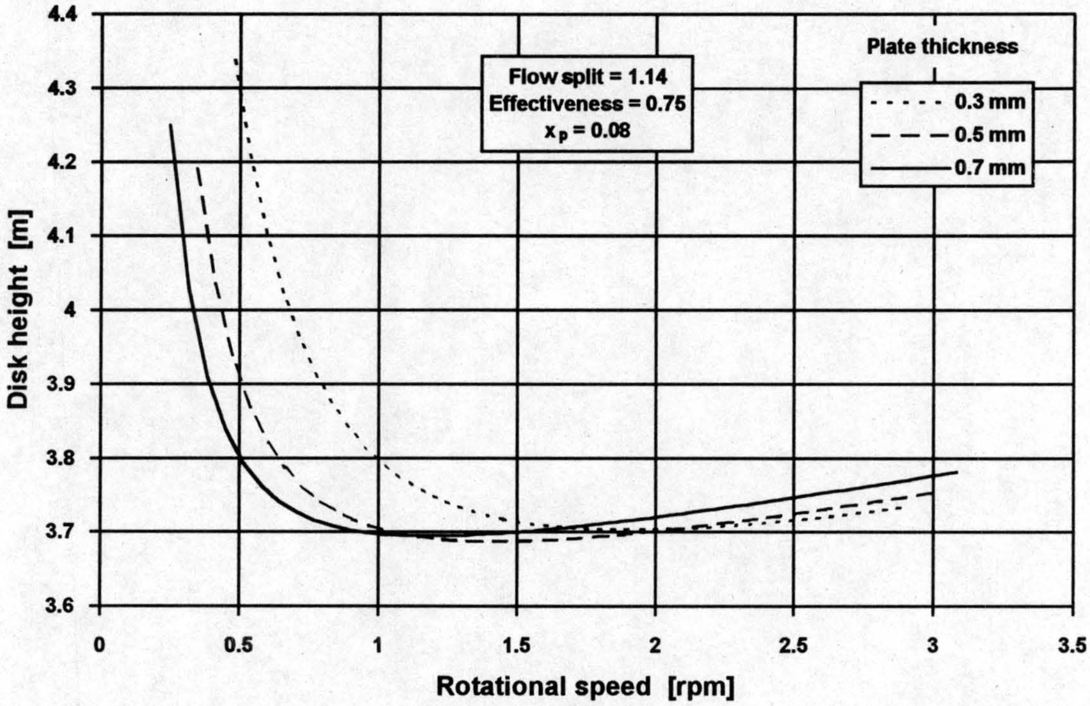

Figure 5.2: Optimum disk speed at minimum disk height for the 11A surface of Type 1 at a spacing of 5 mm.

In figures 5.3 and 5.4 it can be seen how the pressure drop and cost effectiveness parameter are influenced by the disk rotational speed and plate thickness. One expects that the pressure drop curves in figure 5.3 should have the same shape as the disk height curves in figure 5.2 showing a minimum pressure drop at the rotational speed where the disk height is a minimum. The pressure drop curves continue to drop with an increase in rotational speed, even beyond the point of minimum disk height. If the mass flow rates are constant the pressure drop is proportional to the disk height. As explained in Chapter 4 the pressure drop is evaluated over the internal regenerator. The mass flow rates for the hot and cold streams in the internal regenerator decrease with an increase in rotational speed since x_h and x_c increases. The mass flow rates for the internal regenerator can be seen in figure 3.1. The fact that the pressure drop does not show a minimum is an inherent weakness of the model shown in figure 3.1. The current model and proposed flow rates in the internal regenerator are accurate when determining the enthalpy and mass flow rates of the gas streams leaving the actual regenerator, but it is not certain whether the model correctly evaluates the pressure drop over the internal regenerator. Possibly better mass flow rates would be $W_h + x_p/2W_c$ for the hot side and at $(1-x_p/2)W_c$ for the cold side. The issue is however debatable since it is not sure what the influence of the leakage is on the matrix pressure drop.

The cost effectiveness curves in figure 5.4 also fail to show an optimum point. This can be attributed to the fact that the gas supply cost which is related to the pressure drop is the dominating cost. For this reason the optimum cost effectiveness parameter is defined as the value of the cost effectiveness parameter at the optimum disk height.

5.2.2 Effect of the flow split ratio

So far all the results were given for a hot gas to cold gas flow split ratio of 1.14. This was the optimum value obtained in the optimisation process. It was found that the flow split ratio does not have a significant influence on the minimum disk height or the rotational speed where this height occurs. Figure 5.5 shows how the optimum disk height varies with the flow split ratio. The effect of a change in the flow split ratio on the regenerator effectiveness is mainly reflected by changes in the dimensionless groups $(hA)^*$ and A_k^*. The flow split ratio does not have a significant influence on the other dimensionless groups. It was shown in Chapter 3 that the two above mentioned dimensionless groups do not have a significant influence on the regenerator effectiveness and can practically be eliminated from the solution process.

A more important role that the flow split ratio plays in the optimisation process is to balance the pressure drops for the hot and cold sides. Figure 5.6 shows how the hot and cold side pressure drops are influenced by the flow split ratio. It can be seen that the pressure drops are balanced near the optimum ratio of 1.14. This has the advantage of reducing the overall fan sizes needed to supply the gas.

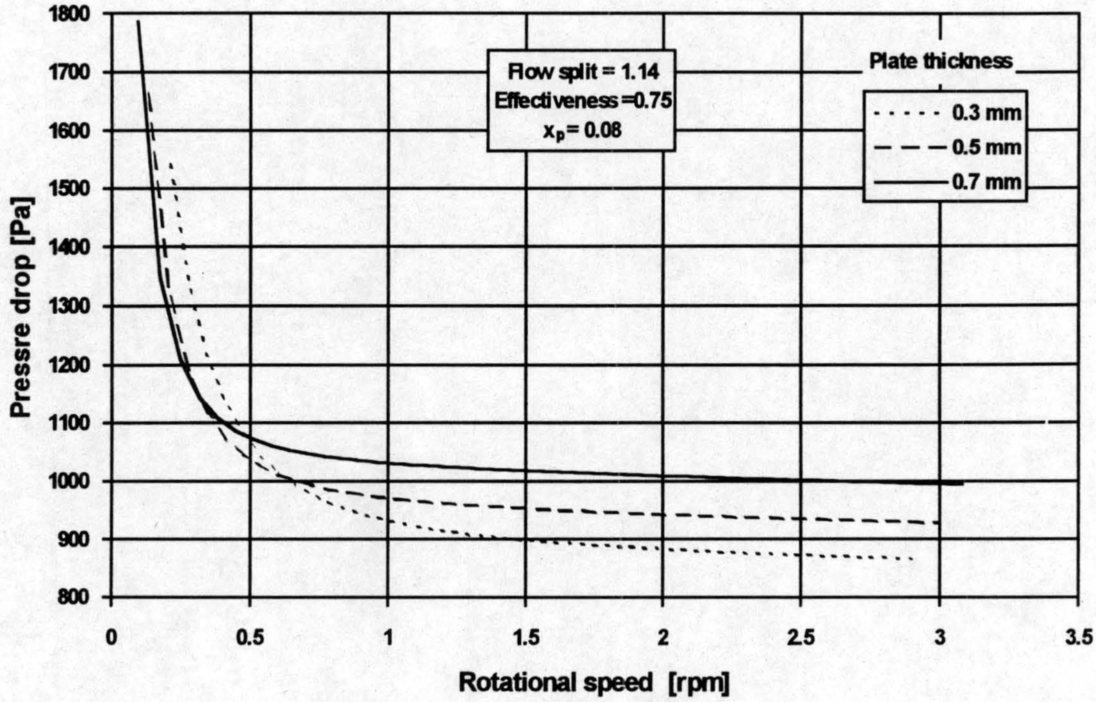

Figure 5.3: Matrix pressure drop at various plate thicknesses for the 11A surface of Type 1 at a spacing of 5 mm.

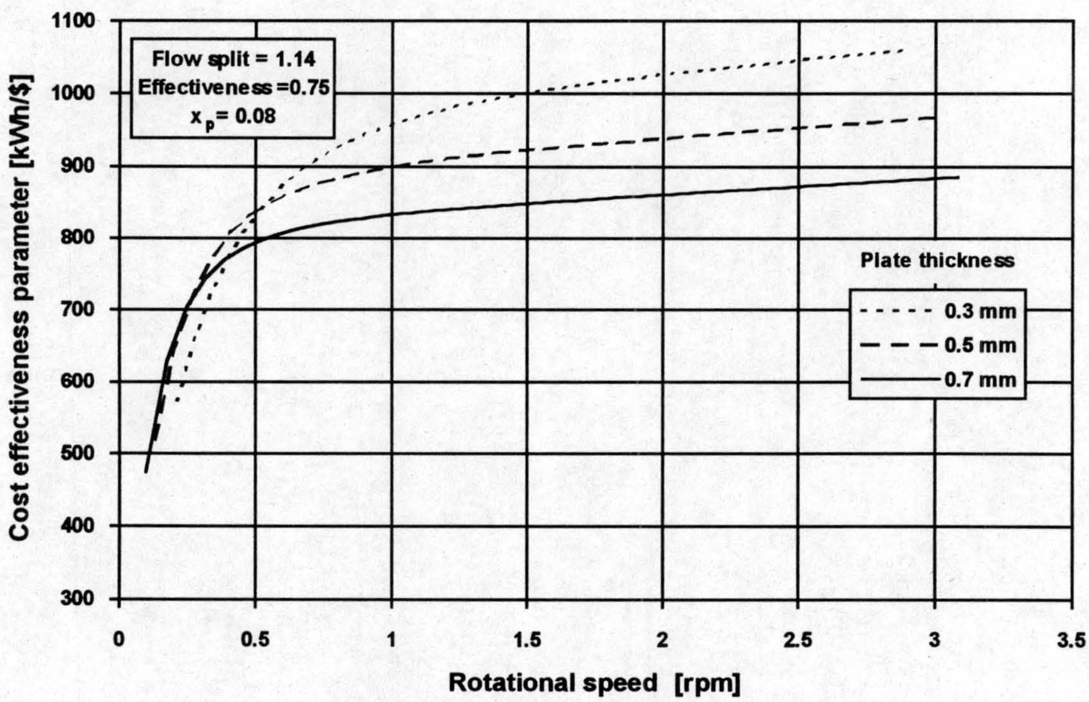

Figure 5.4: Cost effectiveness parameter at various plate thicknesses for the 11A surface of Type 1 at a spacing of 5 mm.

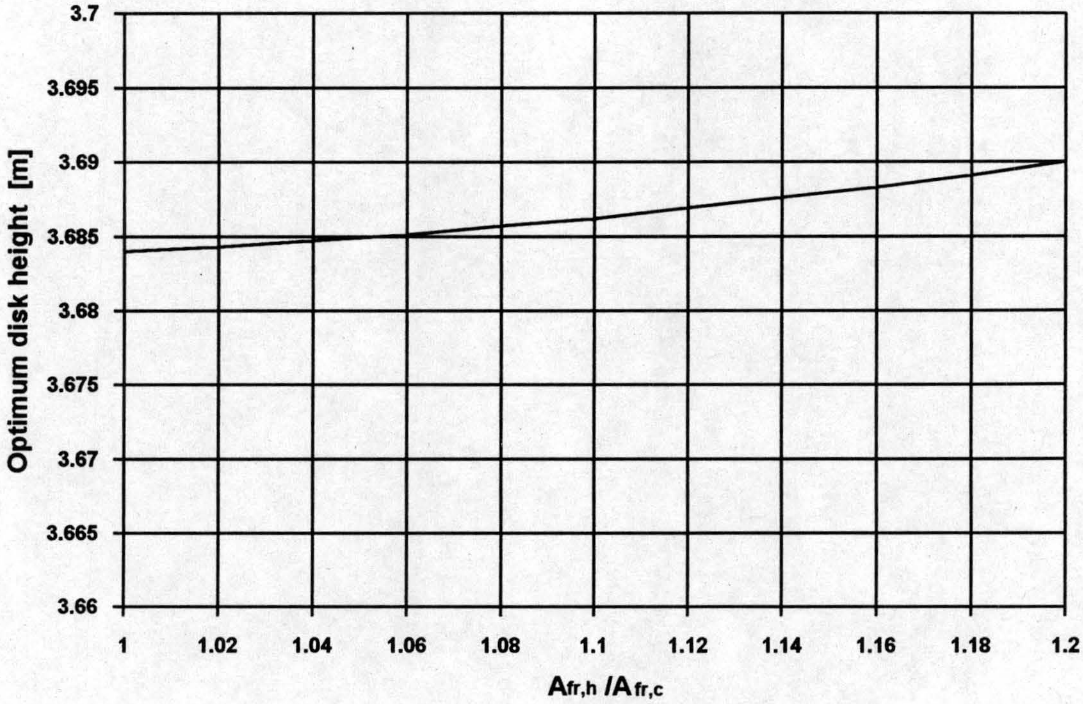

Figure 5.5: Effect of flow split ratio on optimum disk height. The plate thickness is 0.5 mm.

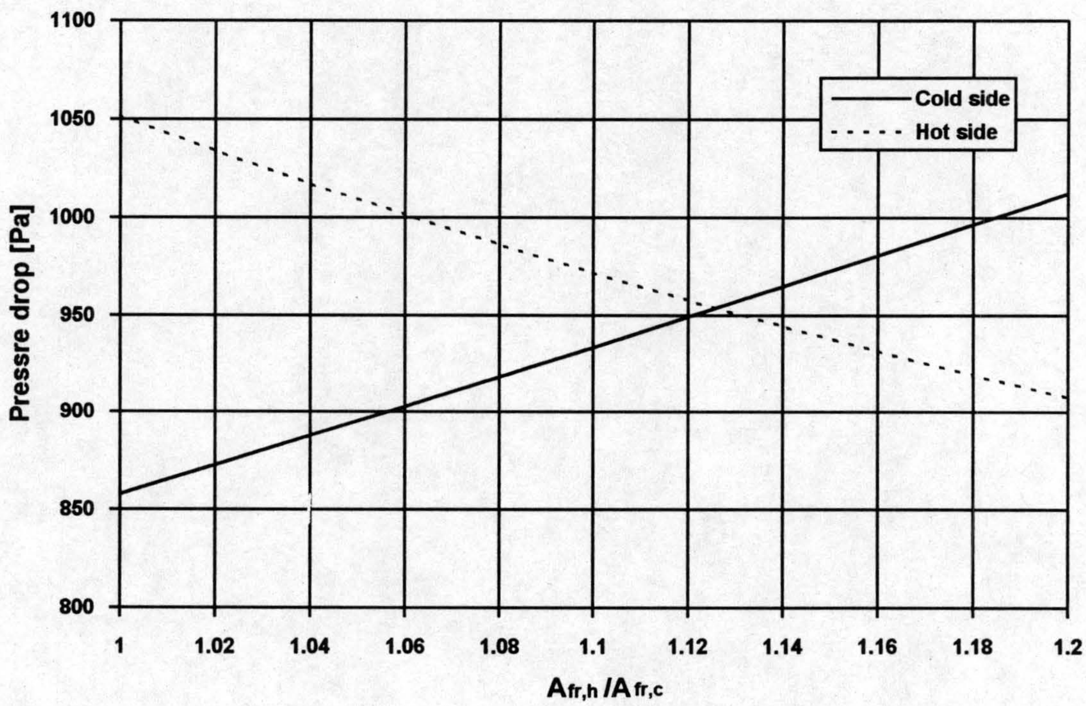

Figure 5.6: Effect of flow split ratio on hot and cold side pressure drop. The plate thickness is 0.5 mm.

5.3 REGENERATOR HEATING SURFACE OPTIMISATION AND SELECTION

In Appendix A it is described how numerous surfaces were tested for their heat transfer and pressure drop characteristics. For every surface at a fixed spacing, pressure drop and heat transfer correlations were determined. The correlations can be seen in tables A.3 to A.7 and graphical representations of the experimental data and correlations can be seen in figures A.14 to A.41.

In section 5.2 it was shown how the rotational speed, flow split ratio, plate thickness and disk height can be optimised for a single surface in a specified application. The next step in the optimisation process is to compare different surfaces with each other at their respective optimum operating conditions. For every surface the entire procedure as described in section 5.2 was repeated at different plate spacings. The optimisation parameters, optimum disk thicknesses and optimum rotational speeds of the surfaces are then compared. This was done for all the Type 2 surfaces at a spacing of 5 mm and all the Type 1 surfaces at a spacing of 5 mm, 3.5 mm and 3 mm.

5.3.1 Discussion of results

Four graphs are plotted for every range of surfaces at a certain spacing. The first type of graph is that which compares the cost effectiveness parameters of the different surfaces. These graphs can be seen in figures 5.7, 5.11, 5.15 and 5.19. Three different plate thicknesses are listed for every surface. In figure 5.7 the cost effectiveness parameter graph for the Type 1 surfaces at a spacing of 5 mm can be seen. It is evident from the graph that for every surface the cost effectiveness parameter increases as the plate thickness decreases. For practical reasons the plate thickness cannot be made too thin. For example in applications where the hot gas contains sulphur trioxide and the matrix temperature falls below the acid dew point, corrosion will occur. This necessitates the use of thicker sheet thicknesses or corrosion resistant materials. Abrasion of the heating surfaces can occur if the gases contain small particles of some nature. The designer should therefore choose the thinnest practical sheet thickness, taking into consideration the above mentioned factors and the expected life of the regenerator. In figure 5.7 the 1A surface which is the normal flat surface is the most cost effective with the 11A, 3A and 12B surfaces also doing well. Similar trends can be seen in figures 5.11, 5.15. Figure 5.19. is for the Type 2 surfaces at a spacing of 5 mm. The exception perhaps is the 11A surface which has the highest cost effectiveness parameter at a spacing of 3.5 mm.

In Appendix A it can be seen from the graphs of the test results of the 11-series of surfaces that the heat transfer rates increases as the height of the waves into the plane of the surface (measurement D in figure D.5) increases. On the other hand the pressure drop increases as well and in proportion it increases more than the heat transfer rate. The effectiveness ratio, Ny/K, therefore decreases with an increase in D. Similarly the cost effectiveness parameter decreases with an increase in D as can be seen in figures 5.7, 5.11 and 5.15. Similar trends can be established for the 3-series and 12-series surfaces of Type 1.

The cost effectiveness parameter is an important criterion in evaluating the performance of a surface. Another factor which should be considered is the disk height. In figures 5.8, 5.12, 5.16 and 5.20 the disk heights for the different surfaces can be seen. It is clear from all the figures that the plate thickness does not have a large influence on the optimum disk height. For the Type 1 surfaces the 1A, 11A, 3A and 12B surfaces have comparable cost effectiveness parameters at the 5 mm and 3.5 mm spacings, but the 1A surface requires by far the largest disk height. This may be a practical drawback. In cases where the gases are not clean, fouling of the surfaces can be anticipated. If the disk height is too large cleaning of the surfaces may become a problem. Space constraints may also limit the allowable disk height. The 1A and 2A surfaces have the highest cost effectiveness parameters of the Type 2 surfaces, but their disk heights are the largest. The disk height decreases as the characteristic heat transfer parameter of the surfaces increases.

One of the major disadvantages of a rotary regenerator is that there is some intermixing of the gas streams. In some applications this is not allowable and then a rotary regenerator cannot be used. In other applications intermixing may be allowable, but the amount of leakage must be limited. A large disk height and a high rotational speed contribute to intermixing. It is therefore necessary to check that the disk rotational speed is within limits. In figures 5.9, 5.13, 5,17 and 5.21 the optimum disk rotational speed for the surfaces can be seen. It is interesting to note that in the cases where the disk height is the largest, the rotational speed is the lowest. This is an advantage since it helps to limit the gas intermixing. It was found that at the optimum operating point the leakage fractions x_c and x_h were very similar for the different surfaces.

The cost effectiveness parameter considers two costs. The cost of the electrical power input to the fans for the gas supply and the matrix material cost. It was found that the electrical power input cost was the dominating cost. For this reason it was decided to vary the unit electricity cost to change the relative importance of the two costs involved. The unit electricity cost was taken as 5 cents for the results discussed so far. Values of 2.5 and 10 cents per unit were also used to see what effect they have on the surface selection. When the unit electricity cost is lowered and therefore the importance of the material cost rises, surfaces like 1A that requires a high disk height will perform less well against its competitors. The opposite is also true. When the unit electricity cost is altered the value of the cost effectiveness parameter changes and it does not make sense to compare them with each other. For this reason a relative cost effectiveness parameter is defined. It is simply the value of the cost effectiveness parameter for the surface divided by the value for the 1A surface. The 1A surface is thus taken as a reference. The effect of the varying unit electricity cost can be seen in figures 5.10, 5.14, 5.18 and 5.22. In these figures the plate thickness was taken constant at 0.5 mm.

From the discussion so far it is evident that it is impossible to say that a specific surface is the most suitable for the application under consideration. The best we can hope for is to highlight a few potentially 'good' surfaces by comparing their cost effectiveness parameters. Which one of these surfaces will be the best for the specific application will ultimately be decided by the practical constraints of the system. For example looking at the Type 1 surfaces we can say that the surfaces 1A, 11A, 3A and 12B have potential. Possible space limitations may cause the 1A surface to be unacceptable. The 11A surface then seems to be the most promising one. If we consider the effect of the plate spacing, the highest cost effectiveness parameters are obtained at the 5 mm spacing. On the other hand the optimum disk height is much higher at the 5 mm spacing than at the 3.5 mm or 3 mm spacing. Once again we may have to consider the less cost effective system if there is a limit on the disk height.

In general the Type 2 surfaces seem to have less potential than the Type 1 surfaces if we consider their cost effectiveness parameters. The Type 2 surfaces on the other hand have a coarser pattern and may be less prone to foaling than the finer patterned Type 1 surfaces.

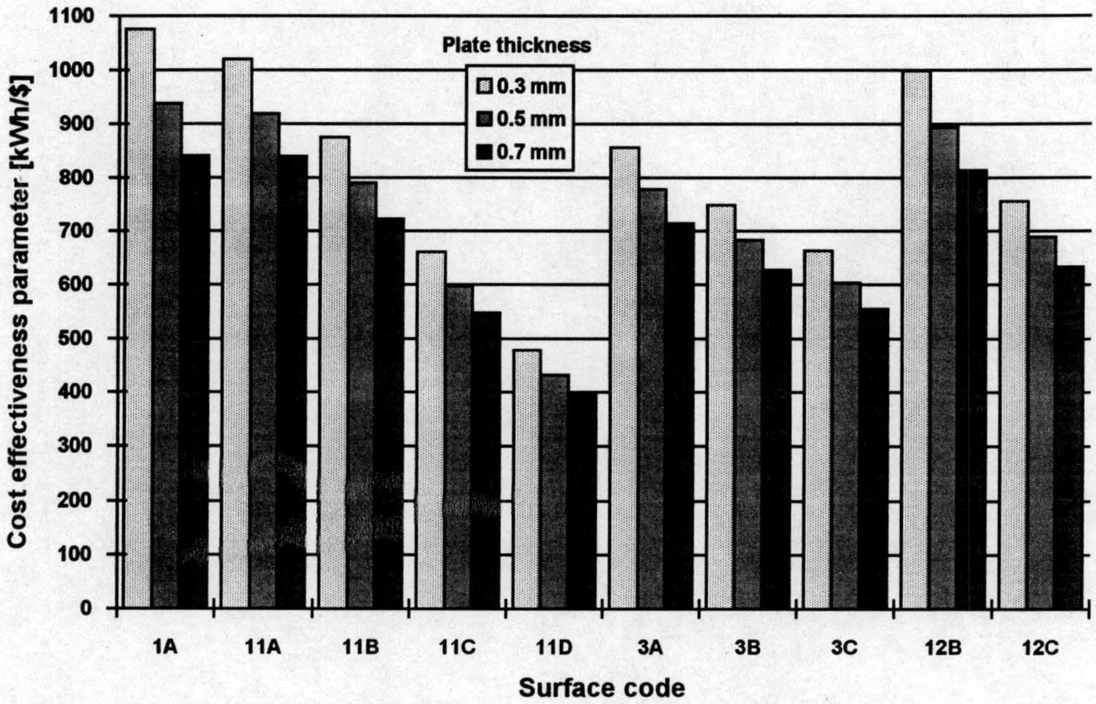

Figure 5.7: Cost effectiveness parameters at the optimum operating point for different surfaces of Type 1 at a spacing of 5 mm.

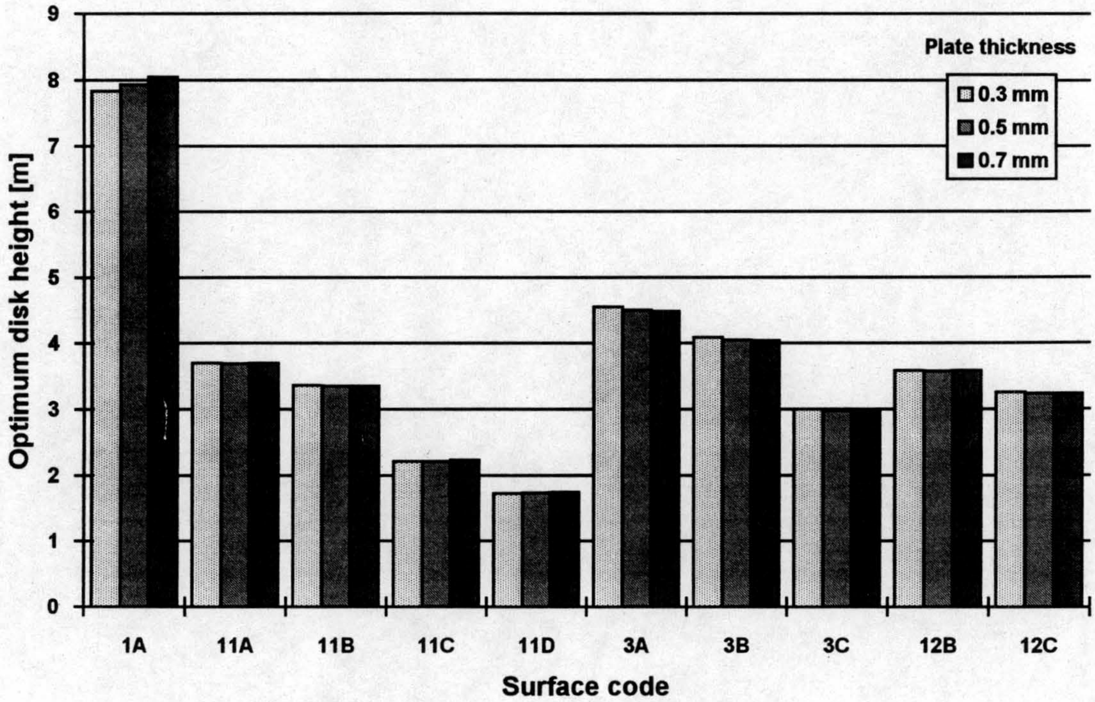

Figure 5.8: Optimum disk height for different surfaces of Type 1 at a spacing of 5 mm.

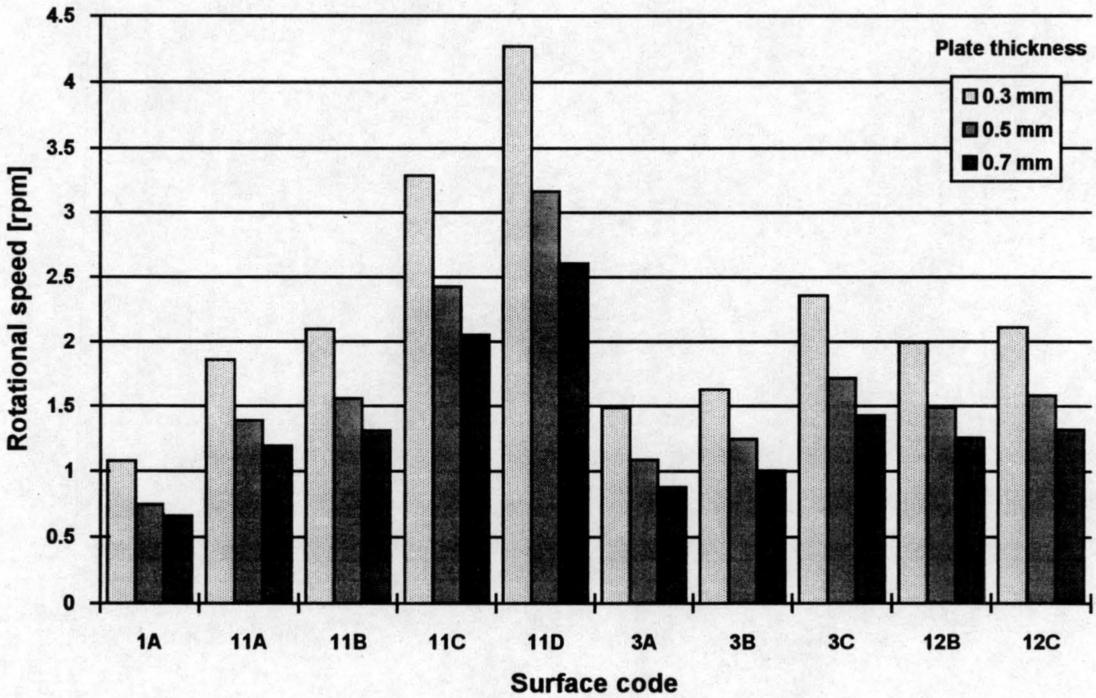

Figure 5.9: Rotational speed at the minimum disk height for different surfaces of Type 1 at a spacing of 5 mm.

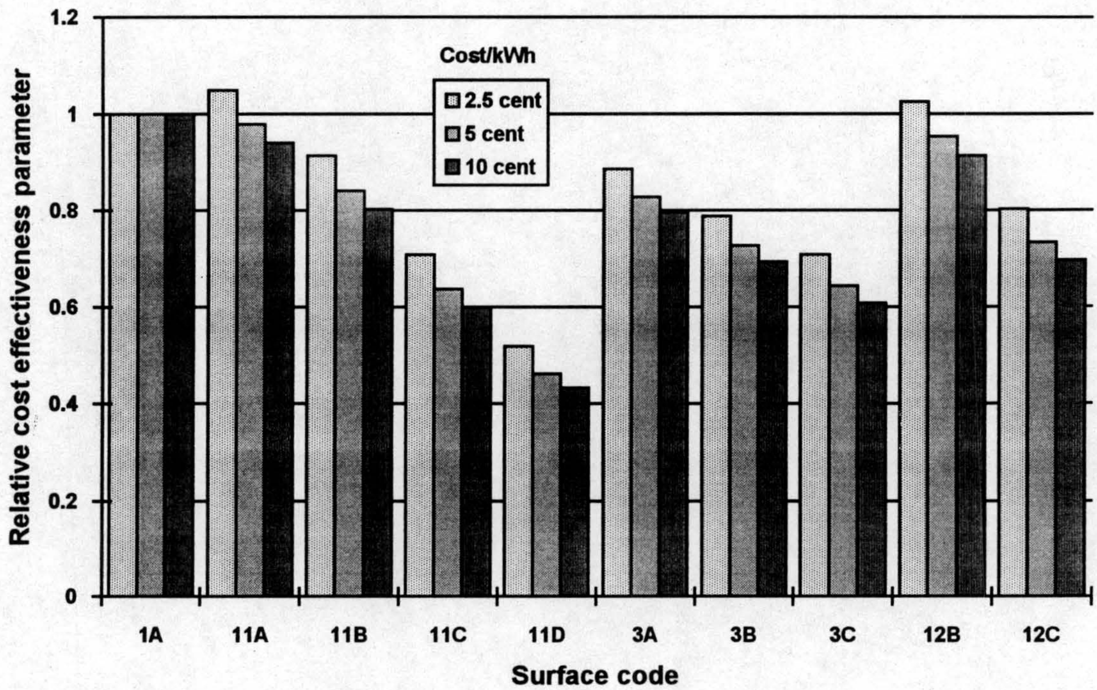

Figure 5.10: The effect of varying electricity cost on the relative cost effectiveness parameter at the optimum operating point for different surfaces of Type 1. The plate thickness is 0.5 mm and the spacing is 5 mm.

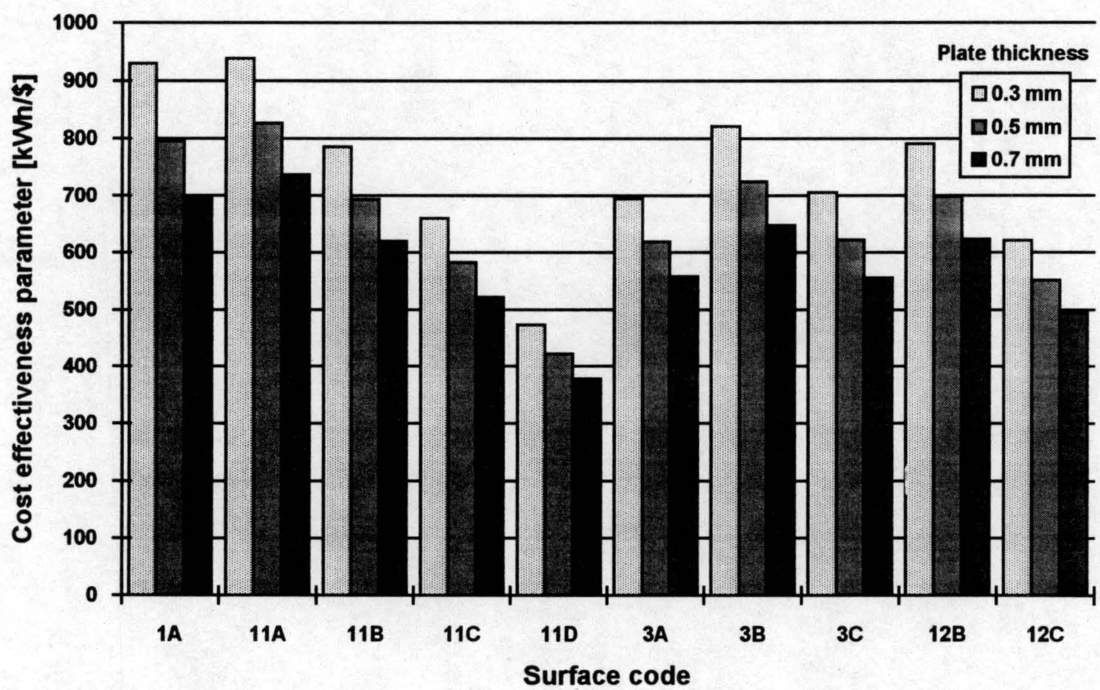

Figure 5.11: Cost effectiveness parameters at the optimum operating point for different surfaces of Type 1 at a spacing of 3.5 mm.

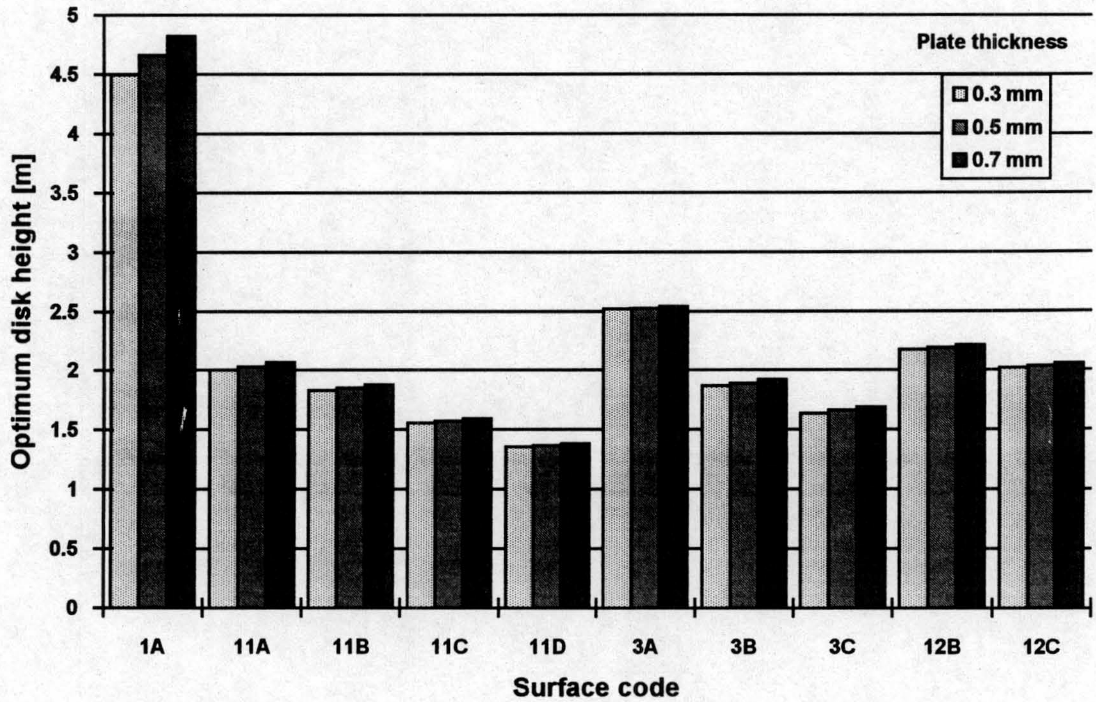

Figure 5.12: Optimum disk height for different surfaces of Type 1 at a spacing of 3.5 mm.

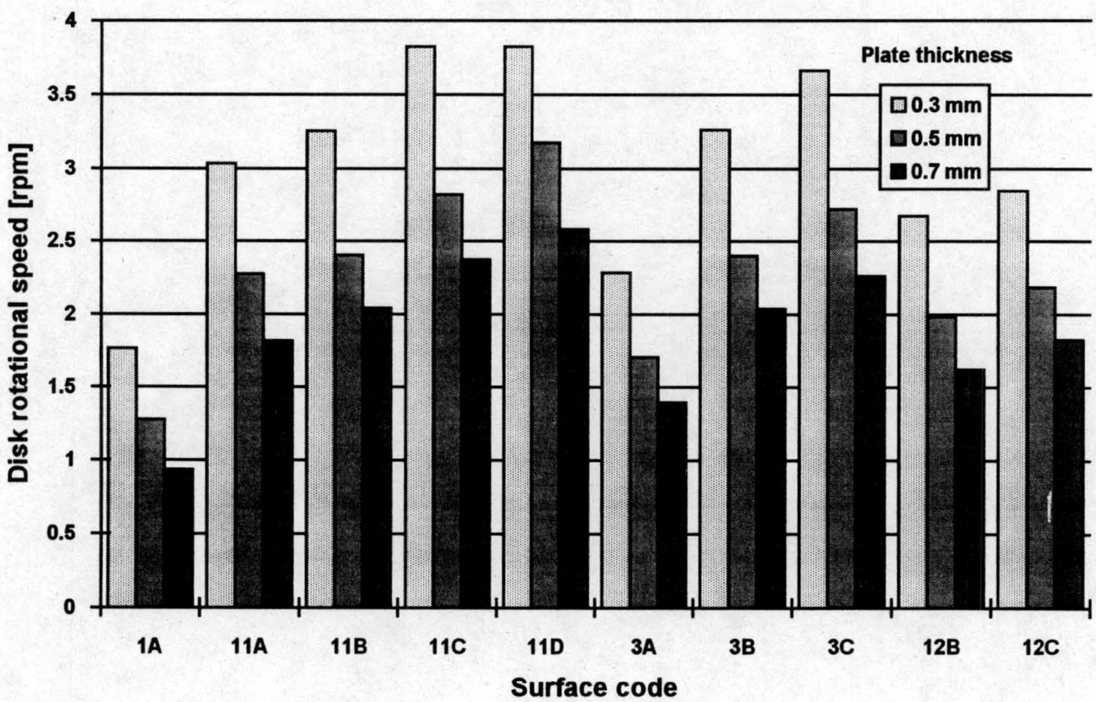

Figure 5.13: Rotational speed at the minimum disk height for different surfaces of Type 1 at a spacing of 3.5 mm.

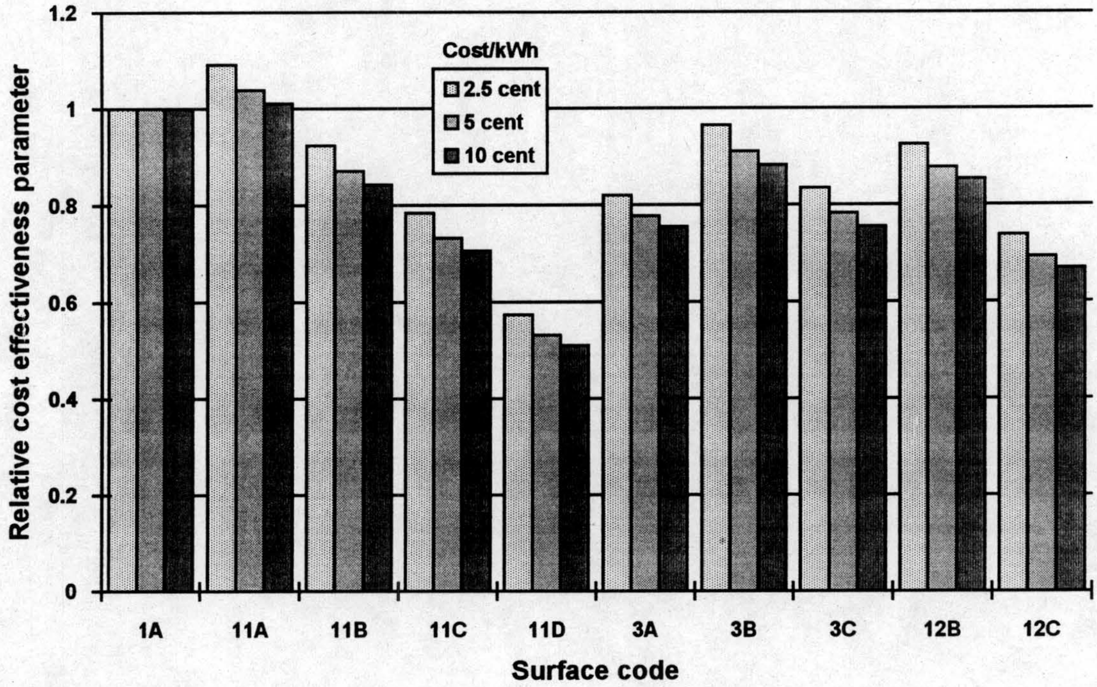

Figure 5.14: The effect of varying electricity cost on the relative cost effectiveness parameter at the optimum operating point for different surfaces of Type 1. The plate thickness is 0.5 mm and the spacing is 3.5 mm.

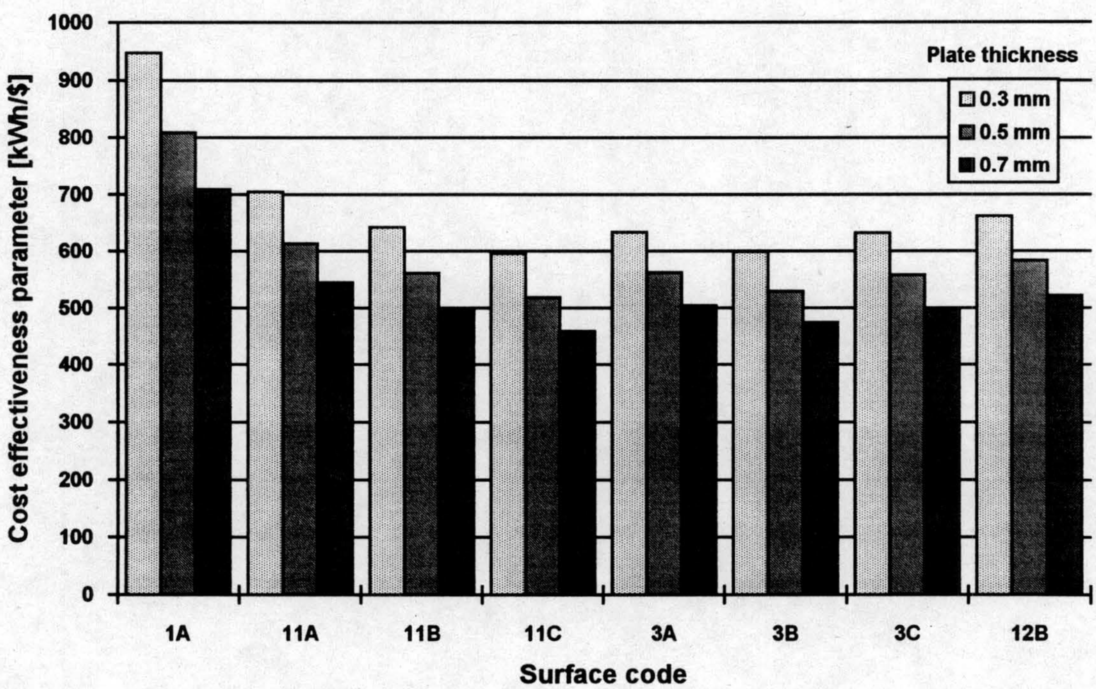

Figure 5.15: Cost effectiveness parameters at the optimum operating point for different surfaces of Type 1 at a spacing of 3 mm.

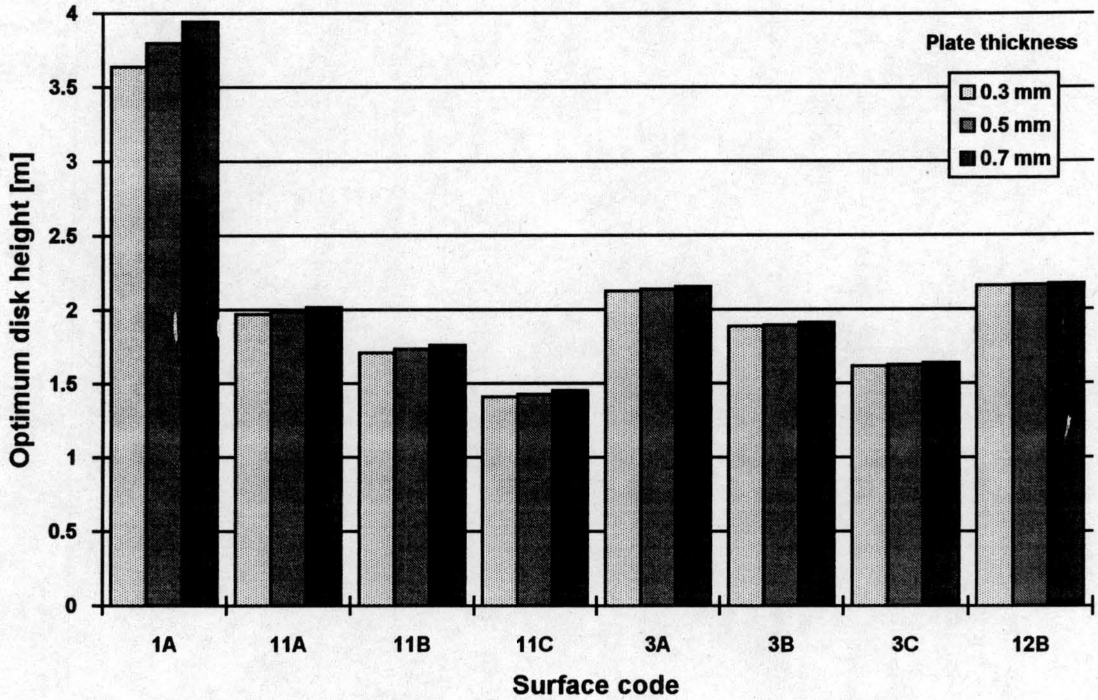

Figure 5.16: Optimum disk height for different surfaces of Type 1 at a spacing of 3 mm.

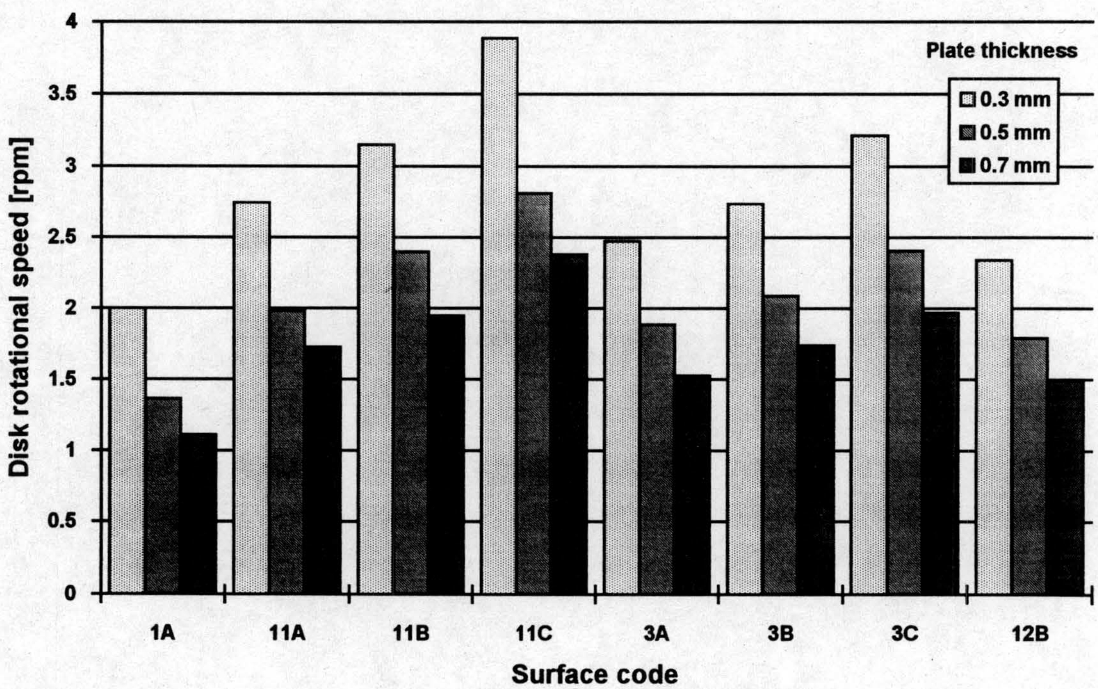

Figure 5.17: Rotational speed at the minimum disk height for different surfaces of Type 1 at a spacing of 3 mm.

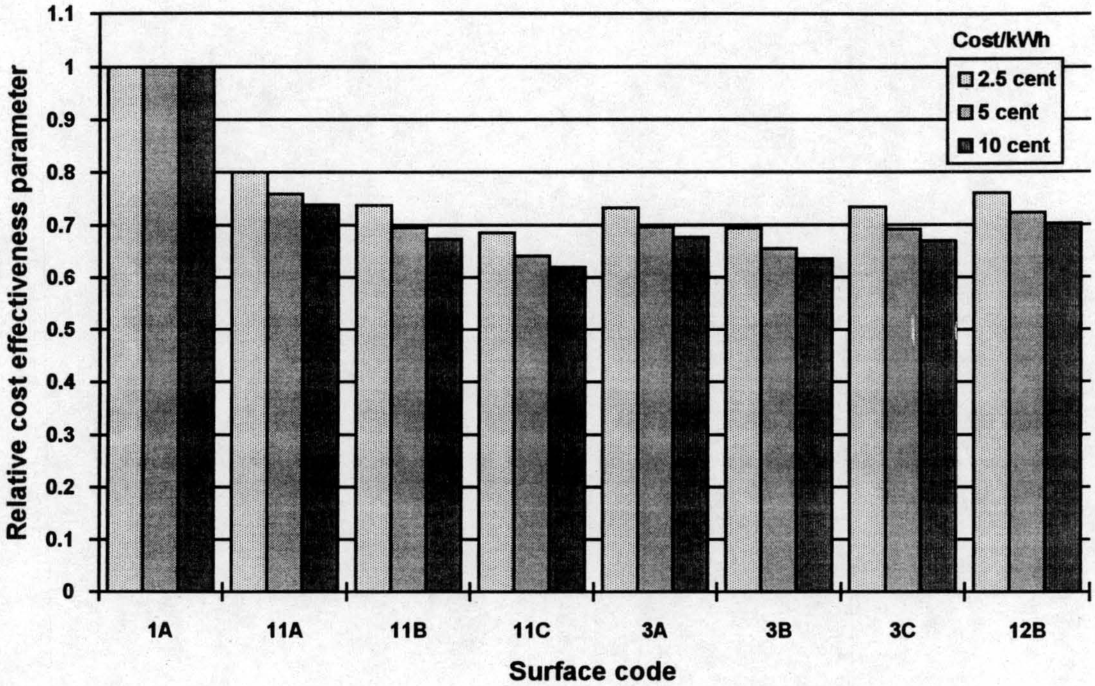

Figure 5.18: The effect of varying electricity cost on the relative cost effectiveness parameter at the optimum operating point for different surfaces of Type 1. The plate thickness is 0.5 mm and the spacing is 3 mm.

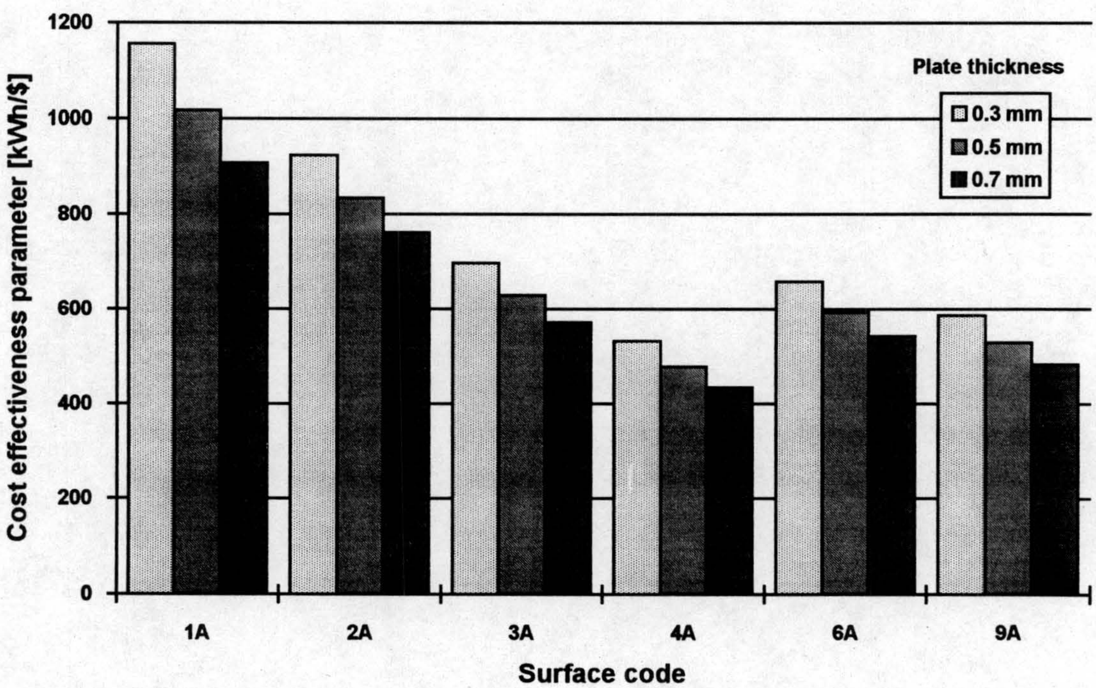

Figure 5.19: Cost effectiveness parameter at the optimum operating point for different surfaces of Type 2 at a spacing of 5 mm.

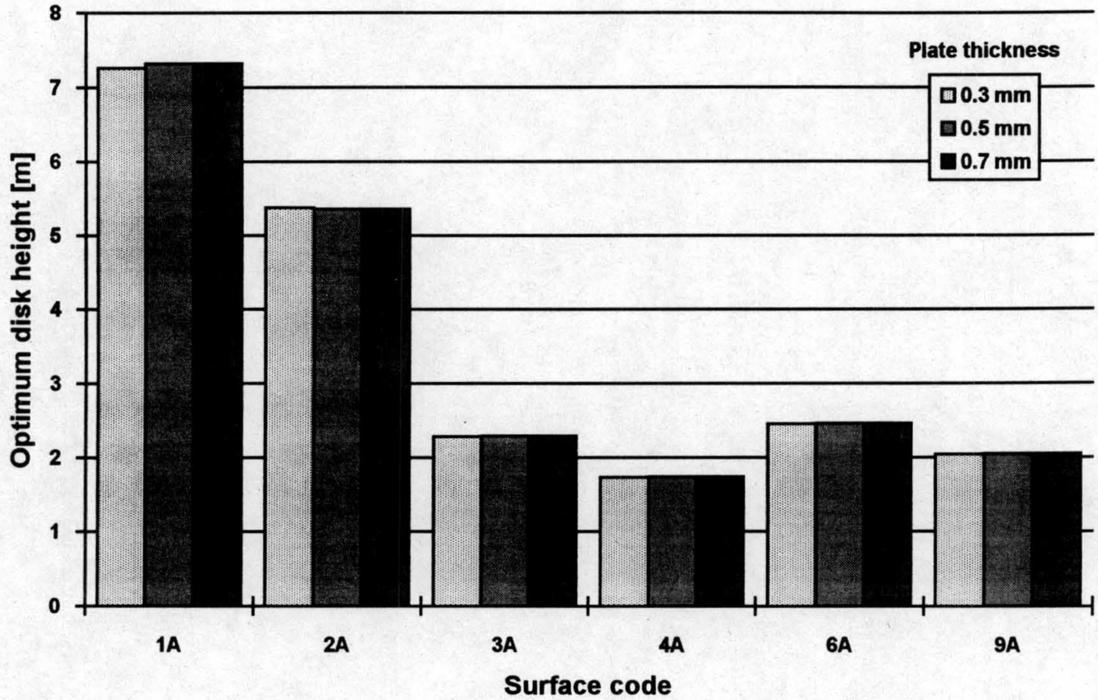

Figure 5.20: Optimum disk height for different surfaces of Type 2 at a spacing of 5 mm.

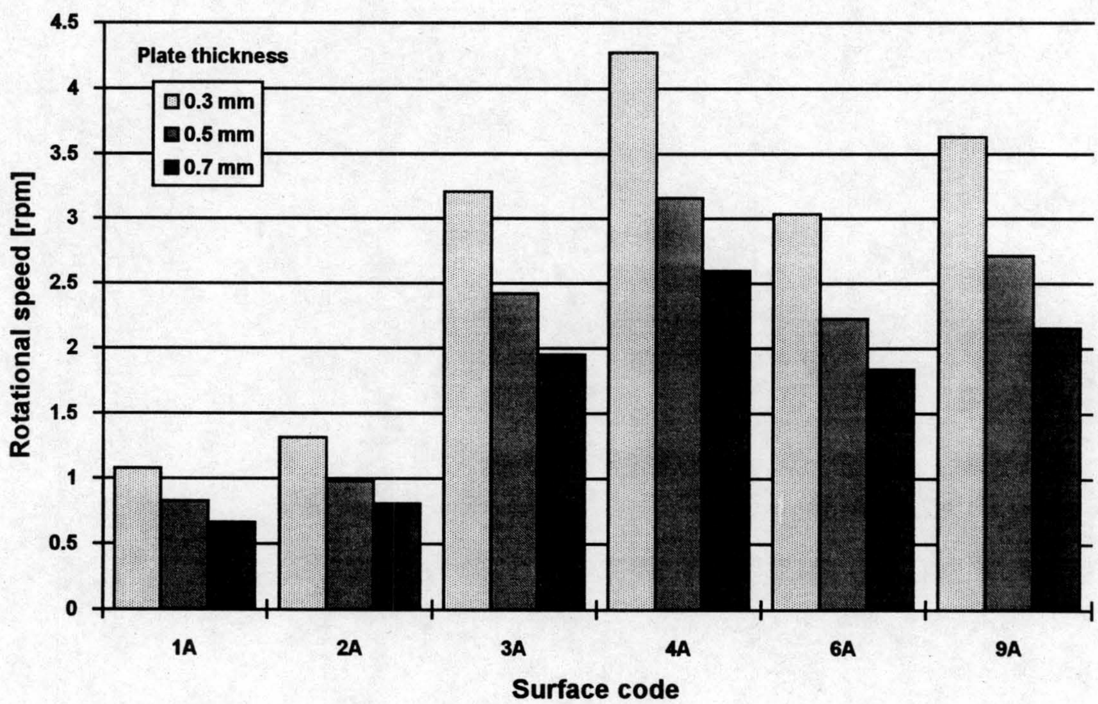

Figure 5.21: Rotational speed at the minimum disk height for different surfaces of Type 2 at a spacing of 5 mm.

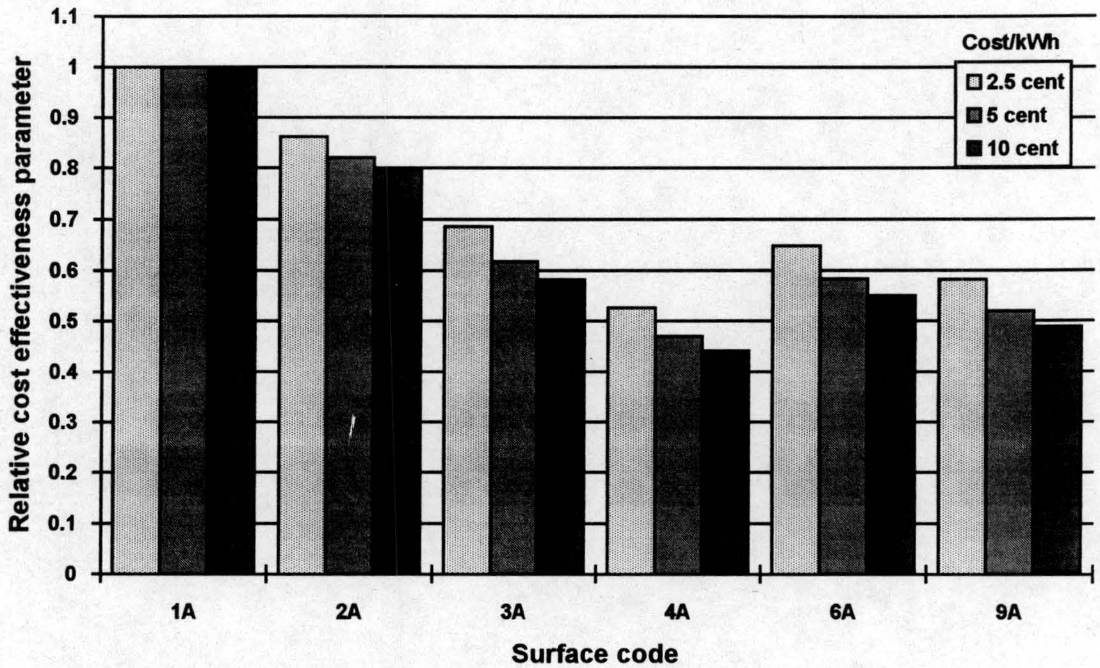

Figure 5.22: The effect of varying electricity cost on the relative cost effectiveness parameter at the optimum operating point for different surfaces of Type 2. The plate thickness is 0.5 mm and the spacing is 5 mm.

CHAPTER 6

CONCLUSION

6.1 DESIGN THEORY AND SOLUTIONS FOR A COUNTERFLOW REGENERATOR

It was shown that in the absence of pressure- or carryover leakage the effectiveness of a rotary regenerator is dependant on six dimensionless parameters.

$$\varepsilon = f\left(Ntu_o, (hA)^*, C_r^*, C^*, \lambda, A_k^*\right)$$

There is no solution available for the full differential equations and boundary conditions. The dimensionless parameters were chosen in such a fashion that the regenerator theory parallels that of recuperators for which theoretical solutions exist. Another advantage of the choice of dimensionless parameters is that two parameters, namely $(hA)^*$ and A_k^* have a minimal influence on the effectiveness. It was shown by various authors that their influence on the effectiveness can be ignored for practical design purposes [58LA1], [64BA1].

Numerous approximate solutions are available for the ideal regenerator, covering the remaining four dimensionless parameters. The approximate theories mainly make use of recuperator analysis. The regenerator theory parallels that of recuperators for the case of infinite rotational speed. The influence of the rotational speed on the effectiveness is then correlated from accurate numerical results. Equation (3.3) is such a correlation which is widely used. Equation (3.9) is presented which is substantially more accurate than equation (3.3), especially at high Ntu_o numbers. Equation (3.8) is also very accurate for accounting for the influence of the rotational speed, but the computing time needed is similar to that of finite difference methods. In section 3.5 an approximate solution method is presented for the effectiveness of an ideal regenerator. The accuracy of the solution method was compared to accurate numerical results covering all six dimensionless parameters. The maximum error was 1.7 % for ranges of the dimensionless parameters which is sufficient to cover all regenerator applications. In Chapter 3 it is also shown how to account for the loss in effectiveness due to pressure- and carryover leakage.

A computer program was written employing both the approximate theory and a finite difference method to thermally evaluate or design a counterflow rotary regenerator. The Design option of the program allows for the optimisation of some of the operating conditions if the regenerator effectiveness is specified. It was shown by an example what the influence of the disk rotational speed, flow split ratio and matrix wall thickness are on the minimum required surface area and the cost effectiveness parameter. The disk rotational speed is the most important optimisation variable if the regenerator matrix is fixed. The required disk height shows a minimum value at the optimal rotational speed. The disk height increases drastically if the rotational speed is lowered beyond a certain value. The designer should make sure that the rotational speed is high enough to avoid this situation, but within limits to avoid excessive fluid intermixing. It was found that the cost effectiveness increases with a decrease in plate thickness. The thinnest possible sheets should therefore be used but practical considerations like corrosion and abrasion should be kept in mind. The flow split ratio does not have a significant effect on the minimum disk height. The flow split ratio can however be used to balance the hot- and cold side pressure drop.

6.2 EXPERIMENTAL TESTING OF HEATING SURFACES AND COMPARISON IN REGENERATOR SYSTEM

Several heating surface shapes and spacings were tested for their heat transfer and pressure drop characteristics. The experimental apparatus was shown to produce reasonably accurate results, taking into consideration the small quantities measured and the transitional nature of the flow. The heat transfer data is presented as a parameter, Ny and the pressure drop data by a loss coefficient K. The effectiveness parameter Ny/K is used to investigate the increase in heat transfer relative to an increase in pressure drop for the enhanced surfaces. A plain flat surface was used as a reference. It was found that mostly when a surface is enhanced to improve the heat transfer rate (Ny) the pressure drop increases even more, resulting in a decrease in Ny/K when compared to a flat surface. The 11A, 3A and 12B surfaces produced the best results relative to the flat surface when their effectiveness ratios are compared.

The effectiveness ratio does not take into consideration the fact that less surface area is required for a specified heat transfer rate when the surfaces are enhanced. The surfaces were therefore compared to each other in a specific application and a cost effectiveness parameter was defined for comparison purposes. The 11A, 3B and 12B surfaces once again produced the best results relative to the flat (1A) surface. The 11A surface seems to be the most promising surface taking into consideration the cost effectiveness parameter and the optimum disk height. It is however difficult to choose the most suitable surface if all the practical limitations of the application are not known.

6.3 RECOMMENDATIONS AND LIMITATIONS

The acquired experimental data can only be used to compare the surfaces among themselves. The size of the surfaces tested was not large enough to establish fully developed hydraulic and thermal conditions. The loss coefficient includes the inlet and exit losses. This results in errors when the correlations are extrapolated to different disk heights. Experimental studies should be conducted under conditions so that the results can be compared to other heating surfaces used in practice. Abrasion, corrosion and fouling tests should be conducted as well since these are important practical considerations for heating surfaces.

The program has the disadvantage that it assumes a single layered layout regenerator matrix. Multi layered layouts are sometimes used for practical reasons. If the program is considered to be upgraded further, this would be the most valuable improvement.

REFERENCES

48HA1 Hahnemann, H.W., Approximate Calculation of Thermal Ratios in Heat Exchangers Including Heat Conduction in Direction of Flow, National Gas Turbine Research Establishment Memorandum No. 36, TPA3/TIB, Ministry of Supply, Millbank, London, SW1, 1948.

51SA1 Saunders, O.A. and Smoleniec, S., Heat Transfer in Regenerators, *IME-ASME General Discussion on Heat Transfer*, pp. 443-445, London, England, September 1951.

53CO1 Coppage, J.E and London, A.L., The Periodic-Flow Regenerator - A Summary of Design Theory, *Trans. ASME*, Vol. 75, pp. 779-787, 1953.

58LA1 Lambertson, T.J., Performance Factors of a Periodic-Flow Heat Exchanger, *Trans. ASME*, Vol. 80, pp. 586-592, 1958.

64BA1 Bahnke, G.D. and Howard, C.P., The Effect of Longitudinal Heat Conduction on Periodic-Flow Heat Exchanger Performance., *J. Eng. Power*, Vol. 86A, pp. 105-120, 1964.

66GR1 Gram, A.J. and Kessler, G.W., New Regenerative Air Heater, *Mechanical Engineering*, pp. 45-47, September 1966.

67KR1 Kroeger, P.G., Performance Deterioration in High Effectiveness Heat Exchangers Due to Axial Heat Conduction Effects., *Advances in Cryogenic Engineering*, Vol. 12, pp. 363-372, 1967.

75GN1 Gnielinski, V., Forsch. Ing. Wessen, Vol. 41, No. 1, 1975.

75SH1 Shah, R.K., A Correlation for Longitudinal Heat Conduction Effects in Periodic-Flow Heat Exchangers, *J. Eng. Power*, Vol. 97A, pp. 453-454, 1975.

75SH2 Shah, R.K., Thermal Entry Length Solutions for Circular Tube and Parallel Plates, Proc. 3rd Natl. Heat Mass Transfer Conf., Indian Inst. Technol., Bombay, Vol. 1, Pap. No. HMT-11-75, 1975.

78SH1 Shah, R.K. and London, A.L., *Laminar Flow Forced Convection in Ducts*, Academic Press, New York, 1978.

79HE1 Heggs, P.J. and Carpenter, K.J., A Modification of the Thermal Regenerator Infinite Conduction Model to Predict the Effects of Intraconduction, *Trans IChemE*, Vol. 57, pp. 228-236, 1979.

79RA1 Razelos, P., An Analytical Solution to the Electric Analog Simulation of the Regenerative Heat Exchanger with Time-Varying Fluid Inlet Temperatures, *Wärme und Stoffubertrag*, Vol. 12, pp. 59-71, 1979.

80HE1 Heggs, P.J., Bansal, L.S., Bond, R.S. and Vazakas, V., Thermal Regenerator Design Charts Including Intraconduction Effects, *Transactions of Industrial Chemical Engineering*, Vol. 58, pp. 265-270, 1980.

81SH1 Shah, R.K., Thermal Design Theory for Regenerators, in *Heat Exchangers: Thermal Hydraulics Fundamentals and Design*, eds. S Kakaç, A.E. Bergles, and F. Mayinger, pp. 721-763, Hemisphere, Washington, DC, 1981.

82AN1 Anon., *Heat Transfer and Fluid Flow Data Book*, General Electric Co., Corporate Research Division, New York, 1982.

82WA1 Warren, I., Ljungstrom Heat Exchangers for Waste Heat Recovery, *Heat Recovery Systems*, Vol. 2, No. 3, pp. 257-271, 1982.

83CH1 Chung-Hsiung Li, A Numerical Finite Difference Method for Performance Evaluation of a Periodic-Flow Heat Exchanger, *Journal of Heat Transfer,* Vol. 105, pp. 611-617, August 1983.

83HA1 Haaland, S.E., Simple and Explicit Formulas for the Friction Factor in Turbulent Pipe Flow, *Trans. ASME J. Fluids Engineering*, Vol. 105, No. 3, pp. 89-90, March 1983.

84 Regeneration and Thermal Energy Storage, in *Thermal and Hydraulic Design of Heat Exchangers*, VDI Verlag, Section 3.15, Hemisphere Publishing Corporation, 1984.

84KA1 Kays, W.M. and London, A.L., *Compact Heat Exchangers*, 2nd ed., McGraw-Hill, New York, 1984.

84WO1 Woodruff, E.B., Lammers, H.B., and Lammers, T.F., *Steam Plant Operation*, Fifth Edition, McGraw-Hill Book Company, New York, 1984.

85BA1 Baclic, B.S., The Application of the Galerkin Method to the Solution of the Symmetric and Balanced Counterflow Regenerator Problem., *J. Heat Transfer*, Vol. 107, pp. 214-221, 1985.

86KR1 Kröger, D.G., Performance Characteristics of Industrial Finned Tubes Presented in Dimensional Form, *Int. J. Heat Mass Transfer*, Vol. 29, No. 8, 1986.

87BA1 Blackwell, B., *Thermodynamic and Transport Properties of Fluids*, Third edition, Great Britain, 1987.

88RO1 Romie, F.E and Baclic, B.S., Methods of Rapid Calculation of the Operation of Asymmetric Counterflow Regenerators, *Journal of Heat Transfer*, Vol. 110, pp. 785-788, August 1988.

88SH1 Shah, R.K., Counterflow Rotary Regenerator Thermal Design Procedures, in *Heat Transfer Equipment Design*, eds. R.K. Shah, E.C. Subbarao and R.A. Mashelkar, pp. 267-296, Hemisphere, New York, 1988.

89SC1 Scaricabarozzi, R., Simple Particular Solutions and Speed Calculation of Regenerators, *Heat Recovery Systems & CHP*, Vol. 9, pp 421-432, 1989.

91LE1 Leong, K.C., Toh, K.C. and Wong, S.H., Microcomputer-Based Design of Rotary Regenerators, *Heat Recovery Systems & CHP*, Vol. 11, No. 6, pp. 461-470, 1991.

90RO1 Romie, F.E., A Table of Regenerator Effectiveness, *Journal of Heat Transfer*, Vol. 112, pp. 497-499, May 1990.

91KA1 Kakaç, S. et. al., *Boilers, Evaporators and Condensers*, John Wiley & Sons, Inc., New York, 1991.

91RO1 Romie, F.E., Treatment of Transverse and Longitudinal Heat Conduction in Regenerators, *J. Heat Transfer*, Vol. 113, pp. 247-249, 1991.

APPENDIX A

Experimental apparatus and procedures for the testing of surfaces for their heat transfer and pressure drop characteristics

A.1 INTRODUCTION

According to the type of transfer process, heat exchangers can be classified into direct contact and indirect contact type heat exchangers. In direct contact types the two transfer fluids mix whereas in indirect contact types the heat transfer is through a separating wall. A regenerator is an example of an indirect contact type heat exchanger. The heat is not transferred through a separating wall, but alternatively stored and rejected by the wall. The hot fluid flows over a matrix and heats up the matrix material. The cold fluid then later flows over the heated matrix and the heat is rejected to the cold fluid. In a regenerator the heat transfer process is usually between two gas streams. The convective heat transfer coefficient for gases can be an order or two lower than for liquids like water. To reduce the size of gas to gas or gas to liquid heat exchangers the heat transfer surface on the gas side must be highly efficient.

An efficient or good surface is one that induces a high heat transfer coefficient between the surface and a fluid while the pressure drop is low. In this experimental study different surfaces were tested for their heat transfer and pressure drop characteristics for potential application in regenerators. The experimental set-up and procedures are described. and it is shown how the data is processed into a form where it can be used for heat exchanger design.

A.2 DESCRIPTION OF EXPERIMENTAL APPARATUS

A.2.1 Test section

A schematic drawing of the test section can be seen in figure A.1. Two plates (1) of the surface to be tested are inserted into the test section where they are set at a prescribed spacing by a spacer (2). An example of a test surface can be seen in figure A.2. A steam chamber block (3) is pressed against the back of each surface. Each steam chamber block (3) houses two steam chambers. The one chamber supplies steam to the back side of the test surface, while the second chamber acts as a guard heater to minimise heat losses to the surroundings. A single steam supply pipe (4) enters each steam chamber block from the side and supplies steam to both steam chambers. The top and bottom plates, (5) and (6), together with the two side plates (8) hold the test section together. Air is blown through the channel that is formed by the two surfaces and the spacers. The test surfaces which are at the steam temperature transfer heat to the air stream. An amount of steam condenses at the back of the test surface to balance the heat transfer to the air stream. The condensate leaves the test section via condensate outlet pipes (9). The steam chambers in contact with the test surfaces are divided into two sections in the direction of air flow.

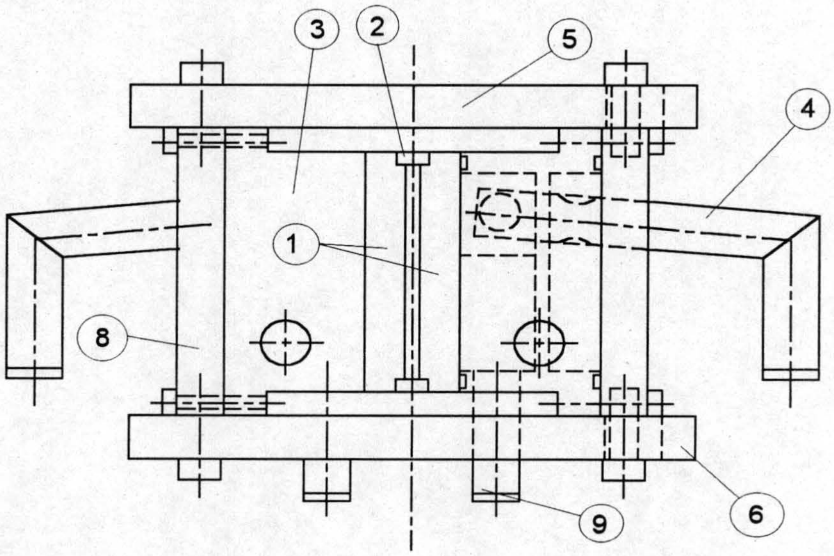

Figure A.1: End view of test section.

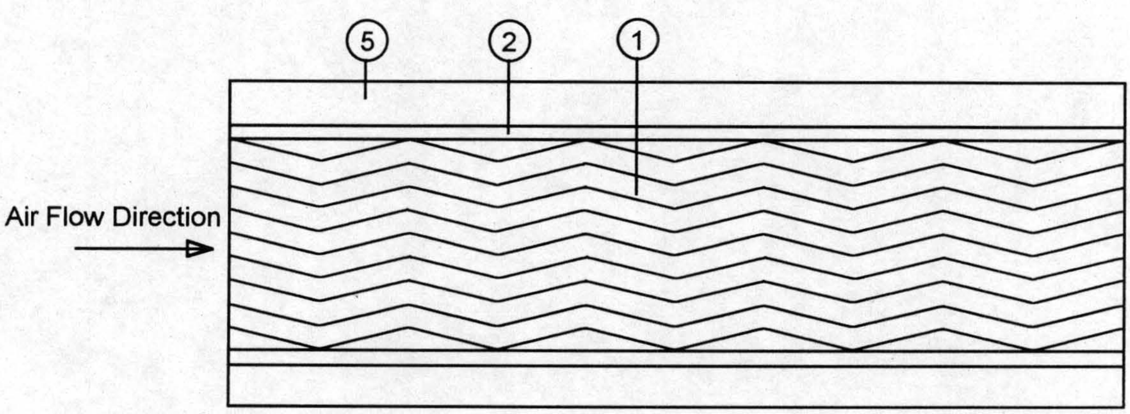

Figure A.2: Side cut-away view of test section showing the test surface.

A.2.2 Air supply

A schematic drawing of the complete experimental set-up is shown in figure A.3. Air flow to the test section is supplied by a high pressure line. The air is then throttled to a lower pressure by a valve that also controls the flow. The air then enters a pipe in which two orifice plates are located in series for the measurement of the air flow rate. The orifices are designed according to the British Standard 1042 Sections 1.1 - 1.4. The uncertainty for the flow rate is usually less than 4 %. The pipe leads to a settling chamber where the velocity is reduced before the air enters the test section. In the settling chamber thermocouples are located to determine the air temperature at the inlet of the test section. An insulation piece is located between the test section and the settling chamber. The function of the insulation piece is to prevent the air in the settling chamber from being preheated before it enters the test section. It also acts as a radiation shield for the thermocouples in the settling chamber.

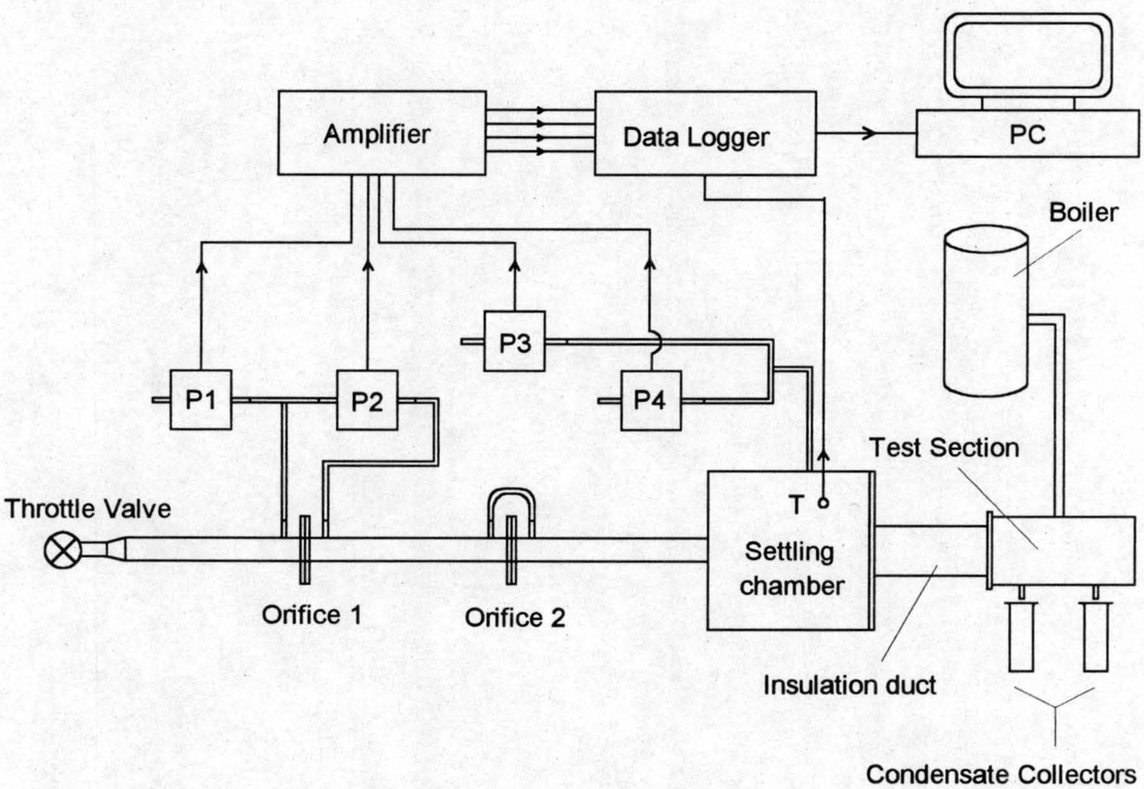

Figure A.3: Schematic representation of experimental set-up.

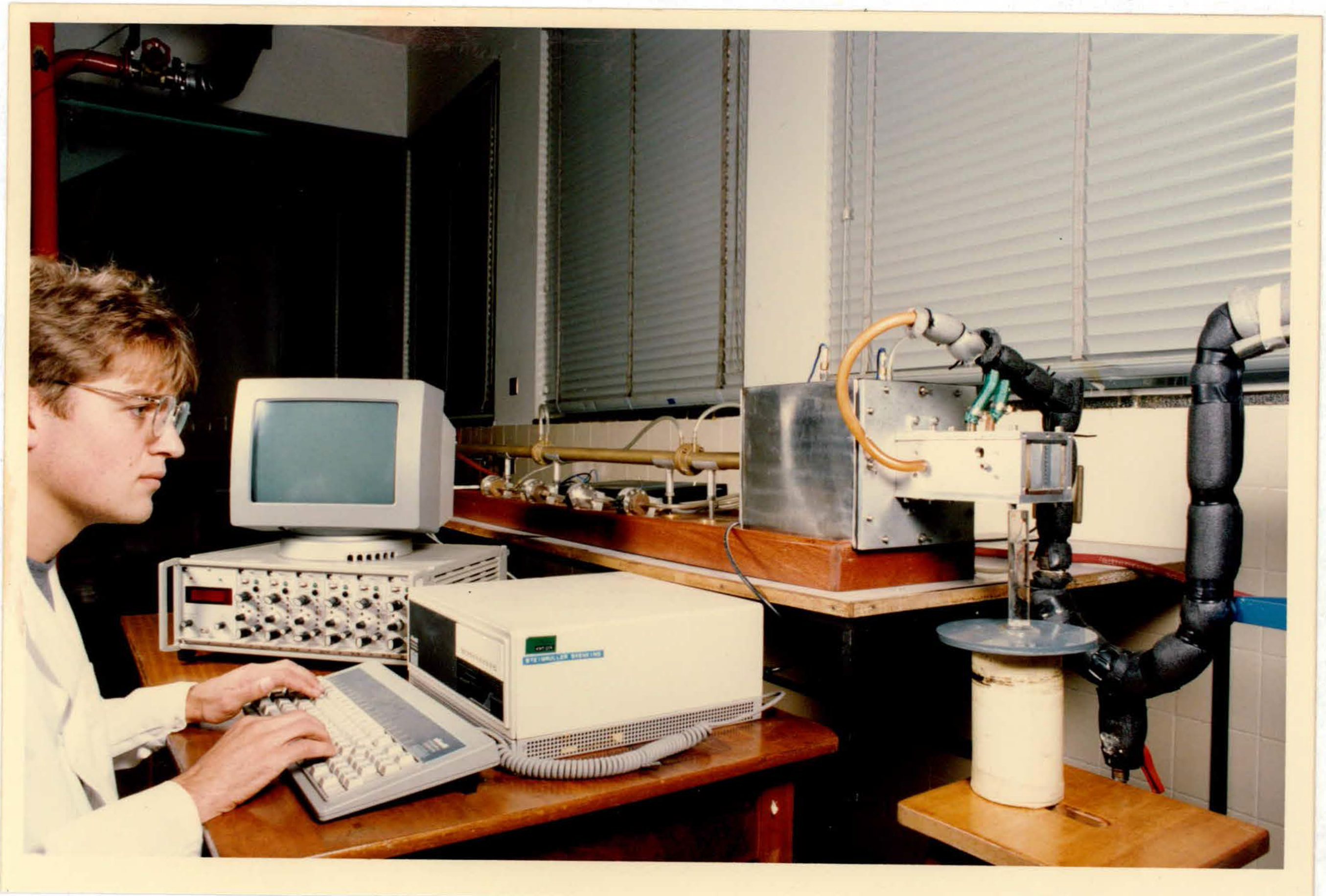

Figure A.4: Photo of experimental set-up.

A.2.3 Data recording

Four HBM differential pressure transducers are used to measure the pressures involved. P2 measures the pressure drop across the orifice. P1 is used to determine the absolute pressure before the orifice plate. P3 and P4 measure the static pressure in the settling chamber. The signals from the transducers go via an HBM KWS3037 bridge amplifier to a Schlumberger multiple voltmeter data logger. The signals from the Type T thermocouples go directly to the data logger. The data logger reads a set of data about every second and sends it to the computer. A Pascal computer program is used to process the signals and store them to a data file. Incorporated into the program are features like integrating and averaging the signals over a period of time. The condensate volume flow rate is determined with measuring cylinders and a stop watch.

A.2.4 Test surfaces

There are several different surfaces that can be categorised into two types. The Type 1 surfaces as shown in figures A.5, A.6 and A.7 are 200 mm long in the direction of the air flow and 50 mm high. Fins are machined out in a wavy pattern on the surface of the surface block. Some of the Type 1 surfaces have additional to the wave pattern on the surface, a wave pattern that goes into the face of the surface.(3 dimensional) The different detailed dimensions of the various surfaces tested are listed in table A.1. The Type 2 surfaces are 200 mm long and 100 mm high. See figures A.9 and A.10 and table A.2 for a listing of the dimensions of the various Type 2 surfaces.

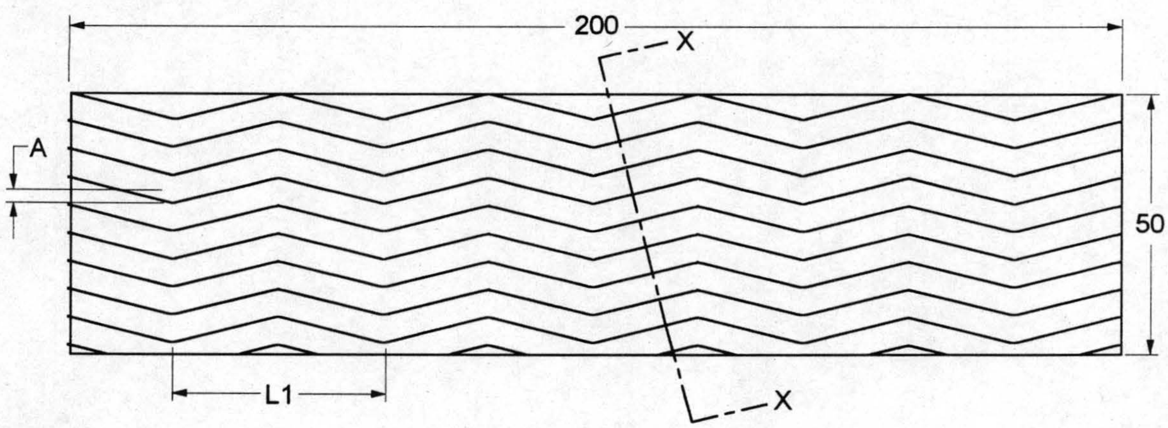

Figure A.5: Plane view of a typical surface of Type 1.

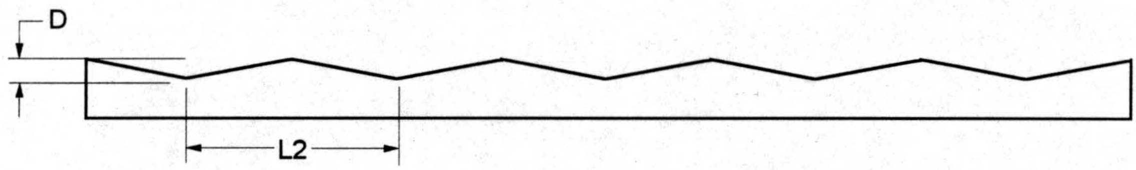

Figure A.6. Side view of a Type 1 surface showing wave pattern into the face of the surface.

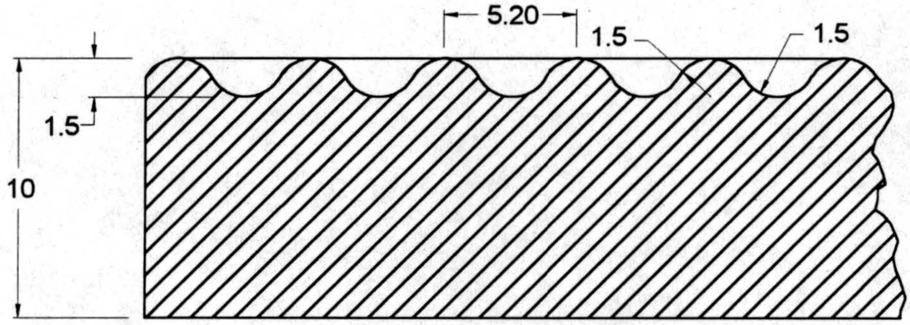

Figure A.7: Cut-away view X-X of Type 1 surface.

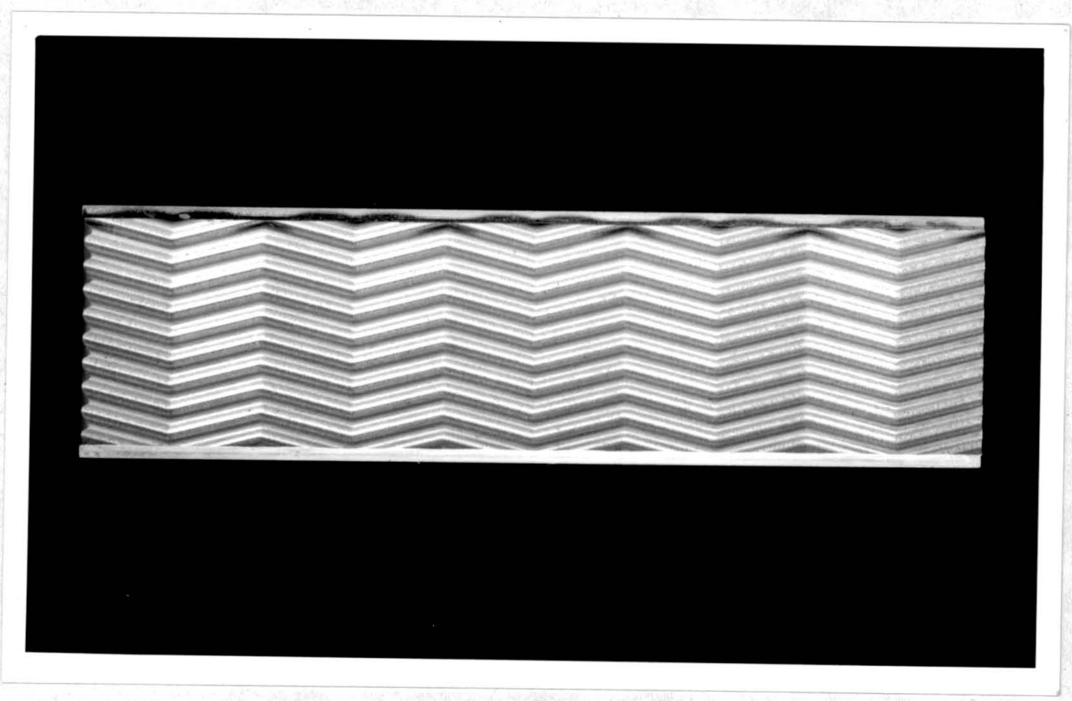

Figure A.8 Plan view photo of a typical surface (surface 3A of Type 1 in this case).

To simplify matters a code will be used to identify the surfaces. The following definitions apply to the Type 1 surfaces.

Table A.1: Surface codes and geometrical definitions for Type 1 surfaces.

Surface code	Description	A (mm)	L1 (mm)	L2 (mm)	D (mm)
1	Flat plate	-	-	-	0
2	Straight fins	0	∞	-	0
3A		2.5	40	-	0
3B		2.5	40	40	2.5
3C		2.5	40	40	5
4		5	40	-	0
5		7.5	40	-	0
6		10	40	-	0
7		2.5	20	-	0
8		2.5	16	-	0
9		2.5	10	-	0
10		1.25	10	-	0
11A,12A		1.25	20	20	0
11B		1.25	20	20	1.25
11C		1.25	20	20	2.5
11D		1.25	20	20	3.75
12B		1.25	20	40	2.5
12C		1.25	20	40	5

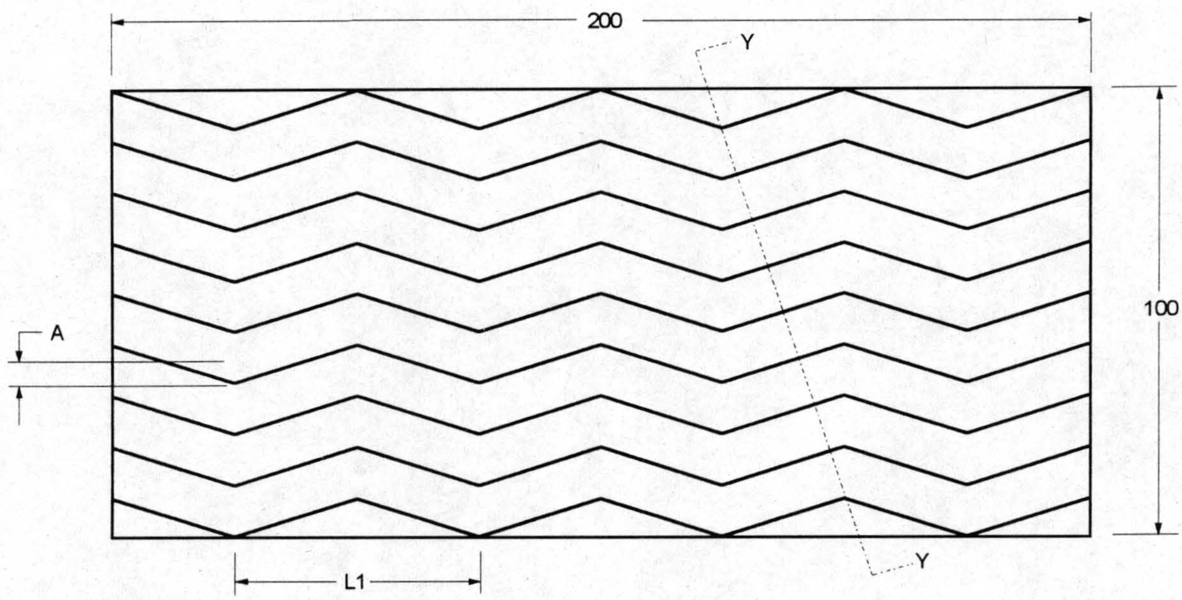

Figure A.9: Plane view of a typical surface of Type 2.

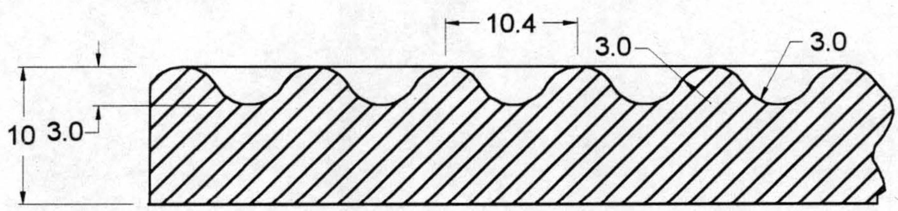

Figure A.10: Cut-away view Y-Y of Type 2 surface.

Table A.2: Surface codes and geometrical definitions for Type 2 surfaces.

Surface code	Description	A (mm)	L1 (mm)	L2 (mm)	D (mm)
1	Flat plate	-	-	-	0
2	Straight fins	0	∞	-	0
3		10	80	-	0
4		15	80	-	0
5		20	80	-	0
6		5	40	-	0
7		10	40	-	0
8		4	32	-	0
9		3.75	24.3	-	0

A.3. EXPERIMENTAL PROCEDURE

A.3.1 Isothermal tests

The pressure drop data is collected under isothermal conditions - i.e. no steam is used and the surfaces are at ambient temperature. Generally the pressure drop will be higher when the surfaces are heated due to the acceleration of the air as it is being heated. During every test (a specific surface at a specific spacing) the air speed over the surface is varied from 2 to 13 m/s in steps of 1m/s. At every air speed the four pressures and the temperature in the settling chamber are recorded. Transducers P3 and P4 record the same pressure, but they cover different ranges. Since some of the pressures are measured relative to atmosphere, the atmospheric pressure is recorded as well. From the schematic layout it can be seen that the total pressure drop across the test surface is the difference in static pressure between points (2) and (3). This is only true if the air velocity between the surfaces is constant. Under isothermal conditions with moderate pressure drops this is approximately true. During the tests however, the static pressure difference between points (1) and (3) were measured. To find the pressure drop Δp2 over the test surface, Δp1 must be subtracted from the measured pressure drop. The insulation piece was previously calibrated so that Δp1 is known for all air flows rates.

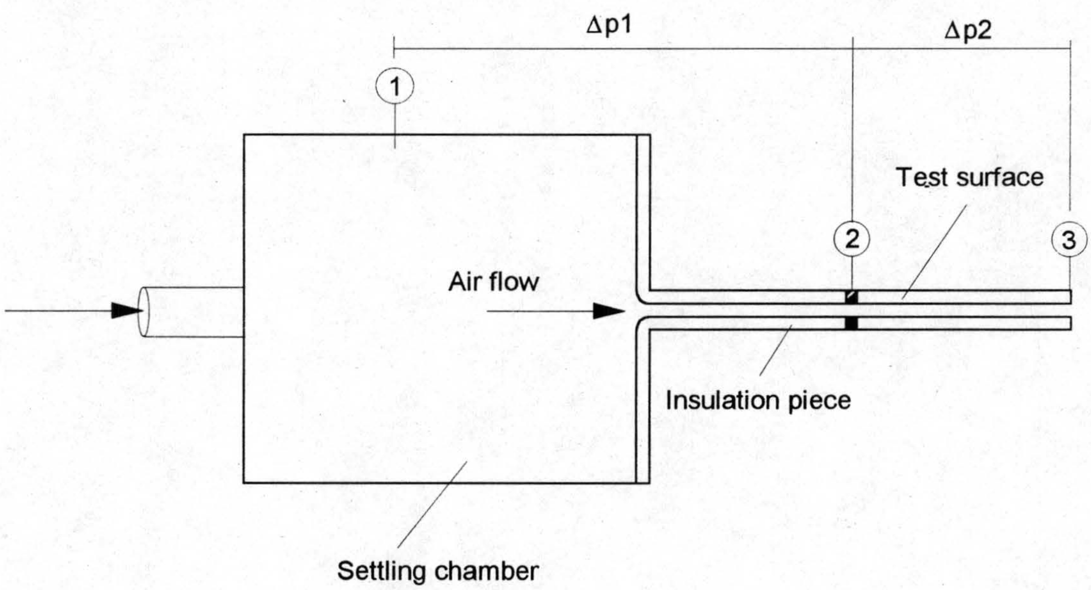

Figure A.11: Schematic layout of apparatus showing location of pressure measuring points.

A.3.2 Thermal tests

During the thermal tests steam is supplied to the steam chambers at the back of the surfaces. Additional to the data recorded for the isothermal tests, the condensate volume flow rates $\dot{V}_1$ and $\dot{V}_2$ are also measured. As mentioned earlier the steam chambers are divided into two sections in the direction of air flow. $\dot{V}_1$ is the condensate flow rate for the first 100 millimetres of the surface and $\dot{V}_2$ the condensate flow rate corresponding to the second 100 millimetres. The air speed is incremented from 2.5 to 12.5 m/s in steps of 2.5 m/s. Before a test starts the system is heated with no air flow until equilibrium is reached. $\dot{V}_1$ and $\dot{V}_2$ are then measured to determine the so called zero reading. The zero reading accounts for steam condensation due to heat transfer through the insulation and possible wet steam.

A.4. INTERPRETATION OF EXPERIMENTAL DATA

A.4.1 Isothermal tests

The method of presenting the heat transfer and pressure drop data in the next two sections is proposed by Kröger [86KR1]. The pressure drop is presented as a loss coefficient K. The loss coefficient is defined as the total pressure drop across the surface, divided by the mean velocity head.

$$K = \frac{\Delta p_t}{0.5\rho_m v^2{}_m} = \frac{\Delta p_s - 0.5\rho_o v^2{}_o + 0.5\rho_i v^2{}_i}{0.5\rho_m v^2{}_m} \tag{A.1}$$

In this case v_o and v_i are equal and the total pressure drop consists only of the static pressure drop.

Every K value must be associated with a flow parameter. In this case the characteristic flow parameter Ry is defined as $m/(\mu A_{fr})$. Ry is the same as a Reynolds number in the absence of an equivalent diameter. Because of the arbitrary nature of the equivalent diameter, many definitions are found in the literature and often lead to confusion.

A sample calculation will now be presented. Consider the following experimental data for 3A surface of Type 2 at a spacing of 5 mm. See table A.2 for the dimensions of the surface.
Atmospheric pressure, p_{atm} = 760 mm Hg
Air temperature, T = 16.31°C
Pressure differential between settling chamber and atmosphere = 116.55 Pa
Pressure drop across orifice plate = 1722.38 Pa
Absolute pressure before orifice plate = 101325+1571.49 = 102 896.49 Pa
Plate spacing = 5 mm
Test surface height = 100 mm (Type 2)

Air properties:

It follows from the data that the absolute temperature of the air T = (273.15+16.31) = 289.46 K. The corresponding viscosity according to equation (D.3) is $\mu_a = 1.798107 \times 10^{-5}$ kg/sm. The mean air density at this temperature is

$$\rho_m = \frac{P}{R.T} = \frac{101325 + 116.55/2}{287.08 \times (273.15 + 16.31)} = 1.22004 \text{ kg/m}^3$$

The air mass flow rate is calculated with the aid of a computer program. The program follows the flow calculation procedure as prescribed in the British Standards 1042 section 1.1. A sample calculation for the air mass flow rate will now follow.

The orifice dimensions are as follows:

Pipe diameter, D = 0.029 m
Orifice diameter, d = 0.00994 m

In general the mass flow rate can be calculated by:

$$m = CE\varepsilon\pi / 4d^2 \sqrt{2\Delta p \rho_u} \qquad \text{(A.2)}$$

The subscript u refers to the upstream condition.
The velocity of approach factor $E = (1-\beta^4)^{-0.5}$ where $\beta = d/D$ (A.3)
The expansibility factor ε is given by $\varepsilon = 1-(0.41 + 0.35\beta^4)\Delta p/(\gamma P_u)$ (A.4)
The pressure drop across the orifice plate Δp = 1722.38 Pa

The discharge coefficient C, is defined as follows:

$$C = 0.5959 + 0.0312\beta^{2.1} - 0.1840\beta^{8} + 0.0029\beta^{2.5}\left(\frac{10^{6}}{Re_{D}}\right)^{0.75} \tag{A.5}$$

$$+0.0900L_{1}\,0.039 - 0.033L'_{2}\beta^{3}$$

The upstream pressure P_u = 102 896.49 Pa. The air density $\rho_u = P_u/RT$ = 1.2382 kg/m³. $\beta = d/D = 0.3427586$. With β known it follows from equation (A.3) that E = 1.006973. From equation (A.4), ε can be calculated.

$$\varepsilon = 1 - (0.41 + 0.35 \times 0.3427586^{2})\frac{1722.38}{1.4 \times 102896.49} = 0.9946062$$

C is a function of Re_D. Re_D is not known at this stage, therefore an iterative procedure will be required. The converged value from the program is: C = 0.609809. From equation (A.1) it follows:

$$m = 0.609809 \times 1.006973 \times 0.9946062\pi / 4 \times 0.00994^{2}\sqrt{2 \times 1722.38 \times 1.2382}$$

$$= 3.0952 \times 10^{-3}\ \mathrm{kg/s}$$

As a check the value for C can be confirmed.

$$Re_{D} = \frac{4m}{\mu D\pi} = \frac{4 \times 3.0952 \times 10^{-3}}{1.798107 \times 10^{-5} \times 0.029 \times \pi} = 7557.82$$

L_1 = 1 and L_2' = 0.47 for this orifice arrangement. From equation (A.5) it follows that C = 0.609825 that is essentially the same as the value of C that was accepted as the converged value.

The mean air speed between the two plates is

$$v_{m} = \frac{m}{\rho_{m}A_{fr}} = \frac{3.0952 \times 10^{-3}}{1.22004 \times 0.005 \times 0.1} = 5.0756\ \mathrm{m/s}$$

To calculate the loss coefficient K for the test surface we need $\Delta p2$, that is the total pressure drop across the test surface. The total pressure drop $\Delta p1 + \Delta p2$ was measured. The insulation duct was previously calibrated so $\Delta p1$ can be calculated. The correlation for $\Delta p1$ is as follows:

$$\frac{\Delta p1}{0.5\rho v_m^2} = 664.7593\,Re^{(-1.20804+0.062179\ln(Re))} \tag{A.6}$$

The Reynolds number in the above correlation is defined in terms of the flow between the two test plates. The two test plates form a rectangular duct with equivalent diameter The equivalent diameter d_e = 4ab/(2a+2b) where a and b are the lengths of the sides of the rectangular duct.

$$d_e = \frac{4 \times 0.005 \times 0.1}{2 \times 0.00.5 + 2 \times 0.1} = 0.0095238 \text{ m}$$

$$Re = \frac{\rho v d_e}{\mu} = \frac{1.22004 \times 5.0756 \times 0.0095238}{1.798107 \times 10^{-5}} = 3279.75$$

From equation (A.6) Δp1 is found to be 34.79 Pa. The total pressure drop Δp1 + Δp2 was measured as 116.55 Pa. The pressure drop across the test bundle Δ p2 can now be calculated as 81.76 Pa.

Finally we calculate the loss coefficient and the corresponding flow parameter.

$$K = \frac{\Delta p2}{0.5\rho_m v^2{}_m} = \frac{81.76}{0.5 \times 1.22004 \times 5.0756^2} = 5.2026$$

$$Ry = \frac{m}{\mu A_{fr}} = \frac{3.0952 \times 10^{-3}}{1.798107 \times 10^{-5} \times 0.005 \times 0.1} = 3.44273 \times 10^5 \text{ m}^{-1}$$

For every surface at a specific spacing the air mass flow rate is varied to find a correlation for the loss coefficient. For the surface under consideration the loss coefficient was correlated as follows:

$$K = 108.5385 Ry^{-0.2378} \qquad (2\times10^5 < Ry < 9\times10^5)$$

A.4.2 Thermal tests

Heat transfer data is usually presented as a Nusselt number ($Nu = hd_e/k$). If the effective diameter is left out again it becomes h/k. The effective finned surface area and the heat exchanger frontal area plays a major role in comparing and optimising heat exchangers. If these parameters are introduced a characteristic heat transfer parameter Ny can be defined.

$$Ny = \frac{he_f A}{kA_{fr} Pr^{0.33}} \tag{A.7}$$

The air side heat transfer coefficient is h, e_f is the fin effectiveness, A is the fin area and A_{fr} is the frontal area. In this case the entire fin is at one temperature and therefore $e_f = 1$. A sample calculation is now presented.

Data recorded:
Atmospheric pressure, $p_{atm} = 757.5$ mm Hg
Atmospheric temperature, T = 19.0 °C
Condensate flow rate based on first 100 mm, $\dot{V}_1 = 0.0681481$ ml/s
Condensate flow rate based on second 100 mm, $\dot{V}_2 = 0.0309302$ ml/s
Zero reading:
Condensate flow rate based on first 100 mm, $\dot{V}_{1,0} = 0.0051445$ ml/s
Condensate flow rate based on second 100 mm, $\dot{V}_{2.0} = 0.0040$ ml/s

The mass flow rate was determined as in the previous example and only the final value is given here.
$m = 3.0652\times10^{-3}$ kg/s
The air is heated and therefore we calculate the air properties at the mean air temperature. The air outlet temperature is found by doing an energy balance between the steam and air

Rate of energy released by steam condensation = Rate of energy to heat the air.

$$(\dot{V}_1 + \dot{V}_2 - \dot{V}_{1,0} - \dot{V}_{2,0})\rho_w i_{fgw} = mc_p (T_{a,o} - T_{a,i}) \tag{A.8}$$

The latent heat of evaporation of water at 100 °C is 2.256896×10^6 J/kg from equation (D.10). The c_p value for air is 1007 J/kg. The density of water at the condensate temperature is taken as 980 kg/m^3. The condensate temperature in the measuring cylinders is not constant but it is believed that the above density is representative of the average temperature.

From equation (A.8) the air outlet temperature is found to be 83.44 °C. This gives a mean air temperature, $T_{a,m}$ of 51.22 °C. According to the left side of equation (A.8) the total heat transfer rate is 198.91 W. The following air properties are calculated at $T_{a,m}$ from equations (D.1) to (D.4).

$\rho_a = 1.08488$ kg/m³
$\mu_a = 1.95757\times10^{-5}$ kg/sm
$c_{p,a} = 1008.09$ J/kgK
$Pr_a = 0.7026$
$k_a = 0.028087$

In a manner similar to the calculations in section A.4.1 the velocity, Re and Ry are calculated. The result is:

V = 5.6338 m/s
Re = 2973.55
Ry = 3.122238×10^5

In order to calculate the heat transfer parameter Ny from equation (A.7) the product hA is needed. The overall heat transfer coefficient U can be expressed in terms of the convective and various other thermal resistances.

$$U = \frac{1}{\frac{1}{h} + \frac{A}{A_c h_c} + \sum_n \frac{A}{A_n} R_n} \tag{A.9}$$

The condensation heat transfer coefficient at the back of the plate is h_c. The summation term represents all the other resistances like conductive and fouling resistances. It was found that h_c is orders of magnitude higher than h and that the conductive resistance through the aluminium plate is small compared to 1/h. Thus equation (A.9) reduces to:

$$hA \approx UA \tag{A.10}$$

For a condenser UA = $Q/\Delta T_{lm}$ where Q is the total heat transfer and ΔT_{lm} is the logarithmic mean temperature difference. Strictly speaking the above relation is only valid when U is a constant. In these experiments U is not constant since the flow is thermally developing. The test surfaces are too short to establish fully thermally developed flow over the greater part.

However for purposes of comparison this approach is adequate and alternatives are limited.

$$\Delta T_{lm} = \frac{T_{a,i} - T_{a,o}}{\ln\left(\frac{T_s - T_{a,o}}{T_s - T_{a,i}}\right)} = \frac{19.00 - 83.44}{\ln\left(\frac{100 - 83.44}{100 - 19.00}\right)} = 40.59\ ^\circ C$$

$$UA = \frac{Q}{\Delta T_{lm}} = \frac{198.91}{40.59} = 4.90046\ W/K$$

From equation (A.7)

$$Ny = \frac{UA}{kA_{fr}\, Pr^{0.33}} = \frac{4.90046}{0.028087 \times 0.005 \times 0.1 \times 0.7026^{0.33}} = 3.920557 \times 10^5\ m^{-1}$$

In this case the correlation between Ny and Ry is: $Ny = 64.1291 Ry^{0.6866}$.

Since the condensate flow rate was measured over the total length of the surface as well as over the first half, a characteristic heat transfer parameter based on the first half was also calculated. From now on we will denote the Ny value based on the entire length (200 mm) as Ny_{200} and The Ny based on the first half as Ny_{100}.

A.5 VERIFICATION OF ACCURACY OF EXPERIMENTAL APPARATUS

No simple theory exists to verify the test results of the wavy surfaces. For this reason a plain flat plate was tested. The two flat plates together with their spacers form a smooth rectangular duct. For rectangular ducts appropriate pressure drop and heat transfer solutions exist which can be compared to the experimental results.

For a plane flat surface of Type 2 at a spacing of 5 mm experimental relationships for K and Ny versus Ry were obtained. The air mass flow rate is such that the flow pattern goes from laminar to the transition and ultimately into the lower turbulent zones. It will now be shown that for both pressure drop and heat transfer the experimental data is in good agreement with the theoretical prediction for laminar and turbulent flow regimes.

A.5.1 Laminar friction factor

The following were experimentally obtained: K = 1.44424 at Ry = 139529. The calculation method is the same as in the previous section.

From the definition of Ry the Reynolds number can be calculated. The equivalent diameter for the rectangular duct is 0.009524 m as was shown earlier.

Since $Re = Ry \times d_e = (139529)(0.009524) = 1328.8$ the flow is laminar. From the definition of K and the definition of the Fanning friction factor, the following relationship holds:
$f = (K \times d_e)/(4L)$
where L is the length of the channel.
The experimental value for the Fanning friction factor can now be calculated.

$f_{exp} = (1.44424)(0.009534)/((4)0.2) = 0.017193$

The exact analytical solution for fRe is known and is in the form of an infinite series. Shah [78SH1] calculated the solution for a few aspect ratios and proposes the following curve fit which agrees within 0.05 % of the exact solution.

$$f\,Re = 24\left[1 - 1.3553\alpha^{*} + 1.9467\alpha^{*2} - 1.7012\alpha^{*3} + 0.9564\alpha^{*4} - 0.2537\alpha^{*5}\right] \qquad (A.11)$$

The aspect ratio α^* is 5/100 = 0.05 for this case. From equation (A.11) it follows that fRe = 22.48546 and subsequently f = 22.48546/1328.8 = 0.0169209. The experimental value of 0.017193 is approximately 1.6 % higher than the theoretical value.

A.5.2 Turbulent friction factor

The following were experimentally obtained: K = 0.632658 at Ry = 797111. As in the case of laminar flow we find the Reynolds number and experimental friction factor.

$Re = 7591.7$
$f_{exp} = 0.0075318$

For smooth ducts Haaland [83HA1] proposes the following relationship for the Fanning friction factor.

$$f = 0.69445\left[\log_{10}\left(\frac{7.7}{Re}\right)^3\right]^{-2} = 0.69445\left[\log_{10}\left(\frac{7.7}{7591.7}\right)^3\right]^{-2} \tag{A.12}$$
$$= 0.0086087$$

The experimental value is about 13 % lower than the theoretical value. Part of the discrepancy can be attributed to the fact the flow is not fully turbulent yet.

A.5.3 Laminar heat transfer coefficient

The following experimental results were obtained: Ny = 81439.17 at Ry = 158574.26. Properties at the mean air temperature, $T_{a,m}$ = 311.91 K are: k_a = 0.0271384 and Pr_a = 0.705816.

From Ry we obtain the Reynolds number.
$Re = Ry \times d_e = (158574.26)(0.009524) = 1510.26$

From the definition of Ny we obtain the experimental heat transfer coefficient.

$$h_{exp} = \frac{NyA_{fr}k_a Pr_a^{0.33}}{A} = \frac{(81439.17)(0.1\times0.005)(0.0271384)(0.705816)^{0.33}}{2(0.005+0.1)0.2} = 23.45\ W/K$$

For a fully developed velocity profile entering between parallel plates at a constant temperature Shah [75SH2] provides the following equation.

$$Nu_T = 7.541 + 0.0235 Re Pr\frac{d_e}{L} \quad \text{for} \quad \frac{L}{RePrd_e} > 0.006 \tag{A.13}$$

The value of 7.541 is for a fully developed temperature profile and the last term accounts for the inlet region. The above equation is applicable for parallel plates. In our case we are dealing with a rectangular duct. We will assume that the term 0.023(Re)(Pr)(d_e/L) is approximately valid for low aspect ratio rectangular ducts. The value of 7.541 will be replaced by the fully developed Nusselt number for a rectangular duct that is given by Shah [78SH1].

$$Nu_T = 7.541\left[1 - 2.610\alpha^* + 4.970\alpha^{*2} - 5.119\alpha^{*3} + 2.702\alpha^{*4} - 0.548\alpha^{*5}\right] \quad (A.14)$$

With an aspect ratio α^* of 5/100 = 0.05 the above relation gives Nu_T = 6.6459. Equation (A.13) now becomes

$$Nu_T = 6.6459 + 0.0235 \, Re \, Pr \frac{d_e}{L} \quad \text{for} \quad \frac{L}{RePrd_e} > 0.006 \quad (A.15)$$

We can now calculate the Nusselt number and the theoretical heat transfer coefficient.

$$Nu_T = 6.6459 + 0.0235 \, Re \, Pr \frac{d_e}{L}$$
$$= 6.6459 + 0.0235(1510.26)(0.705816)\frac{0.009524}{0.2} = 7.8387$$

$$h = Nu_T \frac{k}{d_e} = 7.8387 \frac{0.0271384}{0.009524} = 22.33 \text{ W/K}$$

In this case the experimental value of 23.45 is 5 % higher than the theoretical value.

A.5.4 Turbulent heat transfer coefficient

The following experimental results were obtained: Ny = 313423.9 at Ry = 962297.7. Properties at the mean air temperature, $T_{a,m}$ = 305.33 K are: k_a = 0.0266328 and Pr_a= 0.707661.

As in the laminar flow case we obtain the Reynolds number and heat transfer coefficient.

Re = 9164.74
h_{exp} = 88.657 W/K

For thermally developing turbulent flow Gnielinski [75GN1] proposes the following relation.

$$\mathrm{Nu} = \frac{(f_D/8)(\mathrm{Re}-1000)\,\mathrm{Pr}\left[1+\left(\frac{d_e}{L}\right)^{0.67}\right]}{1+12.7(f_D/8)^{0.5}(\mathrm{Pr}^{0.67}-1)} \tag{A.16}$$

where $f_D = (1.82\log_{10}\mathrm{Re}-1.64)^{-2}$

From the two above relations we find $f_D = 0.03222$ and $\mathrm{Nu} = 31.556$.
Therefore:

$$h = \mathrm{Nu}_T \frac{k}{d_e} = 31.556\frac{0.026633}{0.009524} = 88.244 \text{ W/K}$$

In this case the experimental and calculated heat transfer coefficients are nearly identical.

The rest of the data points and the theoretical prediction for the flat surface of Type 2 at a 5 mm spacing is shown in graphical form in figures A.12 and A.13. Flat plates for the smaller Type 1 surfaces were also tested and compared to theoretical predictions. The largest errors that occurred was in the order of 15 % to 20 % and is usually at transition Reynolds numbers where neither the laminar or turbulent theoretical models are applicable. In general the heat transfer results for the smaller Type 1 surfaces are less accurate than for the Type 2 surfaces. The 'zero reading' for the condensate flow rate is a relatively large fraction of the total condensate flow rate at the Type 1 surfaces. The 'zero readings' that are supposed to be constant were found to vary from case to case and this introduced a certain amount of uncertainty. This is especially profound when the air mass flow rate, and therefore the total condensate flow rate, is low. One possible explanation for the varying 'zero reading' is poor steam quality.

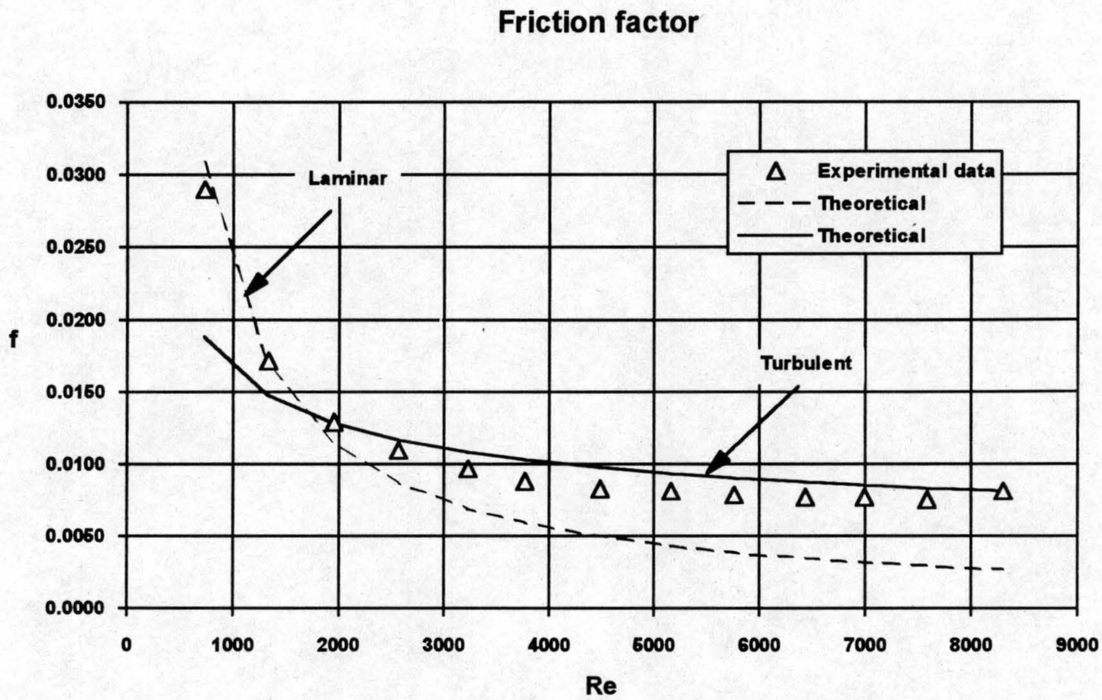

Figure A.12: Comparison of experimental friction factor and theoretical models for the Type 2 flat surface at a 5 mm spacing.

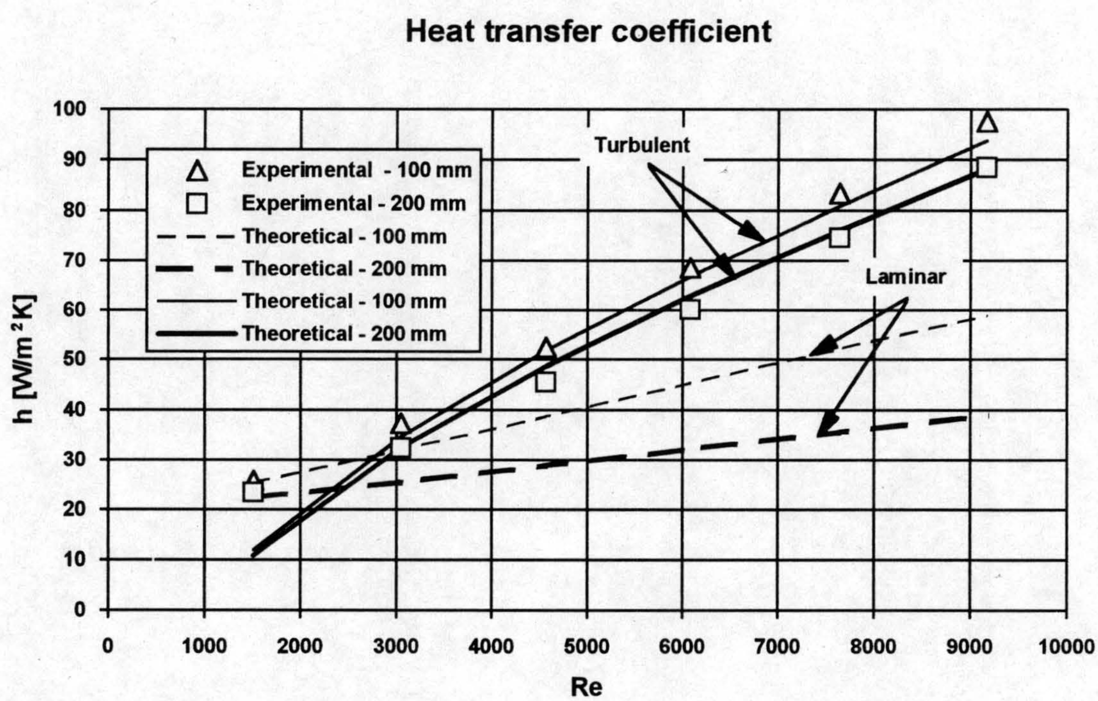

Figure A.13: Comparison of experimental heat transfer coefficient and theoretical models for the Type 2 flat surface at a 5 mm spacing.

A.6. EXPERIMENTAL RESULTS

A.6.1 Correlations

Correlations are presented for K and Ny against the flow parameter Ry. The loss coefficient K is based on the total length of the surface i.e. 200 millimetres. The condensate flow is measured for the first 100 millimetres and for the total length, therefore there are two Ny correlations for every test. Ny_{100} that is based on the first 100 millimetres and Ny_{200} that is based on the total length. Tables A.3 to A.7 list the constants for different surfaces as expressed by equation A.17.

$$\begin{aligned}K_{200} &= a1 \times Ry^{(a2+a3\ln(Ry))}\\ Ny_{100} &= b1 \times Ry^{(b2+b3\ln(Ry))}\\ Ny_{200} &= c1 \times Ry^{(c2+c3\ln(Ry))}\end{aligned} \tag{A.17}$$

Note that the above correlations are only valid for $150\,000 < Ry < 900\,000$. Where two sets of constants are given for a particular surface, the more extensive equation correlates the data more accurately. For every equation a correlation coefficient r^2 is listed.

In view of the large number of tests conducted it is not practical to supply the experimental data as a part of this appendix. The Type 2 surfaces and the 3- and 11 series of Type 1 graphs are presented showing how the correlations relate to the experimental data. The effectiveness ratio Ny/K is an indication of the effectiveness of the surfaces. It is however not sufficient to compare the surfaces with each other with Ny/K as the only criteria. The surfaces must be compared to one another in a specific application and the ultimate criteria must be cost effectiveness.

Table A.3: Correlation coefficients for Type 1 surfaces at a spacing of 2.5 mm.

Surface	a1	a2	a3	r^2	b1	b2	b3	r^2	c1	c2	c3	r^2
1A	88108.7	-0.8153	0	0.941	679.707	0.4369	0	0.906	1761.69	0.4039	0	0.941
1A	$e^{52.8804}$	-7.4303	0.2627	0.983	$e^{51.6770}$	-6.6526	0.2776	0.992	$e^{51.2665}$	-6.4808	0.2700	0.983
3A	4253.71	-0.5106	0	0.981	50.281	0.6897	0	0.998	4.570	0.9200	0	0.992
3B	6132.48	-0.5223	0	0.993	84.116	0.6599	0	0.997	8.355	0.8828	0	0.963
3C	4184.66	-0.4784	0	0.993	60.068	0.6928	0	0.991	8.175	0.9017	0	0.990
11A	4007.55	-0.5144	0	0.992	62.023	0.6715	0	0.999	5.513	0.9031	0	0.990
11B	3921.97	-0.4868	0	0.992	157.853	0.6097	0	0.998	7.039	0.8988	0	0.980
11C	2649.69	-0.4375	0	0.991	77.254	0.6734	0	0.998	10.685	0.8768	0	0.991
11D	1676.3	-0.3738	0	0.983	24.572	0.7733	0	0.997	21.521	0.8340	0	0.996
12B	2129.71	-0.4544	0	0.989	14.812	0.7779	0	0.998	3.555	0.9347	0	0.996
12C	2449.75	-0.4451	0	0.993	60.235	0.6837	0	0.997	20.226	0.8167	0	0.993

Table A.4: Correlation coefficients for Type 1 surfaces at a spacing of 3.0 mm.

Surface	a1	a2	a3	r^2	b1	b2	b3	r^2	c1	c2	c3	r^2
1A	3246.55	-0.5809	0	0.876	40.527	0.6498	0	0.970	267.664	0.5400	0	0.878
1A	$e^{70.8800}$	-10.4311	0.3854	0.991	$e^{31.5268}$	-3.7256	0.1716	0.986	$e^{71.5171}$	-9.8421	0.4078	0.995
3A	1526.15	-0.4457	0	0.980	24.853	0.7298	0	0.999	11.779	0.8302	0	0.993
3B	1876.19	-0.4492	0	0.987	29.4701	0.7250	0	0.998	12.358	0.8360	0	0.997
3C	2034.50	-0.4473	0	0.993	48.137	0.6953	0	0.997	11.933	0.8515	0	0.994
11A	643.128	-0.3790	0	0.990	24.309	0.7277	0	0.997	31.344	0.7571	0	0.991
11B	1261.09	-0.4143	0	0.986	46.429	0.7223	0	0.998	65.006	0.7096	0	0.994
11C	826.242	-0.3579	0	0.989	34.427	0.6734	0	0.998	54.802	0.7391	0	0.991
12B	686.577	-0.3871	0	0.988	10.043	0.7966	0	0.999	6.900	0.8723	0	0.997

Table A.5: Correlation coefficients for Type 1 surfaces at a spacing of 3.5 mm.

Surface	a1	a2	a3	r^2	b1	b2	b3	r^2	c1	c2	c3	r^2
1A	366.148	-0.4173	0	0.794	33.234	0.6425	0	0.923	121.050	0.5856	0	0.875
1A	$e^{66.6411}$	-9.9465	0.3729	0.992	$e^{63.2658}$	-8.7390	0.3674	0.996	$e^{77.3584}$	-10.822	0.4474	0.992
3A	1080.09	-0.4379	0	0.975	26.044	0.7059	0	0.996	11.6631	0.8172	0	0.998
3A	$e^{26.0435}$	-3.5291	0.1208	0.997	-	-	-	-	-	-	-	-
3B	959.71	-0.4169	0	0.985	42.965	0.6793	0	0.999	114.685	0.6562	0	0.994
3C	995.42	-0.3967	0	0.992	100.601	0.6247	0	0.998	138.700	0.6514	0	0.997
11A	1074.92	-0.4431	0	0.997	33.420	0.6911	0	0.997	136.846	0.6360	0	0.992
11B	658.48	-0.3812	0	0.984	17.059	0.7485	0	0.997	89.241	0.6781	0	0.984
11C	652.57	-0.3525	0	0.994	46.959	0.6894	0	0.997	64.928	0.7174	0	0.997
11D	418.38	-0.2792	0	0.987	136.959	0.6248	0	0.995	30.105	0.7909	0	0.999
12B	252.85	-0.3185	0	0.992	13.164	0.7653	0	0.999	26.997	0.7611	0	0.999
12C	583.53	-0.3605	0	0.993	14.921	0.7601	0	0.998	34.698	0.7467	0	0.999

Table A.6: Correlation coefficients for Type 1 surfaces at a spacing of 5 mm.

Surface	a1	a2	a3	r^2	b1	b2	b3	r^2	c1	c2	c3	r^2
1A	436.47	-0.4831	0	0.844	6.452	0.7333	0	0.943	6.816	0.7722	0	0.953
1A	$e^{56.9631}$	-8.5689	0.3202	0.991	$e^{62.8832}$	-8.8404	0.3747	0.997	$e^{60.2979}$	-8.3974	0.3593	0.998
3A	155.546	-0.3425	0	0.998	0.5502	0.9620	0	0.997	1.248	0.9510	0	0.991
3B	147.877	-0.3180	0	0.995	1.048	0.9204	0	0.998	1.863	0.9272	0	0.990
3C	242.777	-0.3221	0	0.995	7.363	0.7909	0	0.995	7.410	0.8401	0	0.978
11A	84.943	-0.2903	0	0.994	5.811	0.7945	0	0.996	9.033	0.8068	0	0.995
11B	57.703	-0.2377	0	0.974	3.691	0.8336	0	0.999	8.704	0.8177	0	0.992
11C	241.032	-0.2958	0	0.993	9.416	0.7779	0	0.997	48.987	0.7112	0	0.996
11D	181.460	-0.2261	0	0.985	39.484	0.6870	0	0.999	87.189	0.6844	0	0.999
12B	27.921	-0.1948	0	0.979	5.083	0.8010	0	0.995	11.761	0.7881	0	0.996
12C	267.383	-0.3476	0	0.994	12.487	0.7466	0	0.999	6.017	0.8505	0	0.994

Table A.7: Correlation coefficients for Type 2 surfaces at a spacing of 5 mm.

Surface	a1	a2	a3	r^2	b1	b2	b3	r^2	c1	c2	c3	r^2
1A	693.724	-0.5213	0	0.920	4.581	0.7621	0	0.986	8.086	0.7621	0	0.976
1A	$e^{39.5880}$	-5.8085	0.2107	0.996	-	-	-		-	-	-	-
2A	114.401	-0.3384	0	0.946	5.395	0.7719	0	0.995	9.110	0.7756	0	0.989
2A	$e^{27.8133}$	-3.9183	0.1385	0.991	-	-	-	-	-	-	-	-
3A	108.538	-0.2378	0	0.991	67.782	0.6330	0	0.998	64.129	0.6866	0	0.997
4A	61.525	-0.1470	0	0.989	66.304	0.6466	0	0.991	131.558	0.6506	0	0.989
6A	235.386	-0.3021	0	0.998	52.960	0.6414	0	0.992	88.060	0.6549	0	0.993
9A	152.393	-0.2422	0	0.998	43.985	0.6677	0	0.995	81.283	0.6764	0	0.997

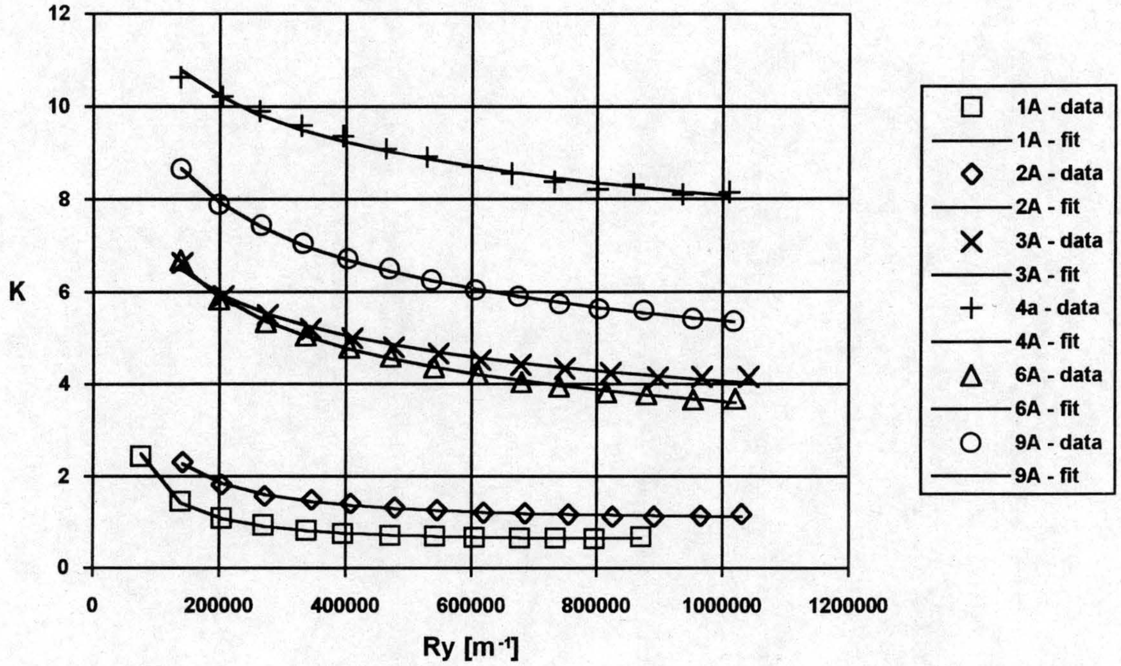

Figure A.14 :Loss coefficient data and curve fits for the Type 2 surfaces at a spacing of 5 mm.

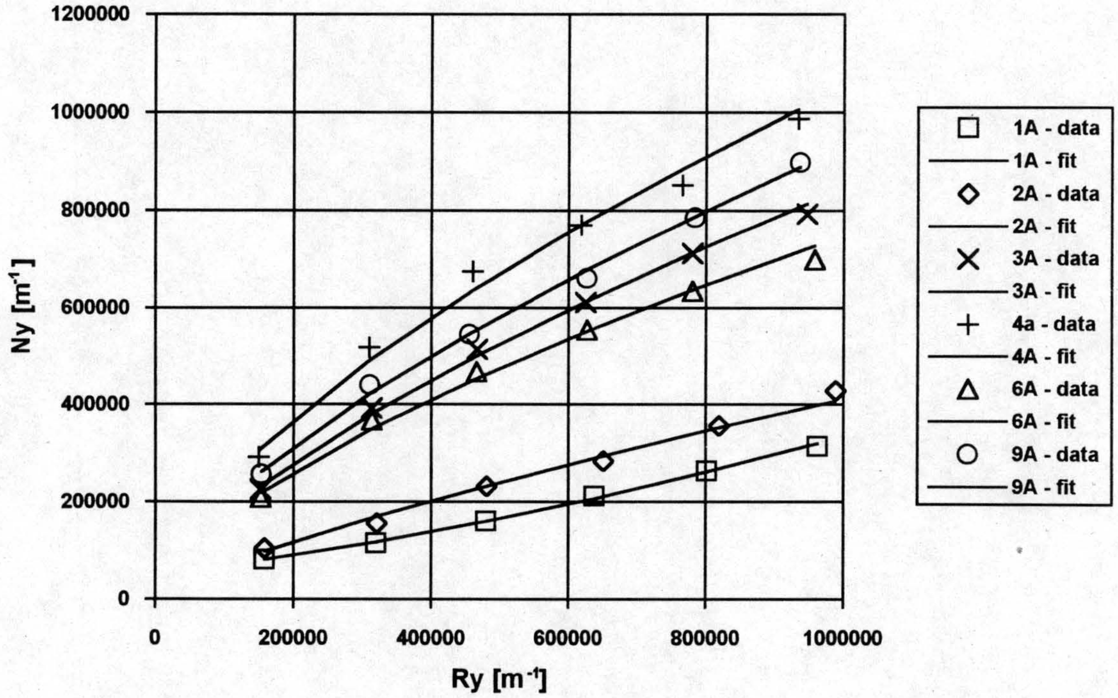

Figure A.15: Heat transfer data and curve fits for the Type 2 surfaces at a spacing of 5 mm.

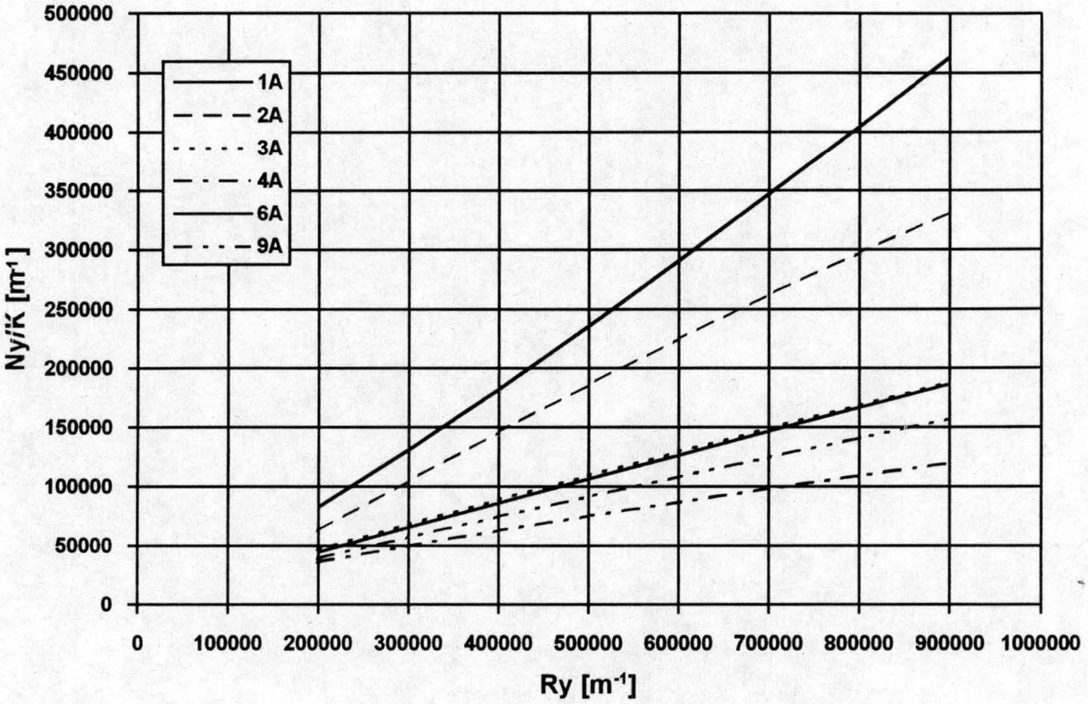

Figure A.16: Effectiveness ratios for the Type 2 surfaces at a spacing of 5 mm (curve fits only).

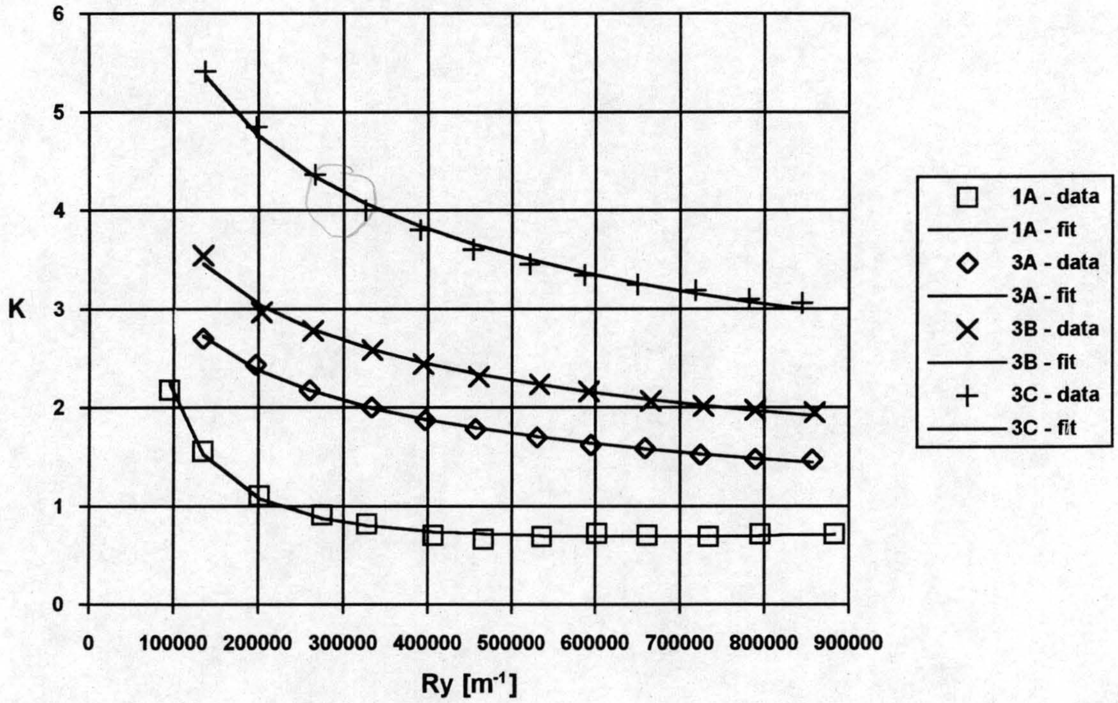

Figure A.17: Loss coefficient data and curve fits for the 3-series of Type 1. The plate spacing is 5 mm.

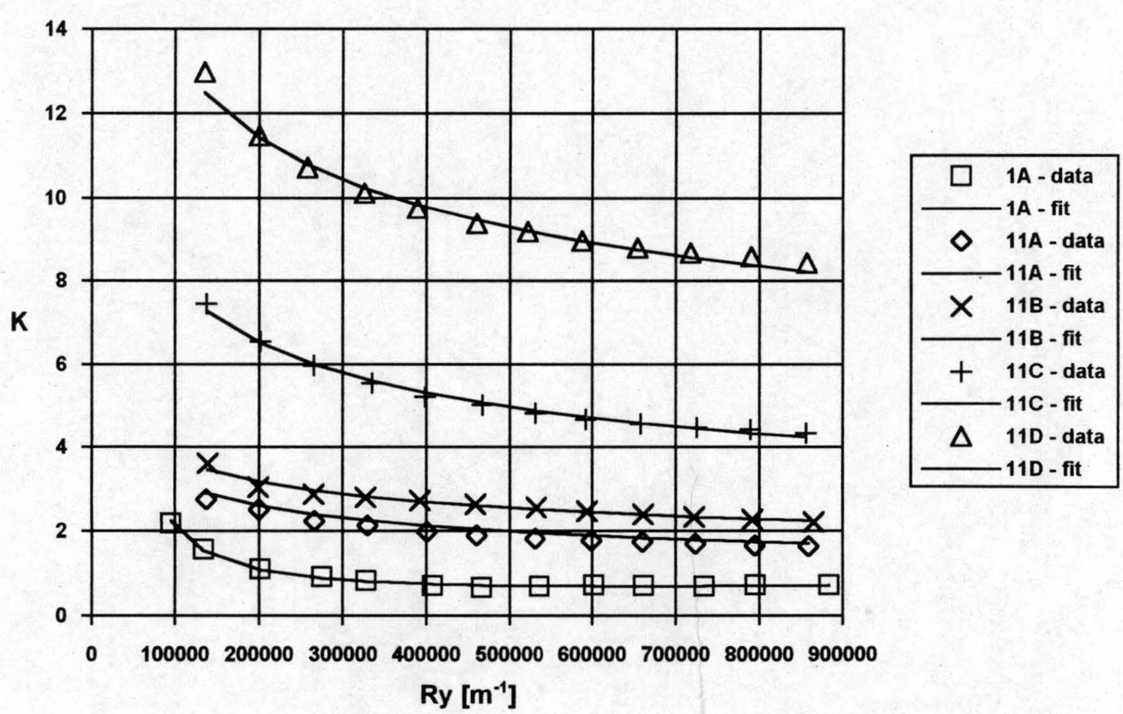

Figure A.18: Loss coefficient data and curve fits for the 11-series of Type 1. The plate spacing is 5 mm.

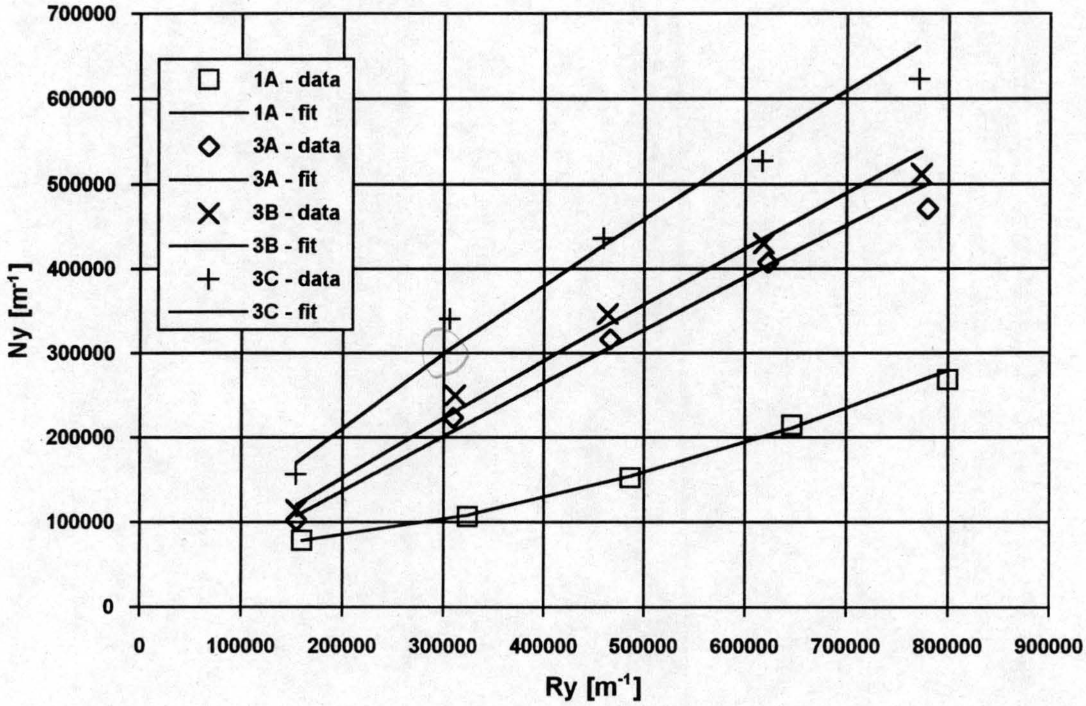

Figure A.19: Heat transfer data and curve fits for the 3-series of Type 1. The plate spacing is 5 mm.

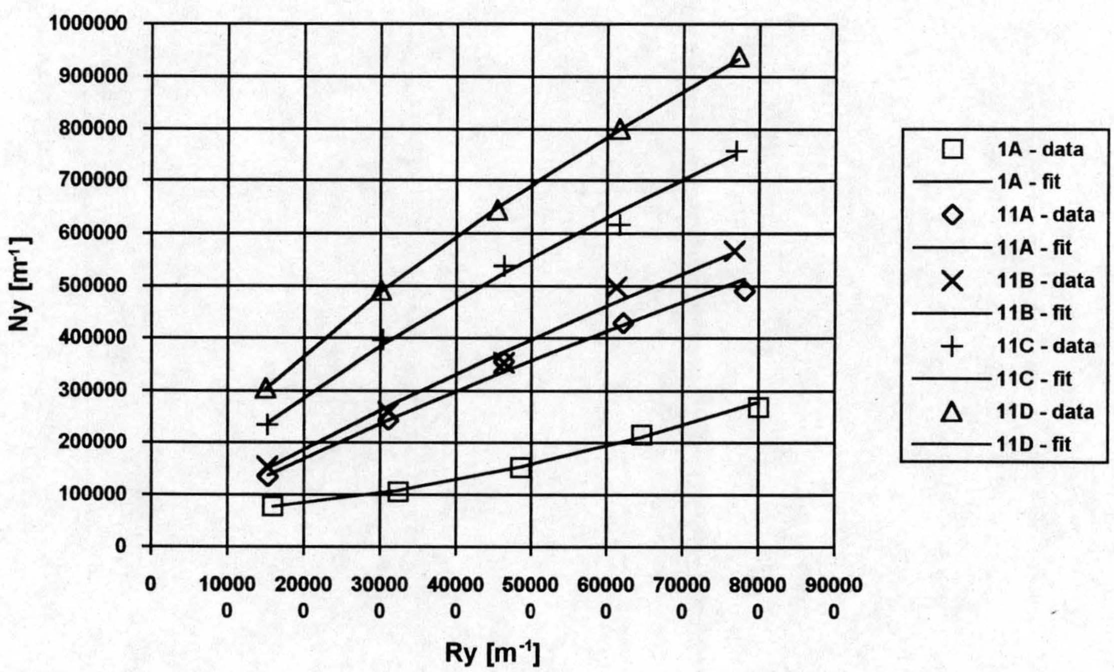

Figure A.20: Heat transfer data and curve fits for the 11-series of Type 1. The plate spacing is 5 mm.

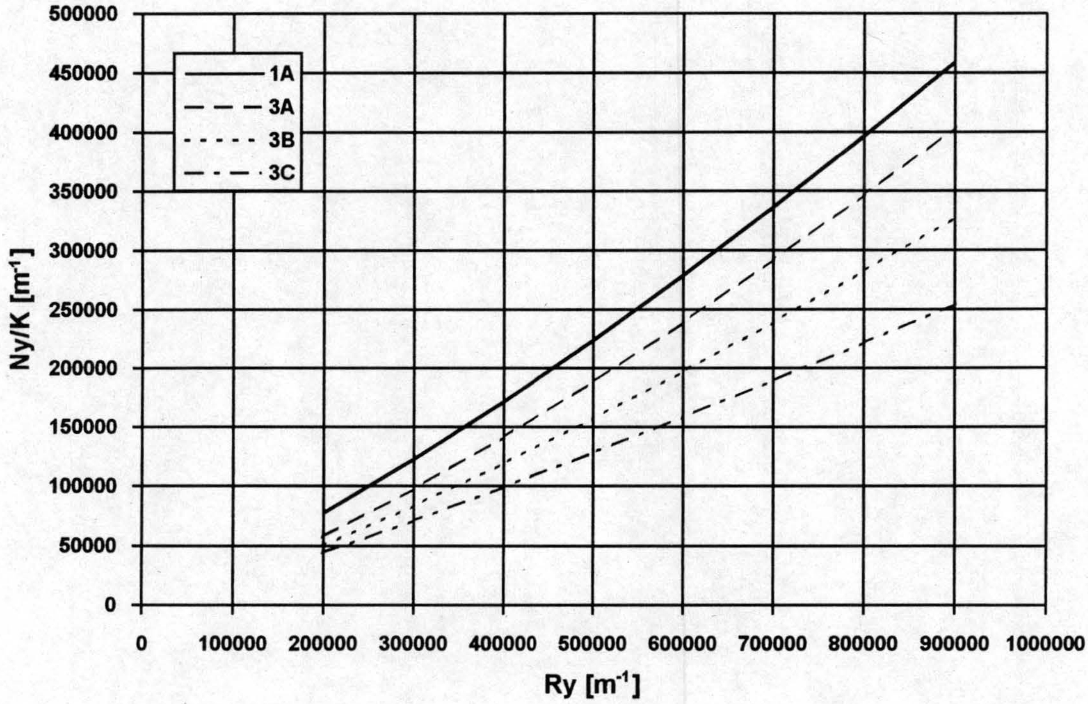

Figure A.21: Effectiveness ratio curve fits for the 3-series of Type 1. The plate spacing is 5 mm.

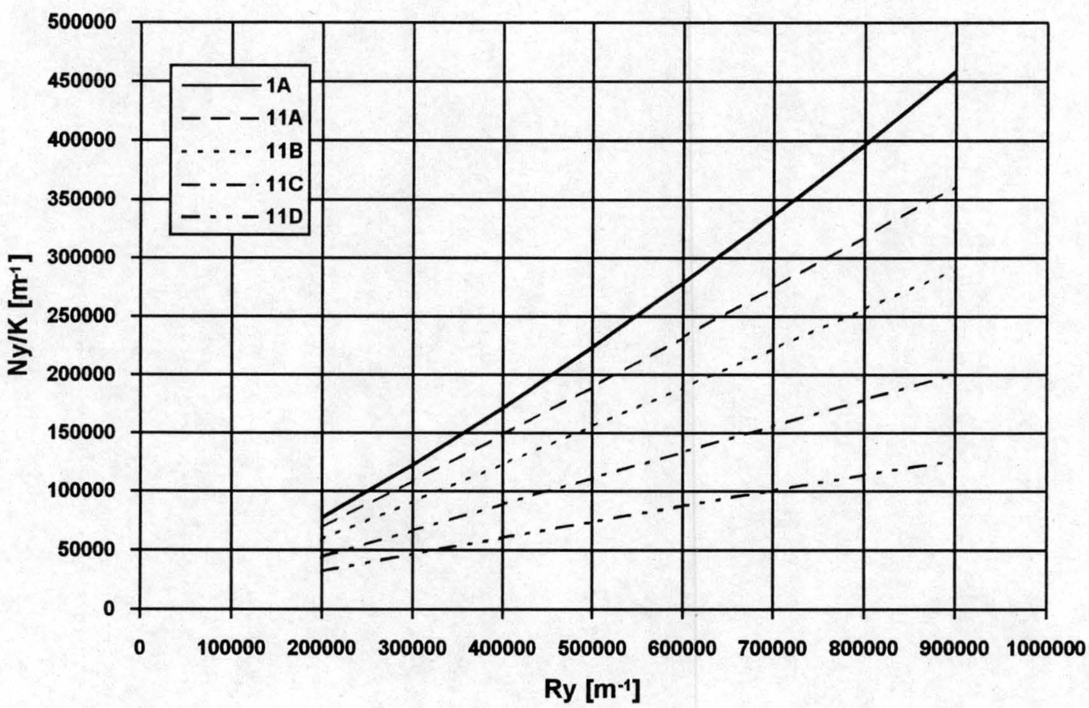

Figure A.22: Effectiveness ratio curve fits for the 11-series of Type 1. The plate spacing is 5 mm.

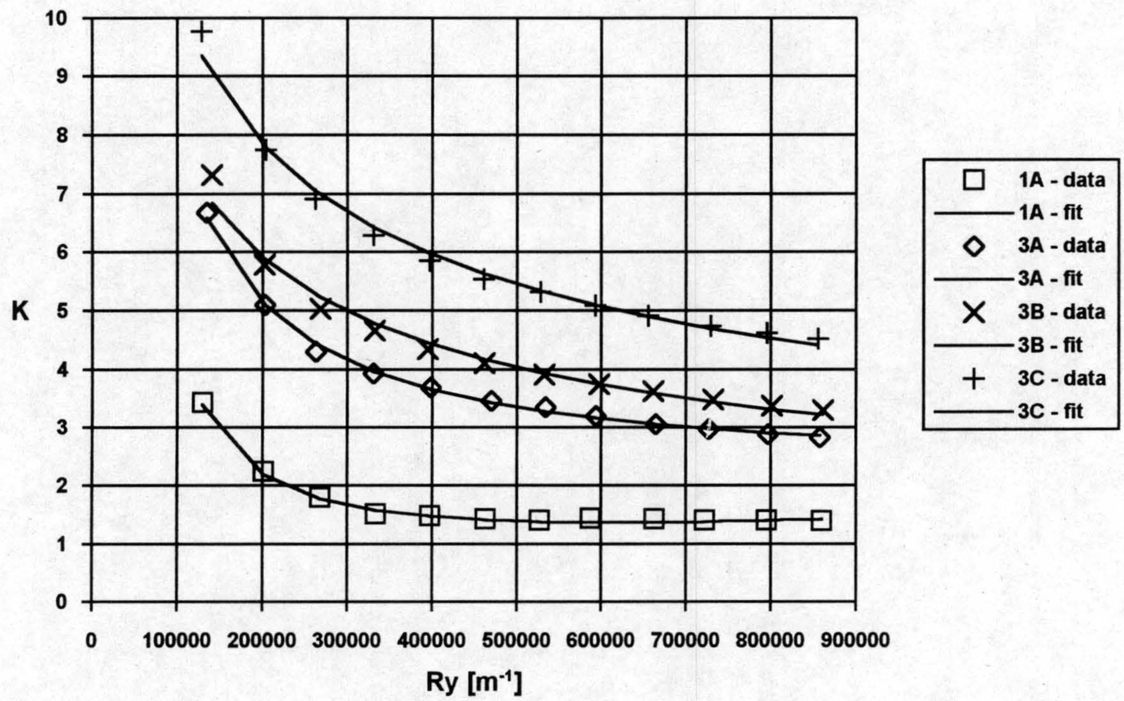

Figure A.23: Loss coefficient data and curve fits for the 3-series of Type 1. The plate spacing is 3.5 mm.

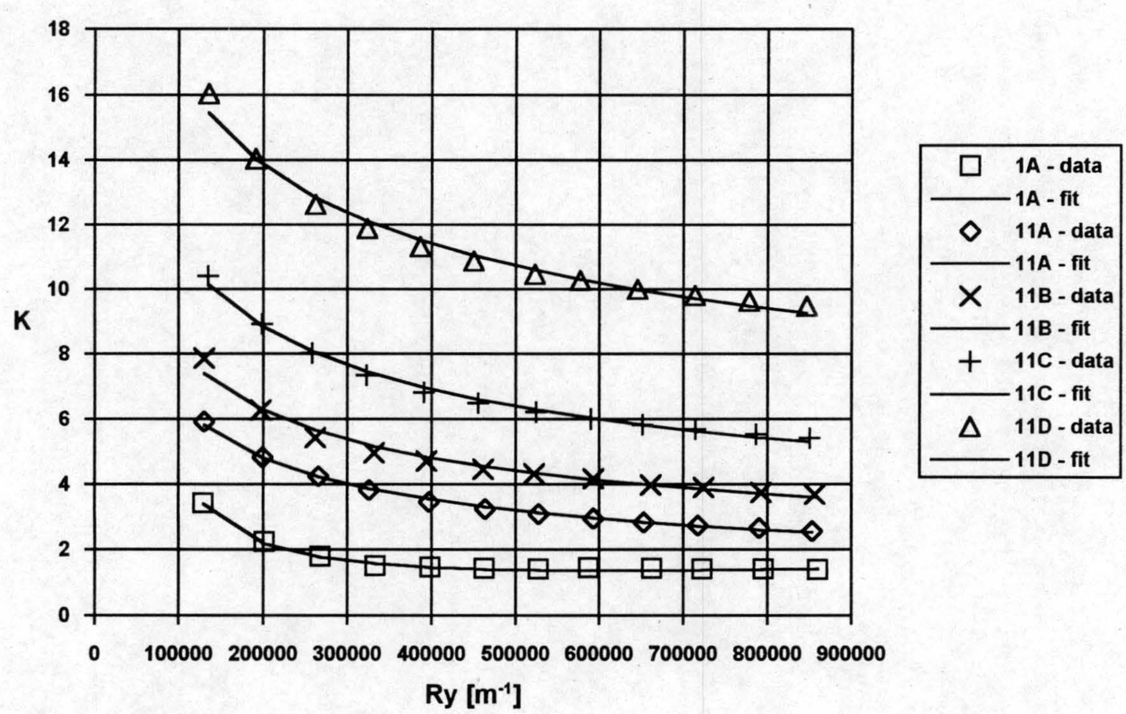

Figure A.24: Loss coefficient data and curve fits for the 11-series of Type 1. The plate spacing is 3.5 mm.

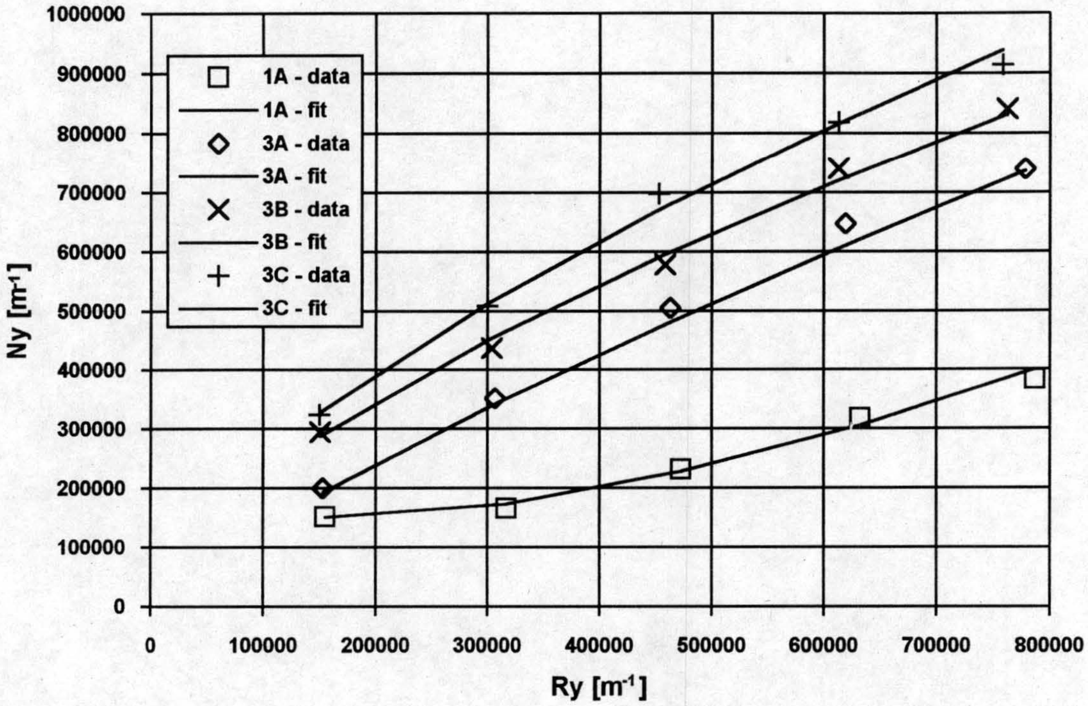

Figure A.25: Heat transfer data and curve fits for the 3-series of Type 1. The plate spacing is 3.5 mm.

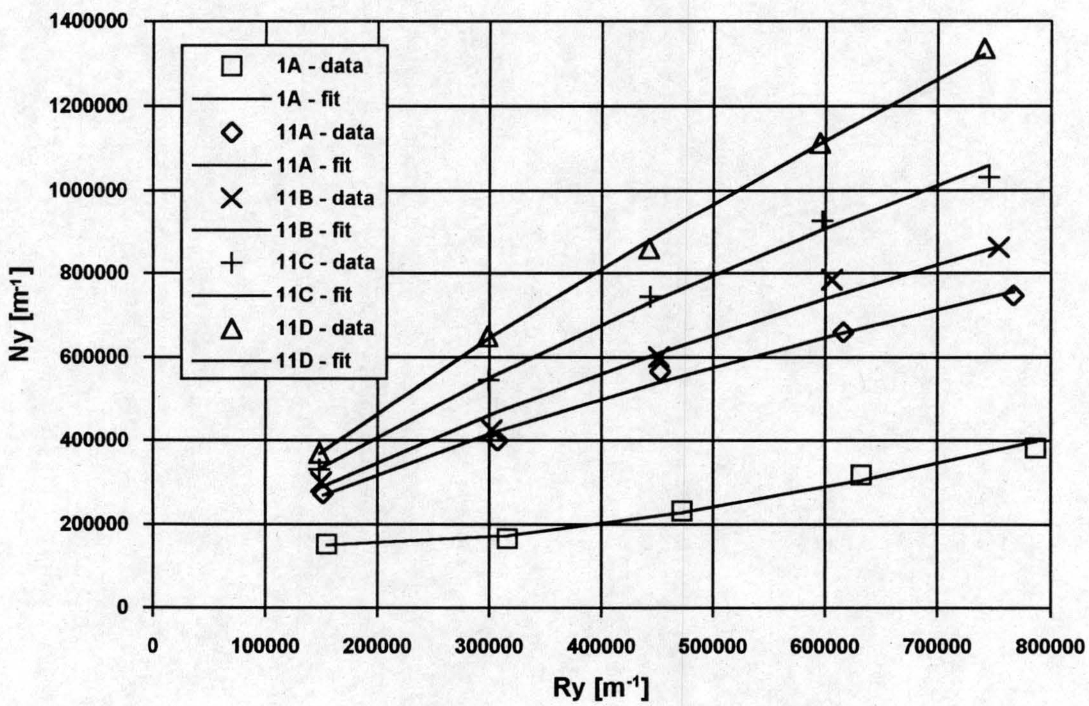

Figure A.26: Heat transfer data and curve fits for the 11-series of Type 1. The plate spacing is 3.5 mm.

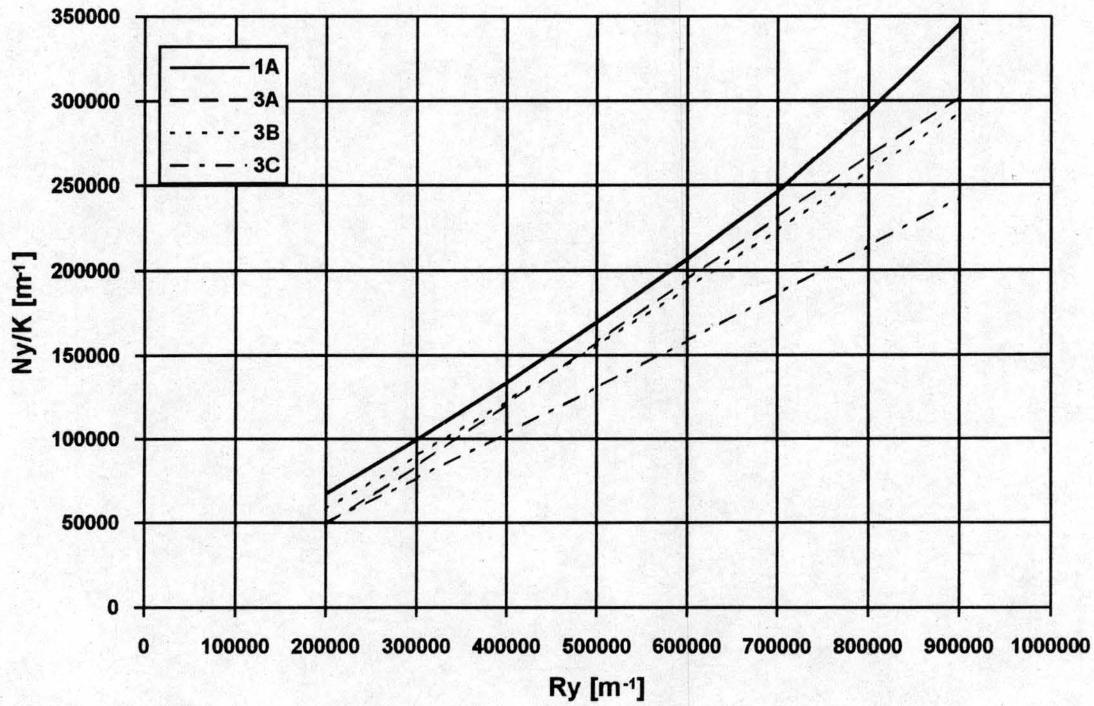

Figure A.27: Effectiveness ratio curve fits for the 3-series of Type 1. The plate spacing is 3.5 mm.

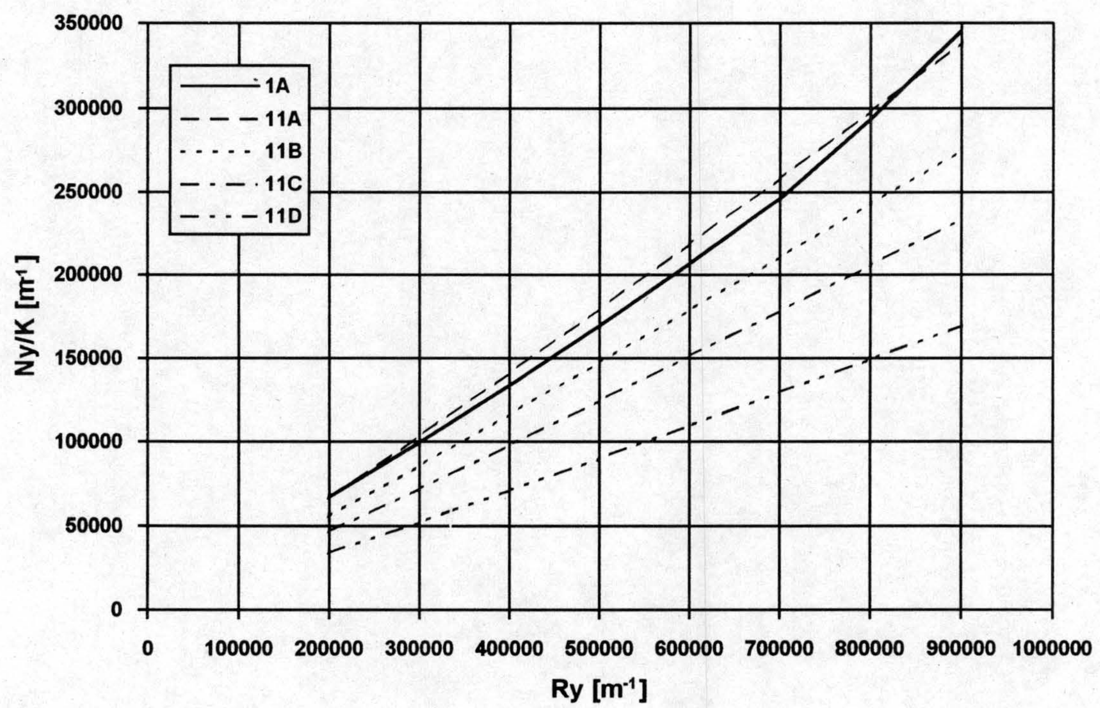

Figure A.28: Heat transfer data and curve fits for the 11-series of Type 1. The plate spacing is 3.5 mm.

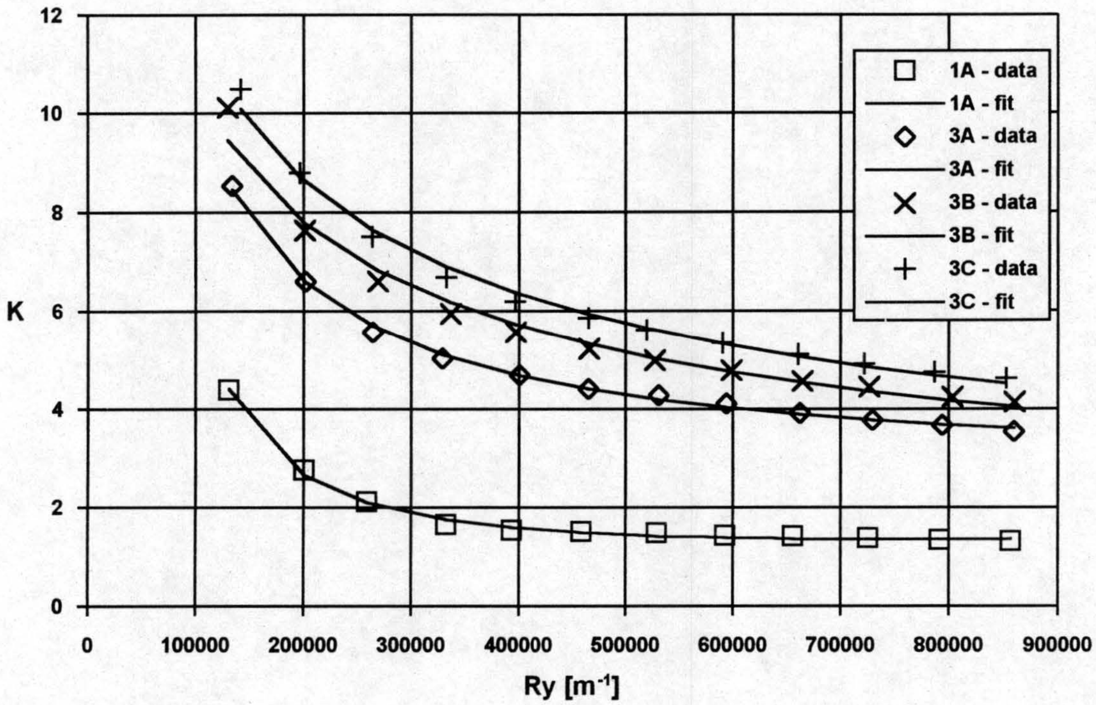

Figure A.29: Loss coefficient data and curve fits for the 3-series of Type 1. The plate spacing is 3 mm.

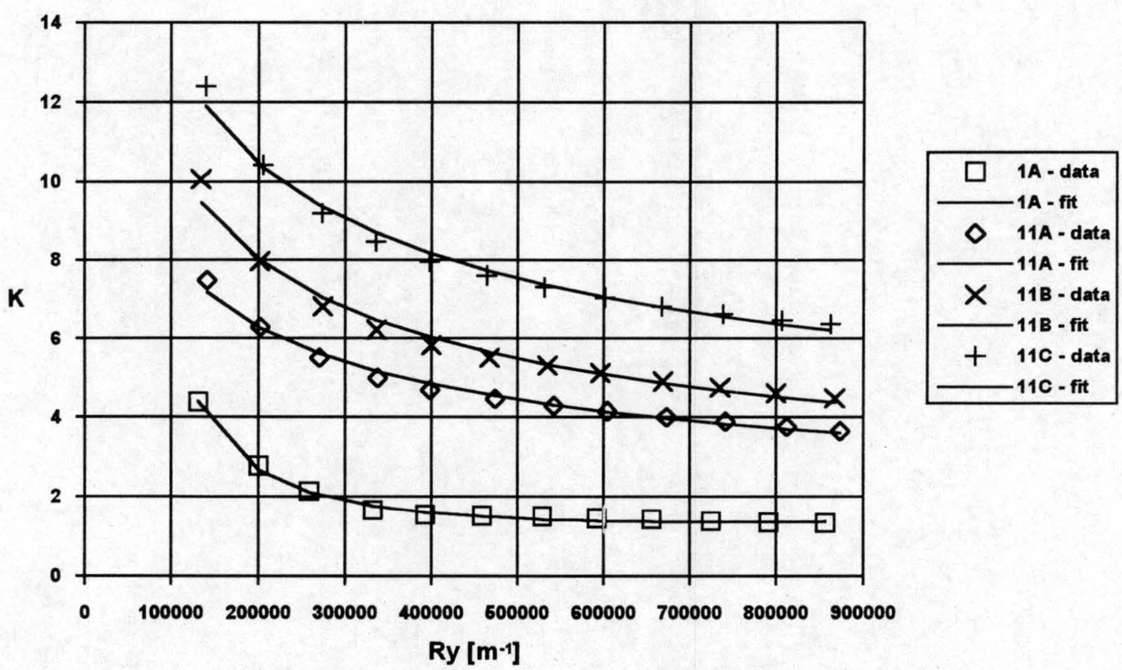

Figure A.30: Loss coefficient data and curve fits for the 11-series of Type 1. The plate spacing is 3 mm.

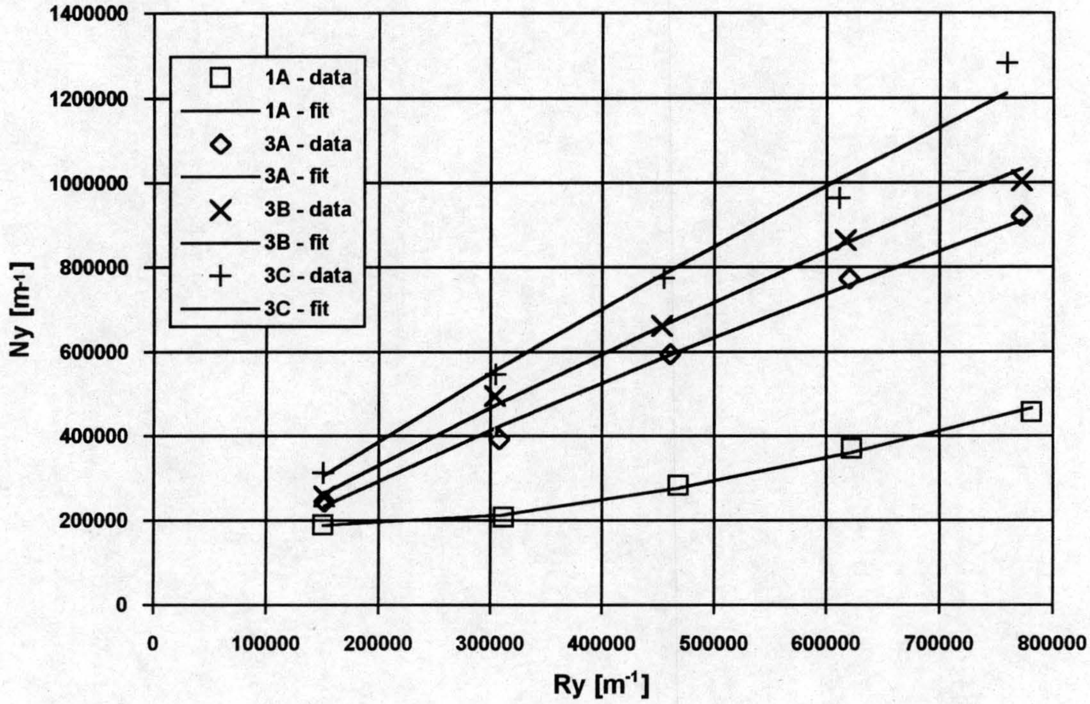

Figure A.31: Heat transfer data and curve fits for the 3-series of Type 1. The plate spacing is 3 mm.

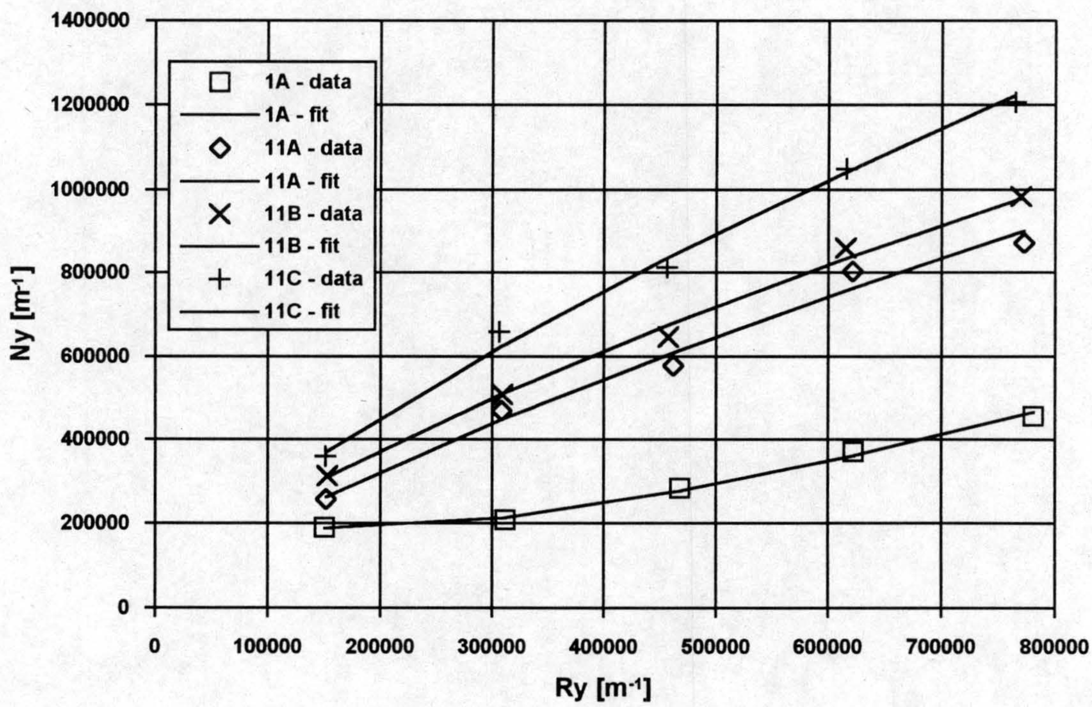

Figure A.32: Heat transfer data and curve fits for the 11-series of Type 1. The plate spacing is 3 mm.

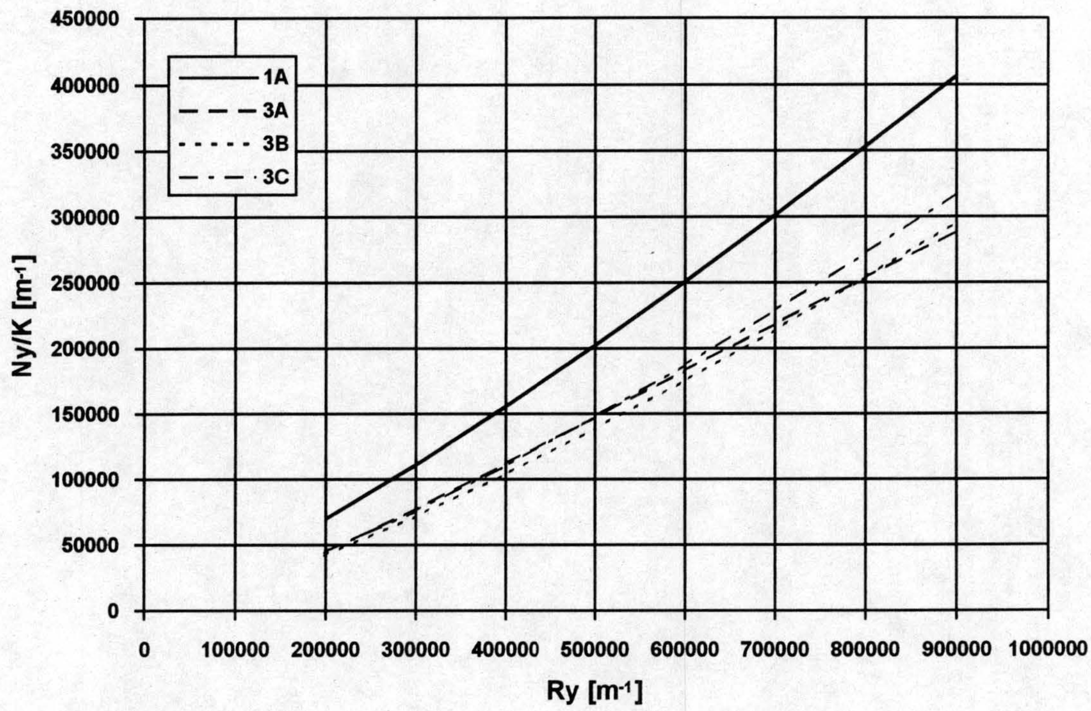

Figure A.33: Effectiveness ratio curve fits for the 3-series of Type 1. The plate spacing is 3 mm.

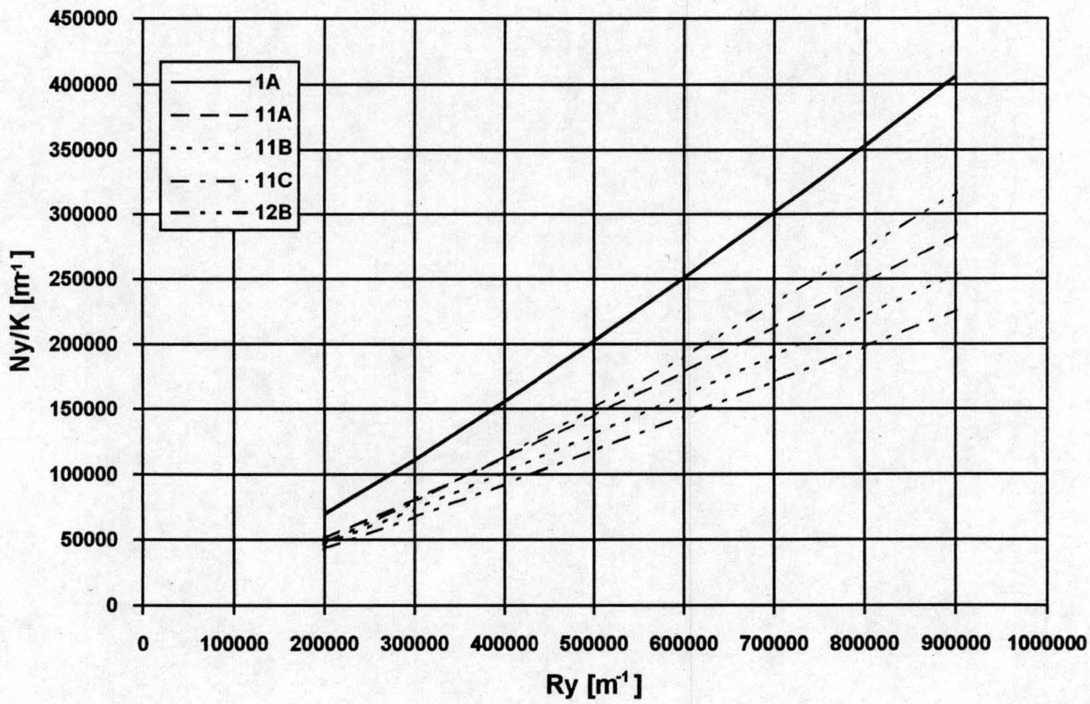

Figure A.34: Effectiveness ratio curve fits for the 11-series of Type 1. The plate spacing is 3 mm.

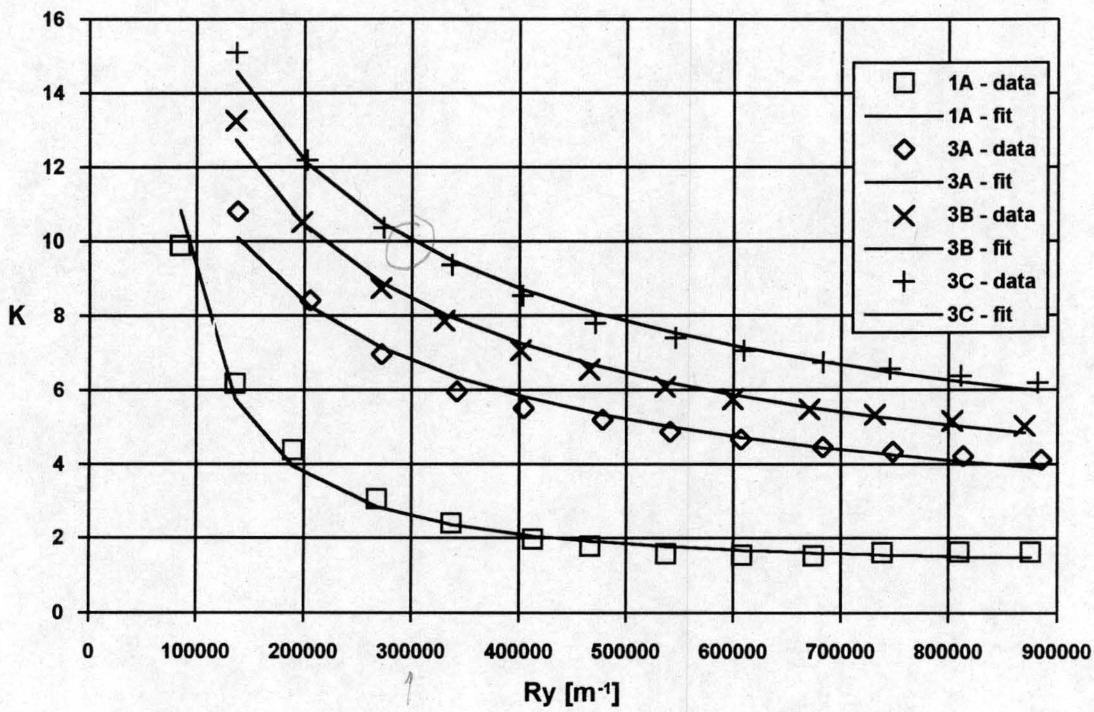

Figure A.35: Loss coefficient data and curve fits for the 3-series of Type 1. The plate spacing is 2.5 mm.

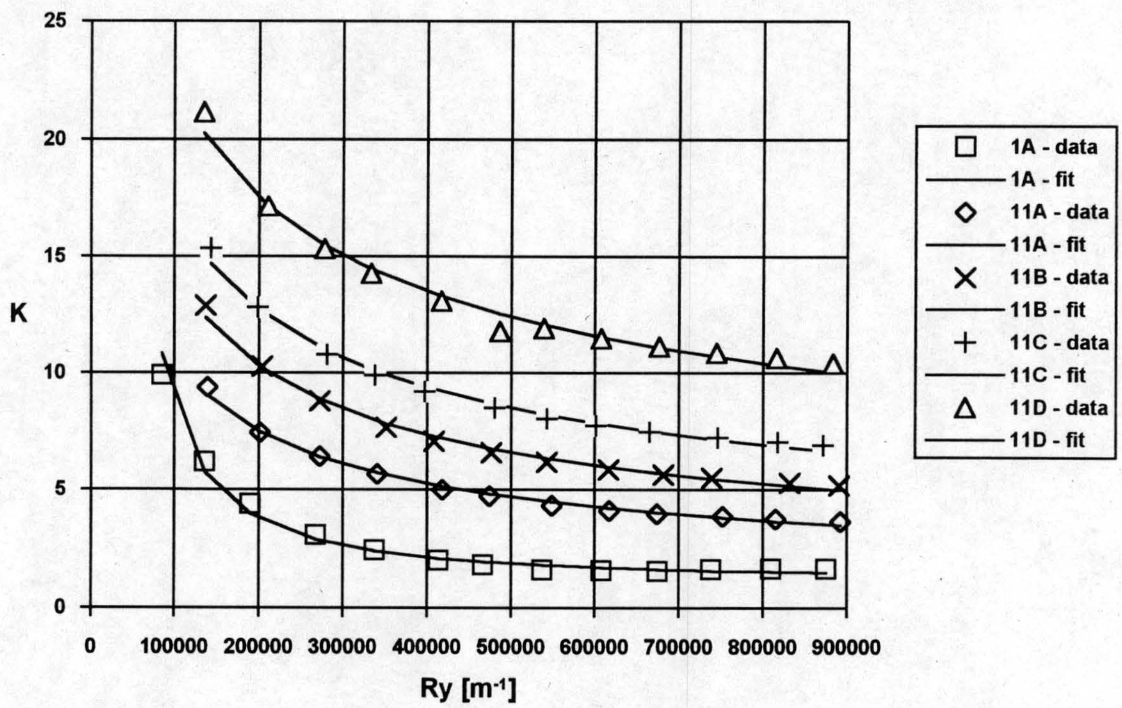

Figure A.36: Loss coefficient data and curve fits for the 11-series of Type 1. The plate spacing is 2.5 mm.

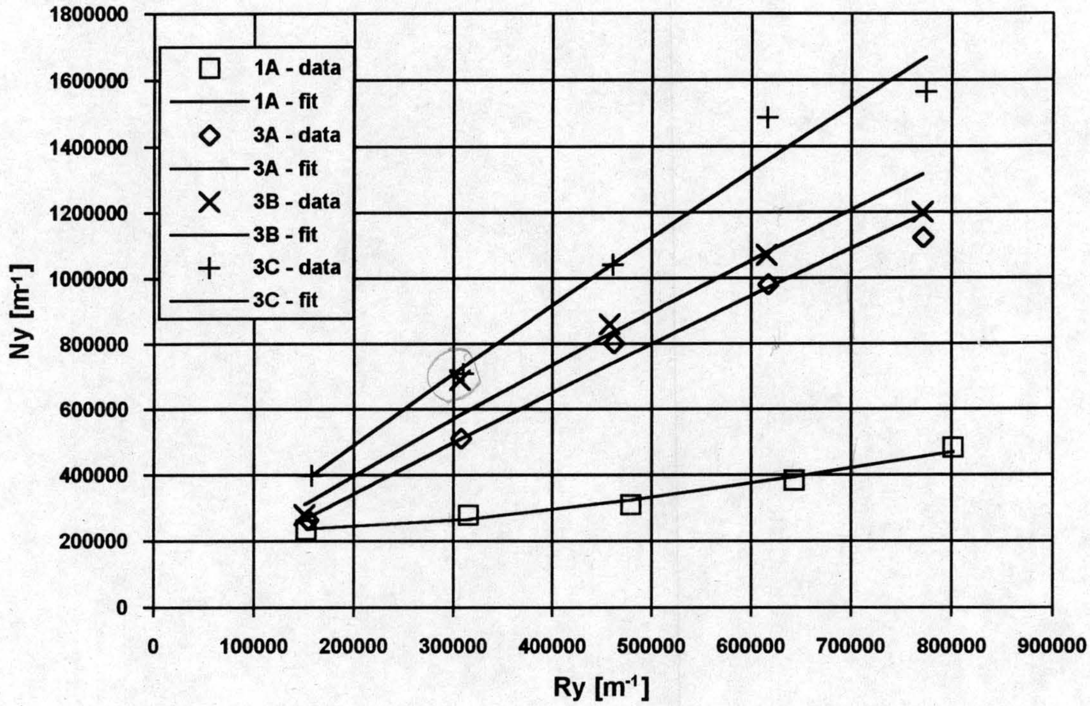

Figure A.37: Heat transfer data and curve fits for the 3-series of Type 1. The plate spacing is 2.5 mm.

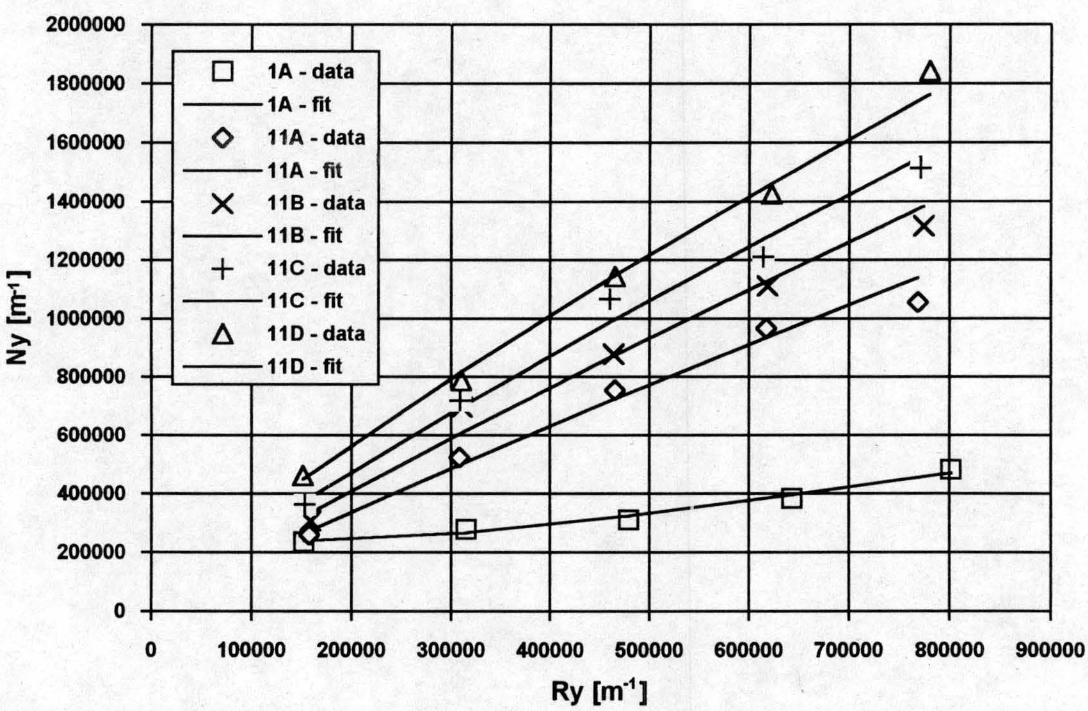

Figure A.39: Heat transfer data and curve fits for the 11-series of Type 1. The plate spacing is 2.5 mm.

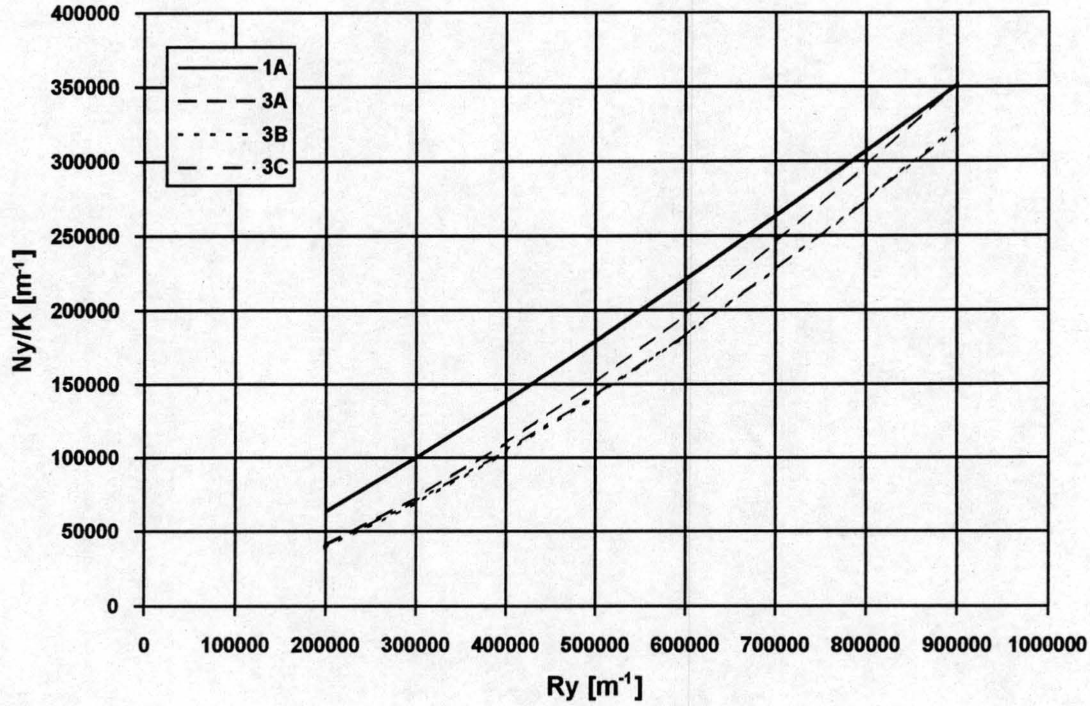

Figure A.40: Effectiveness ratio curve fits for the 3-series of Type 1. The plate spacing is 2.5 mm.

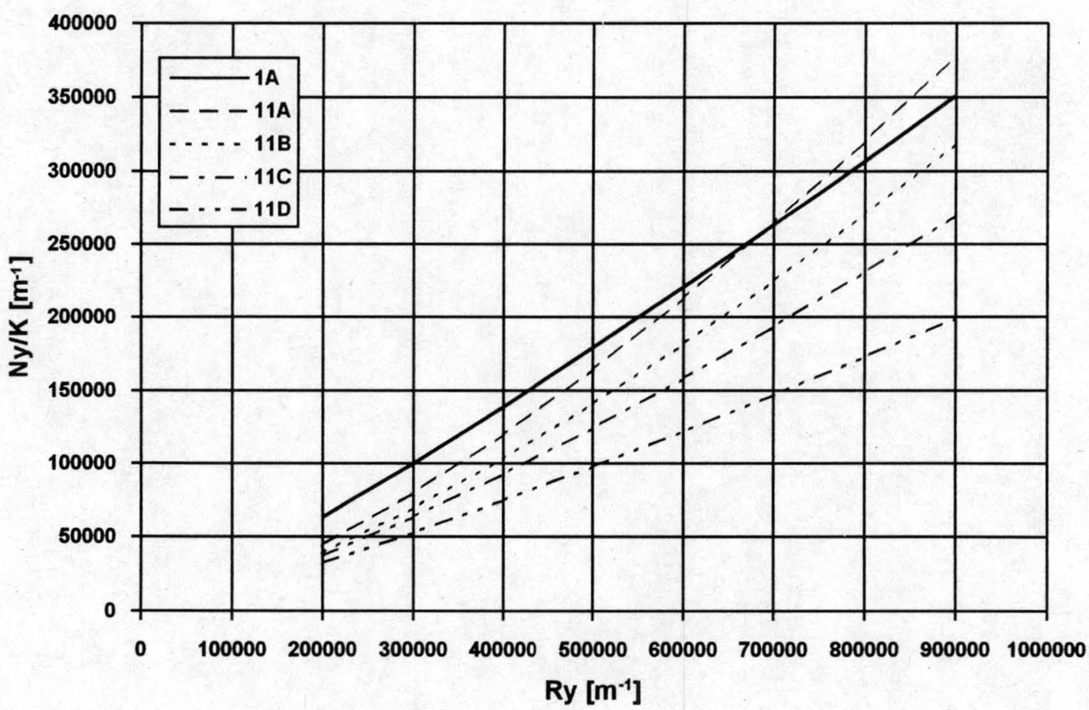

Figure A.41: Effectiveness ratio curve fits for the 11-series of Type 1. The plate spacing is 2.5 mm.

A.7 CONVERSION OF TEST DATA

To convert the empirical equations for heat transfer and pressure drop obtained during the experiments conducted with the apparatus as described above the following definitions and transformations are of relevance to achieve expressions suitable for application in the design of plate fin heat exchangers.

The heat transfer results obtained during the test program may be correlated by the following empirical equations:

$$Ny = \frac{h_a A_a}{k_a \, Pr_a^{0.333} \, A_{fr}} = c1Ry^{(c2+c3\ln(Ry))} \tag{A.18}$$

$$K = \frac{\Delta p}{0.5 \times \rho_a v_a^2} = a1Ry^{(a2+a3\ln(Ry))} \tag{A.19}$$

$$\text{where } Ry = \frac{\rho_a v_a}{\mu_a} \tag{A.20}$$

The test configuration is the special case where the frontal area is equal to the free flow area. In heat exchanger applications the velocity in the above relations is based on the total frontal area. The heat transfer coefficient is replaced by an effective heat transfer coefficient. In effect the tested heat transfer coefficient is multiplied by a fin effectiveness. In heat exchanger design the above relations become

$$Ny_{he} = \frac{h_{a,he} A_{a,he} e_f}{k_a \, Pr_a^{0.333} \, A_{fr,he}} \tag{A.21}$$

$$K_{he} = \frac{\Delta p}{0.5 \times \rho_a v_{a,he}^2} \tag{A.22}$$

$$\text{where } Ry_{he} = \frac{\rho_a v_{a,he}}{\mu_a} \tag{A.23}$$

A.7.1 Loss coefficient transformation

We require that when the air velocity between two fins $v_{a,f}$ is equal to the air velocity between the two surfaces v_a during the experimentation, that the pressure drops must be equal providing the flow length is the same. This leads to the following relationship.

$$Ry = \frac{\rho_a v_a}{\mu_a} = \frac{\rho_a v_{a,f}}{\mu_a} = \frac{\rho_a v_{a,he} A_{fr,he}}{\mu_a A_{o,he}} = Ry_{he} \frac{A_{fr,he}}{A_{o,he}} \tag{A.24}$$

In the above relation $v_{a,he}$ is the air velocity based on the total frontal area of the heat exchanger, $A_{fr,he}$. The free flow area of the heat exchanger is $A_{o,he}$. The equal pressure drop requirement yields:

$$\Delta p = K 0.5 \rho_a v_a^2 = \Delta p_{he} = K_{he} 0.5 \rho_a v_{a,he}^2$$
$$\text{or } K = K_{he} \left(\frac{A_{o,he}}{A_{fr,he}} \right)^2 \tag{A.25}$$

since from continuity $\rho_a v_a A_{o,he} = \rho_a v_{a,he} A_{fr,he}$.

Substitute equations (A.24) and (A.25) into equation (A.20) and find

$$K_{he} \left(\frac{A_{o,he}}{A_{fr,he}} \right)^2 = a1 \left(Ry_{he} \left(\frac{A_{fr,he}}{A_{o,he}} \right) \right)^{\left(a2 + a3 \ln \left(Ry_{he} \left(\frac{A_{fr,he}}{A_{o,he}} \right) \right) \right)}$$

If we assume that the pressure gradient is constant and that the inlet and outlet losses are small compared to the core friction losses we can correct the above equation for any depth of finned tube.

$$K_{he} = a1 \left(Ry_{he} \left(\frac{A_{fr,he}}{A_{o,he}} \right) \right)^{\left(a2 + a3 \ln \left(Ry_{he} \left(\frac{A_{fr,he}}{A_{o,he}} \right) \right) \right)} \left(\frac{L_{he}}{0.2} \right) \left(\frac{A_{o,he}}{A_{fr,he}} \right)^{-2} \tag{A.26a}$$

or equivalently

$$K_{he} = a1\left(Ry_{he}\left(\frac{1}{\sigma_{he}}\right)\right)^{\left(a2+a3\ln\left(Ry_{he}\left(\frac{1}{\sigma_{he}}\right)\right)\right)}\left(\frac{L_{he}}{0.2}\right)\left(\frac{1}{\sigma_{he}}\right)^{2} \tag{A.26b}$$

If a3 = 0 the above relation becomes:

$$K_{he} = a1Ry_{he}^{a2}\left(\frac{A_{fr,he}}{A_{o,he}}\right)^{a2+2}\left(\frac{L_{he}}{0.2}\right) \tag{A.27a}$$

or

$$K_{he} = a1Ry_{he}^{a2}\left(\frac{1}{\sigma_{he}}\right)^{a2+2}\left(\frac{L_{he}}{0.2}\right) \tag{A.27b}$$

A.7.2 Heat transfer parameter transformation

To convert the experimental relationship for Ny we require that when the air velocity between two fins $v_{a,f}$ is equal to the air velocity between the two surfaces v_a during the experimentation, the heat transfer coefficients must be equal.

$$\begin{gathered} h_a = Nyk_a\, Pr_a^{0.333}\frac{A_{fr}}{A_a} = h_{a,he} = Ny_{he}k_a\, Pr_a^{0.333}\frac{A_{fr,he}}{A_{a,he}e_f} \\ \text{or } Ny = Ny_{he}\frac{A_a}{A_{fr}}\frac{A_{fr,he}}{A_{a,he}e_f} \end{gathered} \tag{A.28}$$

Substitute equations (A.24) and (A.28) into equation (A.18) to find:

$$Ny_{he} = c1\left(Ry_{he}\left(\frac{A_{fr,he}}{A_{o,he}}\right)\right)^{\left(c2+c3\ln\left(Ry_{he}\left(\frac{A_{fr,he}}{A_{o,he}}\right)\right)\right)}\left(\frac{A_{a,he}}{A_{fr,he}}\right)\left(\frac{A_{fr}}{A_a}\right)e_f \tag{A.29a}$$

For application to plate fin heat exchangers as in a rotary regenerator, the above relation can be simplified as follows:

$$Ny_{he} = c1\left(Ry_{he}\left(\frac{1}{\sigma_{he}}\right)\right)^{\left(c2+c3\ln\left(Ry_{he}\left(\frac{1}{\sigma_{he}}\right)\right)\right)}\left(\frac{L}{0.2}\right)(\sigma) \tag{A.29b}$$

Note that the fin efficiency for a plate fin heat exchanger is 1.

If c3 = 0 equation (A.29) becomes

$$Ny_{he} = c1Ry_{he}^{c2}\left(\frac{A_{a,he}}{A_{fr,he}}\right)\left(\frac{A_{fr}}{A_{a}}\right)\left(\frac{A_{fr,he}}{A_{o,he}}\right)^{c2} e_f \tag{A.30a}$$

or for plate fin heat exchangers:

$$Ny_{he} = c1Ry_{he}^{c2}\left(\frac{L}{0.2}\right)\left(\frac{1}{\sigma_{he}}\right)^{c2+1} \tag{A.30b}$$

APPENDIX B

Solution method for the effectiveness of a recuperator including the effect of axial or longitudinal heat conduction

The solution by Hahnemann [48HA1] is again reported by Bahnke and Howard [64BA1]. The interested reader is referred to the work of Kroeger [67KR1] where a derivation of the solution can be seen.

The following variables and abbreviations are defined:

$$\sigma \equiv \frac{1}{(hA)^*}$$

$$\Lambda_i \equiv \left[1 + (hA)^*\right] Ntu_o$$

$$\Phi_i \equiv \frac{1}{\lambda}\left[1 + (hA)^*\right] Ntu_o$$

$$\delta_1 = \Lambda_i (C^*\sigma - 1)$$

$$\delta_2 = -\left[\Phi_i(\sigma + 1) + C^*\sigma\Lambda_i^2\right]$$

$$\delta_3 = \sigma\Phi_i\Lambda_i(1 - C^*)$$

$$q = \frac{\delta_3}{2} - \frac{\delta_1\delta_2}{6} + \frac{\delta_1^3}{27}$$

$$p = \frac{\delta_1^2}{9} - \frac{\delta_2}{3}$$

$$\varphi = \cos^{-1}\left(\frac{-q}{\sqrt{p^3}}\right)$$

$$r_1 = 2\sqrt{p}\cos\left(\frac{\varphi}{3}\right) - \frac{\delta_1}{3}$$

$$r_2 = -2\sqrt{p}\,\cos\left(\frac{\varphi}{3} + \frac{\pi}{3}\right) - \frac{\delta_1}{3}$$

$$r_2 = -2\sqrt{p}\,\cos\left(\frac{\varphi}{3} - \frac{\pi}{3}\right) - \frac{\delta_1}{3}$$

The effectiveness is then computed as:

$$E = 1 - \frac{1}{P(1+\sigma C^*)}\left\{\frac{r_1^3(1+\sigma)}{\sigma\Lambda_i\Phi_i}F_1 + \frac{r_1^2}{\sigma\Phi_i}(\sigma^2 C^* - 1)F_2\right\}$$

where

$$F_1 = e^{r_2} - e^{r_3} + \left(\frac{r_2}{r_1}\right)^2 (e^{r_3} - e^{r_1}) + \left(\frac{r_3}{r_1}\right)^2 (e^{r_1} - e^{r_2})$$

$$F_2 = e^{r_2} - e^{r_3} + \left(\frac{r_2}{r_1}\right)(e^{r_3} - e^{r_1}) + \left(\frac{r_3}{r_1}\right)(e^{r_1} - e^{r_2})$$

$$F_3 = (1 - e^{r_1})(e^{r_2} - e^{r_3}) + \left(\frac{r_1}{r_2}\right)(1 - e^{r_2})(e^{r_3} - e^{r_1}) + \left(\frac{r_1}{r_3}\right)(1 - e^{r_3})(e^{r_1} - e^{r_2})$$

$$F_4 = e^{r_1}(e^{r_2} - e^{r_3}) + \left(\frac{r_2}{r_1}\right)^2 e^{r_2}(e^{r_3} - e^{r_1}) + \left(\frac{r_3}{r_1}\right)^2 e^{r_3}(e^{r_1} - e^{r_2})$$

$$F_5 = e^{r_1}(e^{r_2} - e^{r_3}) + \left(\frac{r_2}{r_1}\right) e^{r_2}(e^{r_3} - e^{r_1}) + \left(\frac{r_3}{r_1}\right) e^{r_3}(e^{r_1} - e^{r_2})$$

$$P = F_3 + \frac{1}{(1+\sigma C^*)}\left\{\frac{r_1^3(1+\sigma)}{\sigma\Lambda_i\Phi_i}F_1 + \frac{r_1^3}{\Lambda_i\Phi_i}F_4 - \frac{r_1^2}{\sigma\Phi_i}F_2 + \frac{\sigma r_1^2 C^*}{\Phi_i}F_5\right\}$$

For the special case for a balanced symmetric recuperator the above solution reduces to

$$E = 1 - \left[1 + Ntu_o - \kappa Ntu_o^3 / a^2\right]^{-1}$$

where

$$\kappa = 4 - \frac{8}{a}\left[1 - (1 - e^{-a})/\sinh(a)\right]$$

$$a = 2\sqrt{Ntu_o^2 + Mo_o}$$

$$Mo_o = \frac{Ntu_o}{\lambda}$$

Note: This solution was derived with the assumption that the number of transfer units are equal on each side ($Ntu_h = Ntu_c$). This implies that $(hA)^*$ must be taken as $1/C^*$ and not the actual value. The error introduced by this assumption is very small as it was previously shown that the influence of $(hA)^*$ on the effectiveness is negligible.

APPENDIX C

Numerical scheme for the solution of a counterflow regenerator including the effect of longitudinal heat conduction

The regenerator thermal problem can be solved by discretisizing the basic governing differential equations as derived in Chapter 2 or alternatively a direct finite difference scheme can be used. Such a scheme was developed by Lambertson [58LA1] and later extended by Bahnke and Howard [64BA1] to include the effect of longitudinal heat conduction. The scheme of Bahnke and Howard [64BA1] and the method of solution that was used in the program described in Chapter 4 will be presented here.

The following idealisations were made:

1. The thermal resistance of the matrix wall is zero in the radial direction as well as in the direction of the matrix rotation.

2. The thermal properties of the fluids and the matrix material are constant with temperature and time.

3. There is no pressure- or carryover leakage between the two fluids.

4. The convective heat transfer coefficients are constant over the flow length.

5. The fluids pass in a counterflow fashion and regular periodic conditions are established.

6. The fluid inlet temperatures are constant with position and time.

For this direct finite difference method the rotor is divided into a finite number of elements. Each element is seen as a heat exchanger with a fluid stream and a matrix metal 'stream' in cross flow. Energy balances are then written for each element. The element itself is considered to be fixed in space with the metal and fluid stream flowing through it. There is a heat transfer area associated with each element.

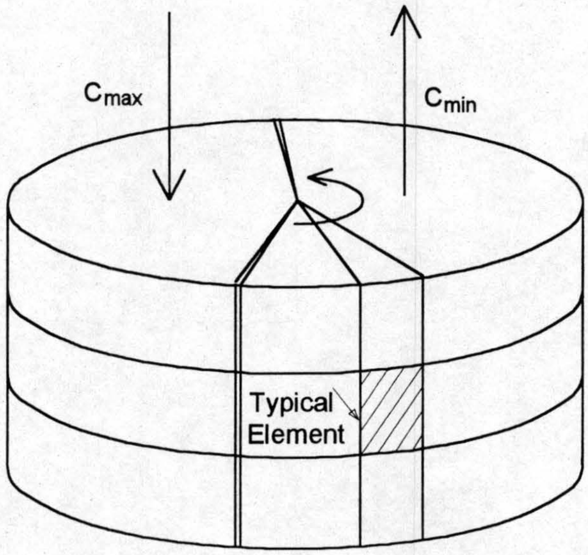

Figure C.1: Regenerator matrix showing flow arrangement and typical element.

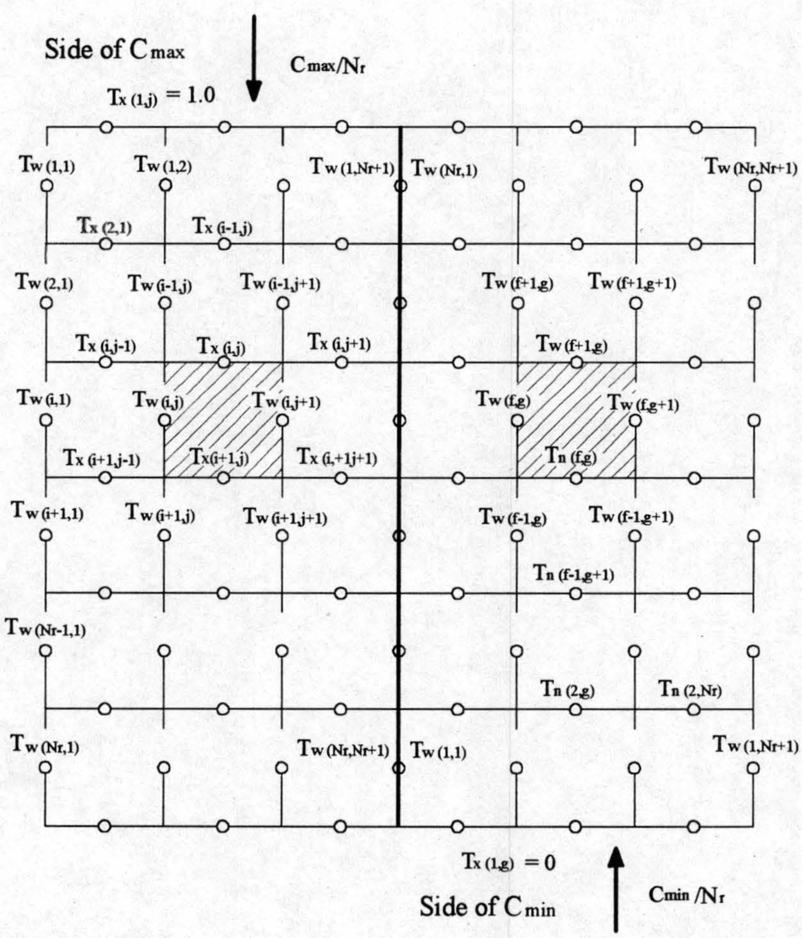

Figure C.2: Schematic representation of regenerator elements.

Consider a fluid element on the side of C_{max} as can be seen in figure C.2. The maximum fluid side will be denoted by 'x' and the minimum fluid side by 'n'. The number of radial divisions on the maximum fluid side is N_x and the number of axial divisions is N_r. The temperature of the maximum fluid is T_x while the minimum fluid temperature is T_n. The matrix temperature will be denoted by T_w. The convective heat transfer rate must be equal to the rate of change of enthalpy of the fluid stream in the absence of heat conduction in the fluid itself, therefore:

$$\frac{(hA)_x}{N_x N_r}\Delta T_{avg} = \frac{C_{max}}{N_x}\left[T_{x(i,j)} - T_{x(i+1,j)}\right] \tag{C.1}$$

where ΔT_{avg} is taken as the arithmetic mean temperature difference between the fluid and the matrix.

$$\Delta T_{avg} = 0.5\left[T_{x(i,j)} - T_{x(i+1,j)}\right] - 0.5\left[T_{w(i,j)} - T_{w(i,j+1)}\right]$$

An energy balance on the element requires that the energy supplied by convection plus the net energy influx due to conduction from neighbouring elements must be equal to the energy stored in the element. $A_{k,x}$ is the total solid area for longitudinal heat conduction on the maximum fluid side, L is the total disk thickness and k is the thermal conductivity of the matrix material.

$$\begin{aligned}&\frac{C_{max}}{N_x}\left[T_{x(i,j)} - T_{x(i+1,j)}\right] + k\frac{A_{k,x}N_r}{2LN_x}\left[(T_{w(i-1,j)} - T_{w(i-1,j+1)}) - (T_{w(i,j)} - T_{w(i,j+1)})\right]\\ &-k\frac{A_{k,x}N_r}{2LN_x}\left[(T_{w(i,j)} - T_{w(i,j+1)}) - (T_{w(i+1,j)} - T_{w(i+1,j+1)})\right] = \frac{C_r}{N_r}\left[T_{w(i,j+1)} - T_{w(i,j)}\right]\end{aligned} \tag{C.2}$$

Equation (C.2) can be arranged to find the outlet fluid temperature.

$$T_{x(i,j+1)} = D_4 T_{x(i,j)} + D_5\left[T_{w(i,j)} - T_{w(i,j+1)}\right] \tag{C.3}$$

The outlet matrix temperature can be found by combining equations (C.1) and (C.2).

$$T_{w(i,j+1)} = D_1 T_{x(i,j)} - D_2 T_{w(i,j)} + D_3\left[T_{w(i-1,j)} + T_{w(i-1,j+1)} + T_{w(i+1,j)} + T_{w(i+1,j+1)}\right] \tag{C.4}$$

The boundary conditions are that the longitudinal heat conduction is zero at the ends. For the top and bottom rows equation (C.4) will be different, because of the no-heat-conduction boundary condition that applies there. For the top row equation (C.4) becomes

$$T_{w(1,j+1)} = D_6 T_{x(1,j)} - D_7 T_{w(1,j)} + D_8\left[T_{w(2,j)} + T_{w(2,j+1)}\right] \tag{C.5}$$

For the bottom row:

$$T_{w(Nr,j+1)} = D_6 T_{x(Nr,j)} - D_7 T_{w(Nr,j)} + D_8\left[T_{w(Nr-1,j)} + T_{w(Nr-1,j+1)}\right] \tag{C.6}$$

In a similar fashion finite difference equations can be written for the minimum side.

$$T_{n(f+1,g)} = F_4 T_{n(f,g)} + F_5\left[T_{w(f,g)} + T_{w(f,g+1)}\right] \tag{C.7}$$

$$T_{w(f,g+1)} = F_1 T_{n(f,g)} - F_2 T_{w(f,g)} + F_3\left[T_{w(f-1,g)} + T_{w(f-1,g+1)} + T_{w(f+1,g)} + T_{w(f+1,g+1)}\right] \tag{C.8}$$

$$T_{w(Nr,g+1)} = F_6 T_{n(Nr,g)} - F_7 T_{w(Nr,g)} + F_8\left[T_{w(Nr-1g)} + T_{w(Nr-1,g+1)}\right] \tag{C.9}$$

$$T_{w(1,g+1)} = F_6 T_{n(1,g)} - F_7 T_{w(Nr,j)} + F_8\left[T_{w(2,g)} + T_{w(2,g+1)}\right] \tag{C.10}$$

With the dimensionless parameters $Ntu_o, C^*, C_r^*, A_k^*, (hA)^*$ and λ defined as in chapter 1 the coefficients D_i and F_i in the above equations are defined as follows:

$$C_1 = \frac{C^* Ntu_o}{2N_r}\left[1 + \frac{1}{(hA)^*}\right] \qquad E_1 = \frac{Ntu_o}{2N_r}\left[1 + (hA)^*\right]$$

$$C_2 = C^* C_r^* \frac{N_x}{N_r} \qquad E_2 = C_r^* \frac{N_n}{N_r}$$

$$C_3 = C^* \lambda \frac{1}{1 + A_k^*} \frac{N_r}{2} \qquad E_3 = \lambda \frac{A_k^*}{1 + A_k^*} \frac{N_r}{2}$$

$$C_4 = C_1 + (1 + C_1)(C_2 + 2C_3) \qquad E_4 = E_1 + (1 + E_1)(E_2 + 2E_3)$$

$$C_5 = C_1 + (1 + C_1)(C_2 + C_3) \qquad E_5 = E_1 + (1 + E_1)(E_2 + E_3)$$

$$D_1 = \frac{2C_1}{C_4} \qquad F_1 = \frac{2E_1}{E_4}$$

$$D_2 = \frac{C_1 + (1 + C_1)(2C_3 - C_2)}{C_4} \qquad F_2 = \frac{E_1 + (1 + E_1)(2E_3 - E_2)}{E_4}$$

$$D_3 = \frac{(1 + C_1)C_3}{C_4} \qquad F_3 = \frac{(1 + E_1)E_3}{E_4}$$

$$D_4 = \frac{1 - C_1}{1 + C_1} \qquad F_4 = \frac{1 - E_1}{1 + E_1}$$

$$D_5 = \frac{C_1}{1 + C_1} \qquad F_5 = \frac{E_1}{1 + E_1}$$

$$D_6 = \frac{2C_1}{C_5} \qquad F_6 = \frac{2E_1}{E_5}$$

$$D_7 = \frac{C_1 + (1 + C_1)(C_3 - C_2)}{C_5} \qquad F_7 = \frac{E_1 + (1 + E_1)(E_3 - E_2)}{E_5}$$

$$D_8 = \frac{(1 + C_1)C_3}{C_5} \qquad F_8 = \frac{(1 + E_1)E_3}{E_5}$$

Solution Method

We see from equations (C.3) and (C.7) that the outlet fluid temperatures are dependant on the matrix 'stream' outlet temperatures. The matrix outlet temperature for a specific element is dependant again on matrix temperatures of neighbouring elements. There is thus no simple method of stepping through all the elements to arrive at an answer. An iteration process will be required.

First we assume an initial temperature distribution for the matrix. This can be taken as the average of the maximum- and minimum fluid inlet temperatures. To simplify calculations we can select a temperature scale between 0 and 1. The maximum fluid inlet temperature is taken as 1 and the minimum fluid inlet temperature as 0.

The calculation process is started on the left column on the maximum fluid inlet side. The fluid inlet temperature of this element is known from the boundary condition, $T_{x(1,j)} = 1.0$. The outlet temperatures of this element can then be calculated by making use of the initial guess for the matrix temperatures. It should be recognised that the matrix temperatures on the left edge of the maximum side are physically the same as the matrix temperatures on the right edge of the minimum fluid side. By stepping down in the first column of the maximum side the outlet temperature of the first column can be determined. In a similar fashion all the fluid outlet temperatures on the maximum side can be determined. We then start on the inlet side of the minimum fluid and determine all the outlet temperatures. The newest matrix temperatures must always be used to speed up the process. After the process is completed once, a new matrix temperature distribution will exist that will be used as the starting values for the next iteration.

The fluid outlet temperatures on each side can be used to calculate the effectiveness. The effectiveness is defined as

$$\varepsilon = \frac{C_{min}\left(\bar{T}_{n,o} - \bar{T}_{n,i}\right)}{C_{min}\left(\bar{T}_{x,i} - \bar{T}_{n,i}\right)} = \frac{C_{max}\left(\bar{T}_{x,i} - \bar{T}_{x,o}\right)}{C_{min}\left(\bar{T}_{x,i} - \bar{T}_{n,i}\right)}$$

$$\varepsilon = \frac{\left(\bar{T}_{n,o} - 0\right)}{(1-0)} = \frac{\left(1 - \bar{T}_{x,o}\right)}{C^*(1-0)} = \sum_{k=1}^{Nn} T_{n(Nr+1,k)} = \frac{1}{C^*}\left(1 - \sum_{k=1}^{Nx} T_{x(Nr+1,k)}\right)$$

The above equation gives us two methods of calculating the effectiveness. The two methods will give the same answer if the solution is converged. In the program the convergence criterion was set as

$$\left|\frac{\varepsilon_x}{\varepsilon_n} - 1\right| \le 1 \times 10^{-5}$$

The accuracy is dependent on the number of subdivisions. Furthermore the number of subdivisions should be increased if the size and rotational speed of the regenerator increases. A high rotational speed requires more radial divisions and a 'long' regenerator requires more axial divisions. If this is not done the accuracy decreases and the numerical method becomes unstable and sometimes fails to converge. A high rotational speed is equivalent to a high C_r^* and a high Ntu_o number is an indication of a 'long' regenerator. The following method was used to automatically adjust the number of increments.

$N_x = N_n = \text{Constant} + \Delta N_n$

$N_r = \text{Constant} + \Delta N_r$

where

$\Delta N_n = \text{Round}(1.5C_r^*)$

$\Delta N_r = \text{Round}(0.02Ntu_o)$

The constants 1.5 and 0.02 were determined by trial and error. The computing time increases dramatically if the number of subdivisions is increased. To be more time efficient the effectiveness for a specific set of parameters is evaluated with $N_{n1} = 12 + \Delta N_n$ and $N_{r1} = 12 + \Delta N_r$ divisions. We denote this effectiveness ε_1 The effectiveness is then evaluated again with $N_{n2} = 16 + \Delta N_n$ and $N_{r2} = 16 = \Delta N_r$ divisions. This effectiveness is ε_2. We can then extrapolate to zero element area to find a more accurate effectiveness.

$$\varepsilon = \frac{\varepsilon_1 - \varepsilon_2}{\left(\frac{1}{N_{n1}N_{r1}} - \frac{1}{N_{n2}N_{r2}}\right) \Big/ N_{n1}N_{r1} - \varepsilon_1}$$

This method produced answers accurate to 4 or 5 significant figures when compared to calculations with more divisions, while the computing time and storage space needed is much less.

APPENDIX D

THERMOPHYSICAL PROPERTIES OF FLUIDS

The thermophysical properties of dry air from 220 K to 380 K at standard atmospheric pressure (101325 N/m^2)

Density

$\rho_a = P/RT$ kg/m^3 (D.1)

where R = 287.08 J/kgK

Specific heat [82AN1]

$c_{pa} = a + bT + cT^2 + dT^3$ J/kgK (D.2)

$a = 1.045356 \times 10^{3}$
$b = -3.161783 \times 10^{-1}$
$c = 7.083814 \times 10^{-4}$
$d = -2.705209 \times 10^{-7}$

Dynamic viscosity [82AN1]

$\mu_a = a + bT + cT^2 + dT^3$ kg/ms (D.3)

$a = 2.287973 \times 10^{-6}$
$b = 6.259793 \times 10^{-8}$
$c = -3.131956 \times 10^{-11}$
$d = 8.150380 \times 10^{-15}$

Thermal conductivity

$k_a = a + bT + cT^2 + dT^3$ W/mK (D.4)

$a = -4.937787 \times 10^{-4}$
$b = 1.018087 \times 10^{-4}$
$c = -4.627937 \times 10^{-8}$
$d = 1.250603 \times 10^{-11}$

The thermophysical properties of dry air from 100 K to 2000 K at standard atmospheric pressure (101325 N/m²)

Equations (D.5) to (D.8) are curve fits by the author from tabulated data found in the literature.

Density

$\rho_a = P/RT$ kg/m^3 (D.5)
where $R = 287.08$ J/kgK

Specific heat [87BA1]

$c_p = a + bT + cT^2 + dT^3 + eT^4$ J/kgK (D.6)

$a = 1.051967546 \times 10^{3}$
$b = -3.723763121 \times 10^{-1}$
$c = 9.270461698 \times 10^{-4}$
$d = -5.979265899 \times 10^{-7}$
$e = 1.318061482 \times 10^{-10}$

Dynamic viscosity [87BA1]

$\mu_a = a + bT + cT^2 + dT^3 + eT^4$ kg/ms (D.7)

$a = 5.842550139 \times 10^{-8}$
$b = 7.603632610 \times 10^{-8}$
$c = -5.672930923 \times 10^{-11}$
$d = 2.796817228 \times 10^{-14}$
$e = -5.002783115 \times 10^{-18}$

Thermal conductivity [87BA1]

$k_a = a + bT + cT^2 + dT^3 + eT^4$ W/mK (D.8)

$a = -3.8103889465 \times 10^{-3}$
$b = 1.3206459224 \times 10^{-4}$
$c = -1.1733457586 \times 10^{-7}$

$d = 6.8751900235 \times 10^{-11}$
$e = -1.2768478798 \times 10^{-14}$

The thermophysical properties of saturated water liquid from 273.15 K to 380 K

Density

$$\rho_w = (a + bT + cT^2 + dT^6)^{-1} \quad kg/m^3 \tag{D.9}$$

$a = 1.49343 \times 10^{-3}$
$b = -3.7164 \times 10^{-6}$
$c = 7.09782 \times 10^{-9}$
$d = -1.90321 \times 10^{-20}$

Latent heat of vaporation

$$i_{fgw} = a + bT + cT^2 + dT^3 \quad J/kg \tag{D.10}$$

$a = 3.4831814 \times 10^{6}$
$b = -5.8627703 \times 10^{3}$
$c = 1.2139568 \times 10^{1}$
$d = -1.40290431 \times 10^{-2}$